Correlated 2D Electron Aspects of the Quantum Hall Effect

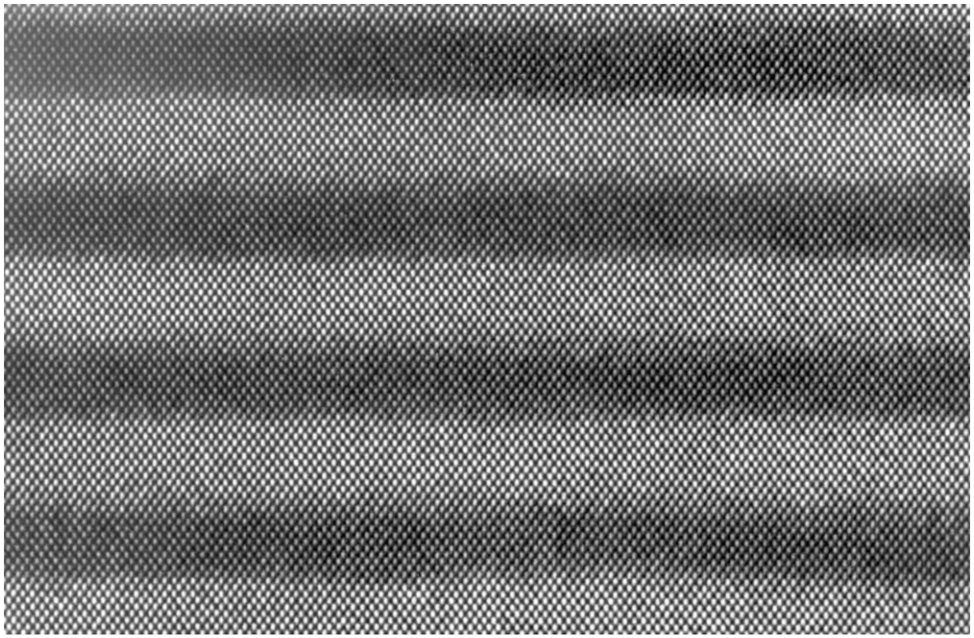

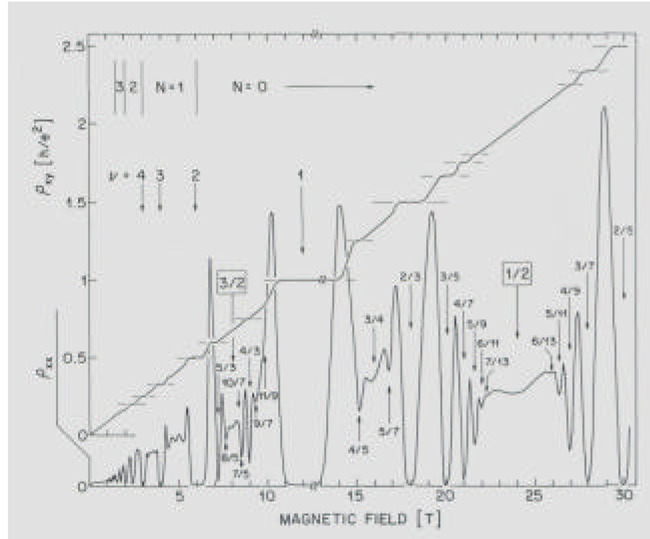

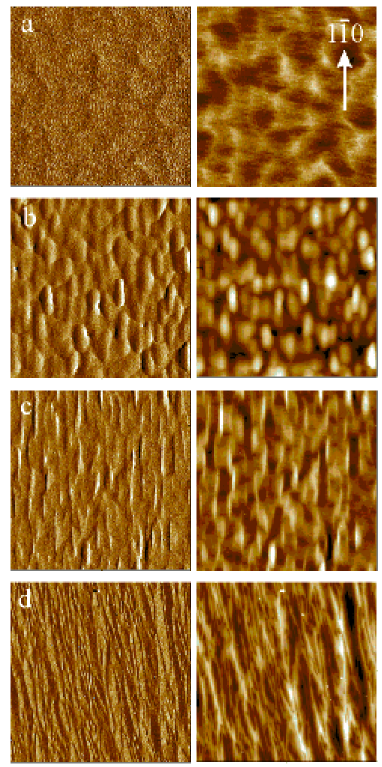

Magnetic field spectrum of the correlated 2D electron system:
Electron interactions lead to a range of manifestations

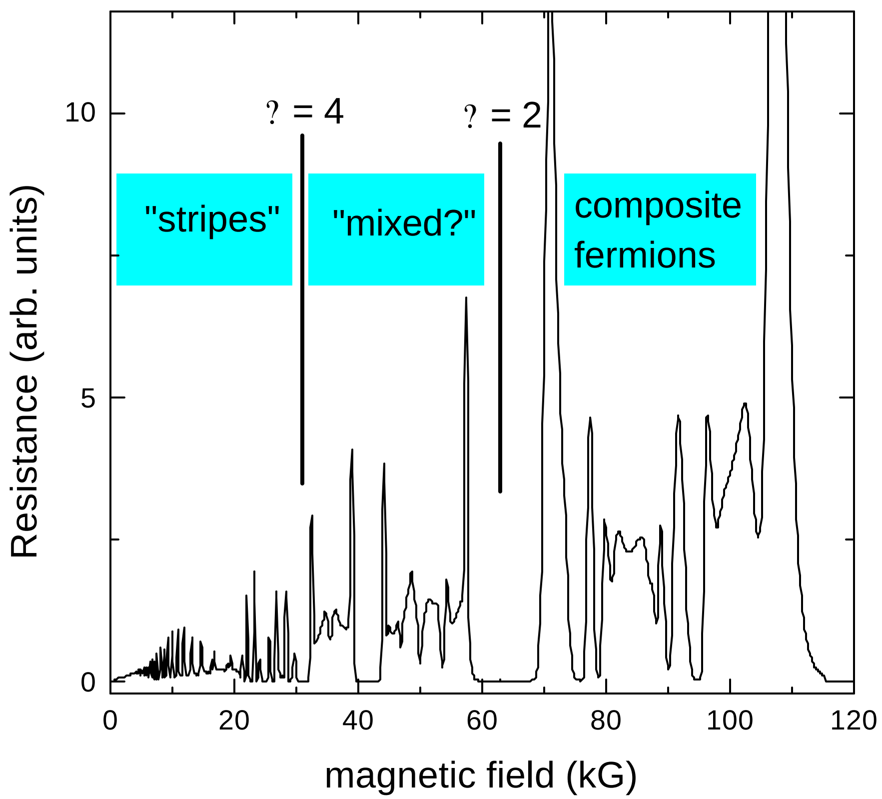

Outline:

I. Introduction: materials, transport, Hall effects

II. Composite particles – FQHE, statistical transformations

III. Quasiparticle charge and statistics

   A. Vortex picture
   B. Early measurements of fractional charge
   C. Noise measurements and fractional charge
   D. Potential Statistical tests

IV. Higher Landau levels

V. Other parts of spectrum: non-equilibrium effects, electron solid?

VI. Multicomponent systems: Bilayers

III. Quasiparticle charge and statistics

A. Vortex picture

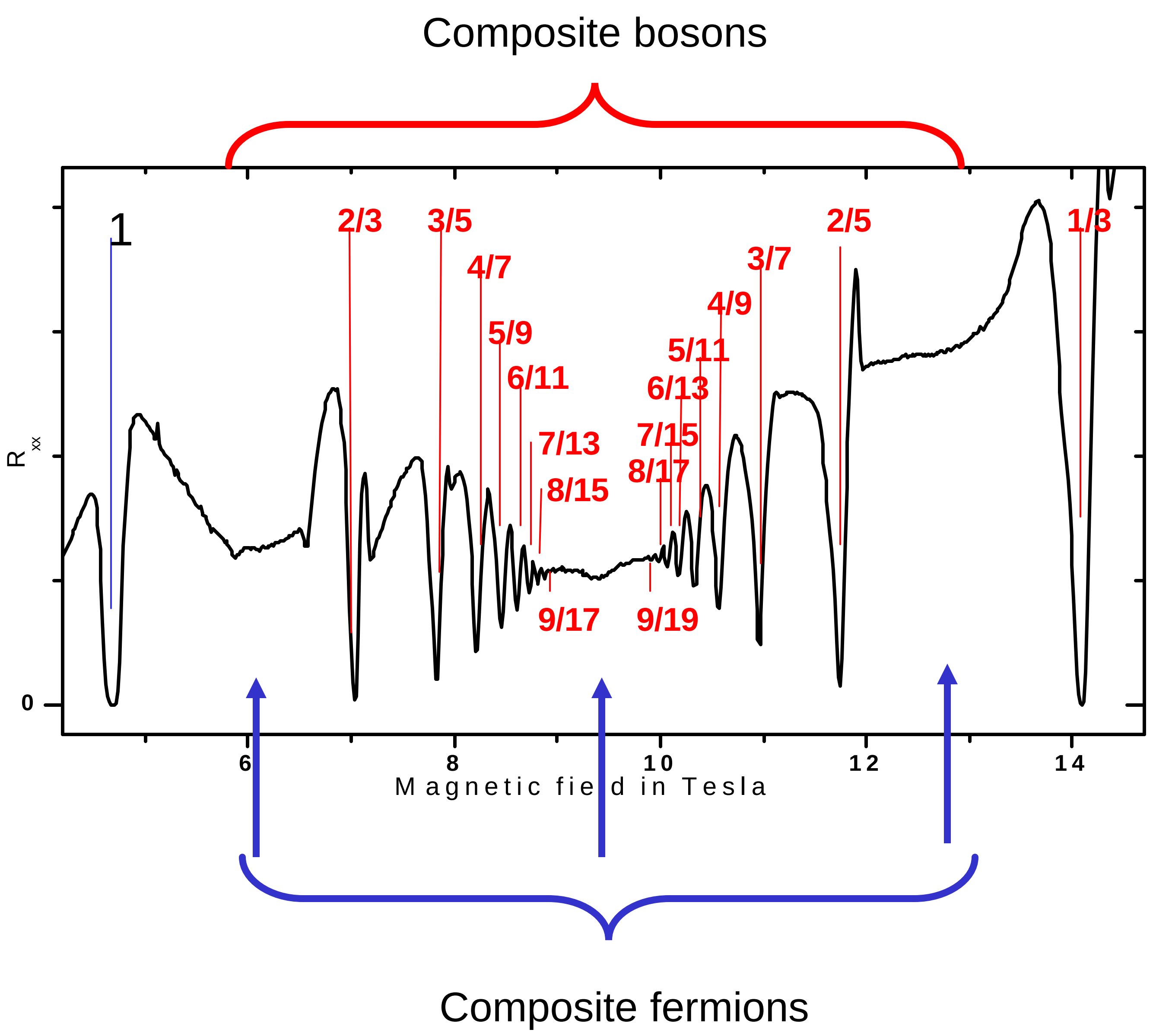

III. Quasiparticle charge and statistics

A. Vortex picture

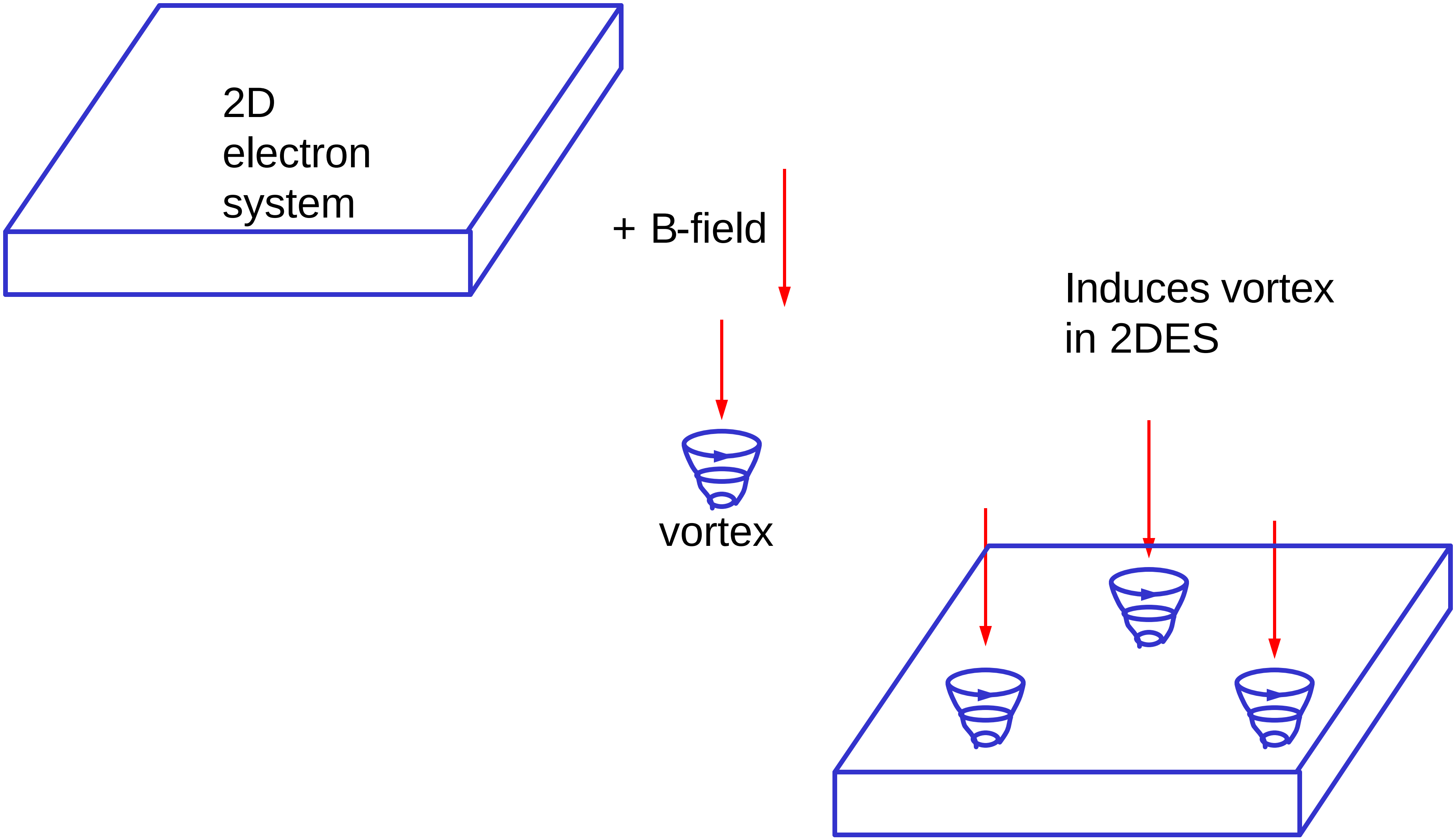

III. Quasiparticle charge and statistics

A. Vortex picture

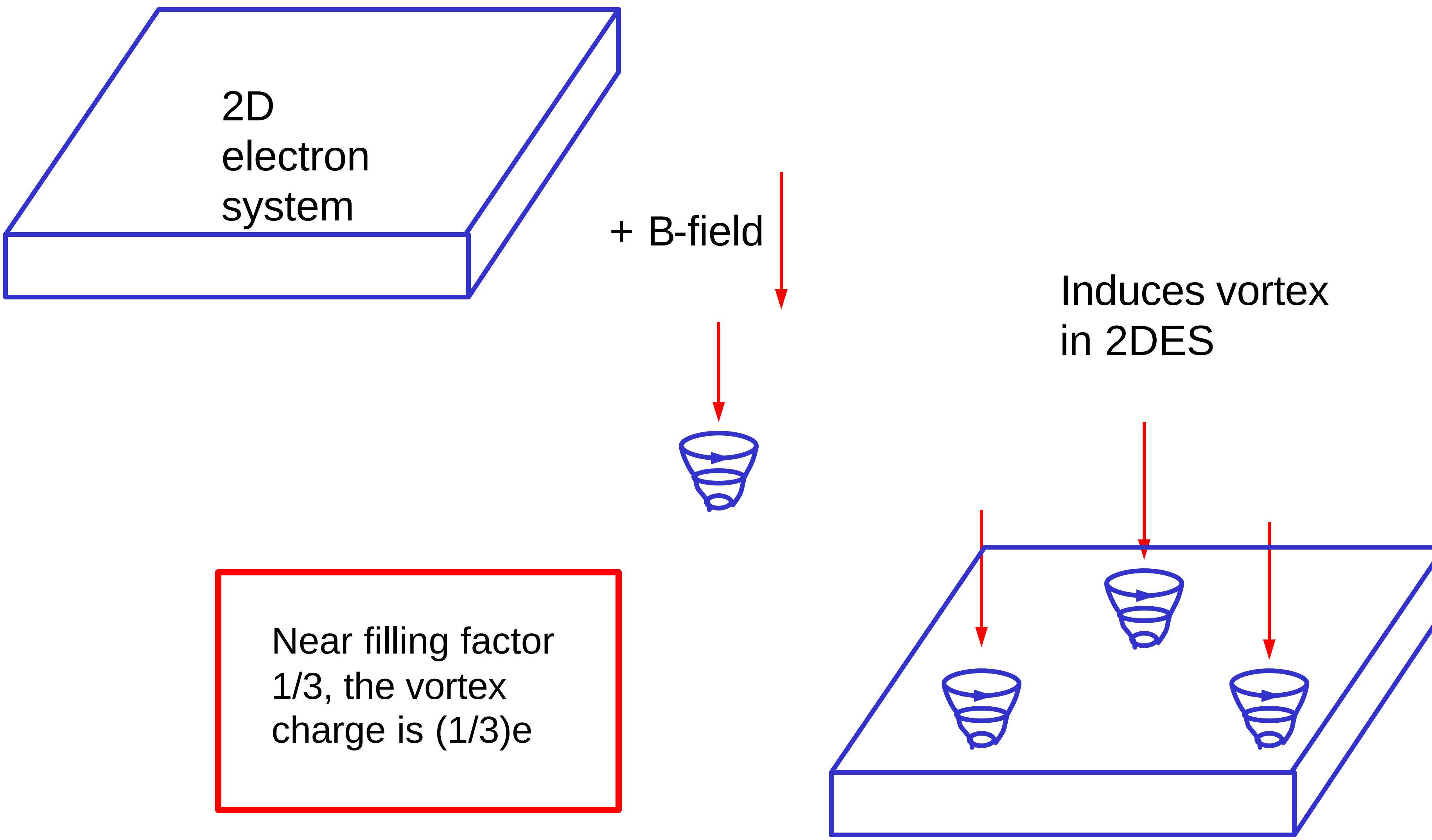

Near filling factor 1/3, the vortex charge is (1/3)e

III. Quasiparticle charge and statistics

A. Vortex picture

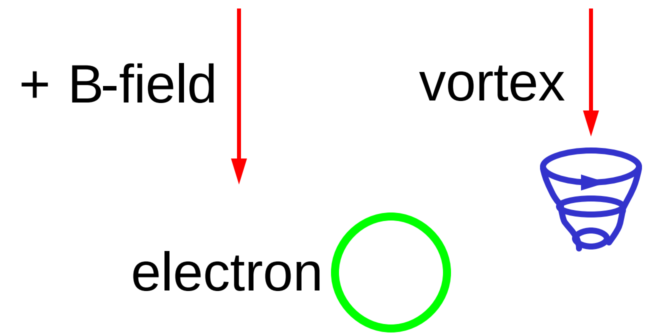

Now consider an electron

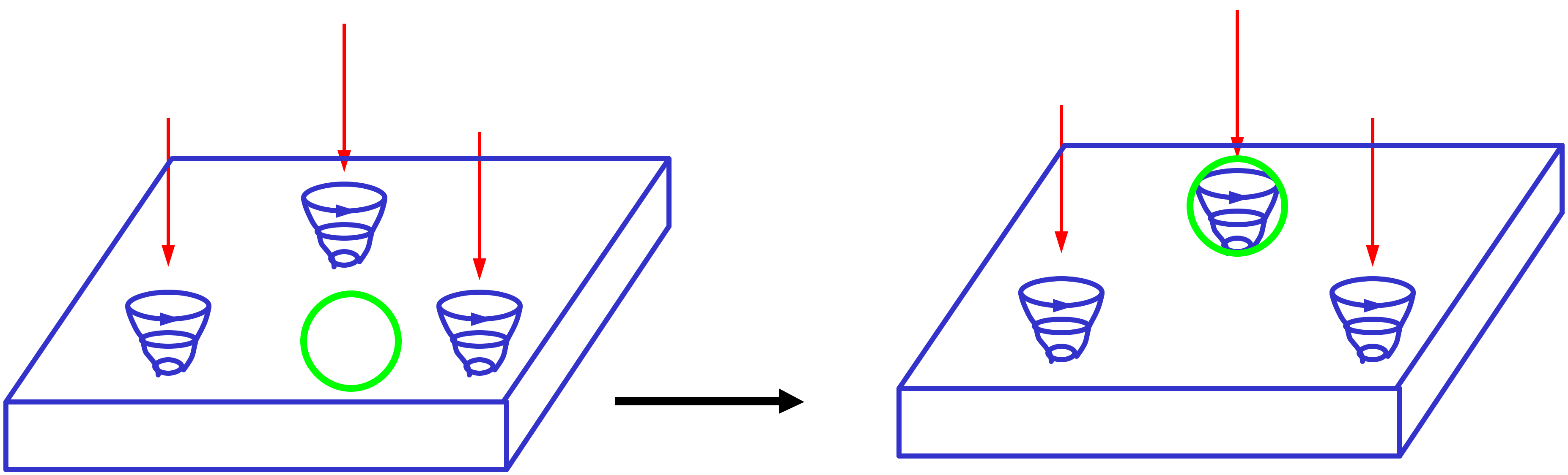

superpose vortex on electron: exclusion principle, + lowers energy

III. Quasiparticle charge and statistics

A. Vortex picture

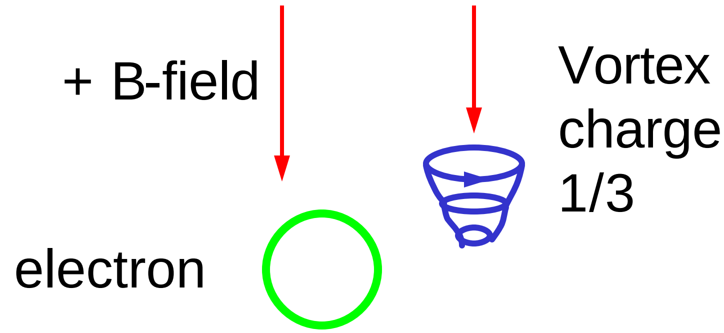

Now consider an electron

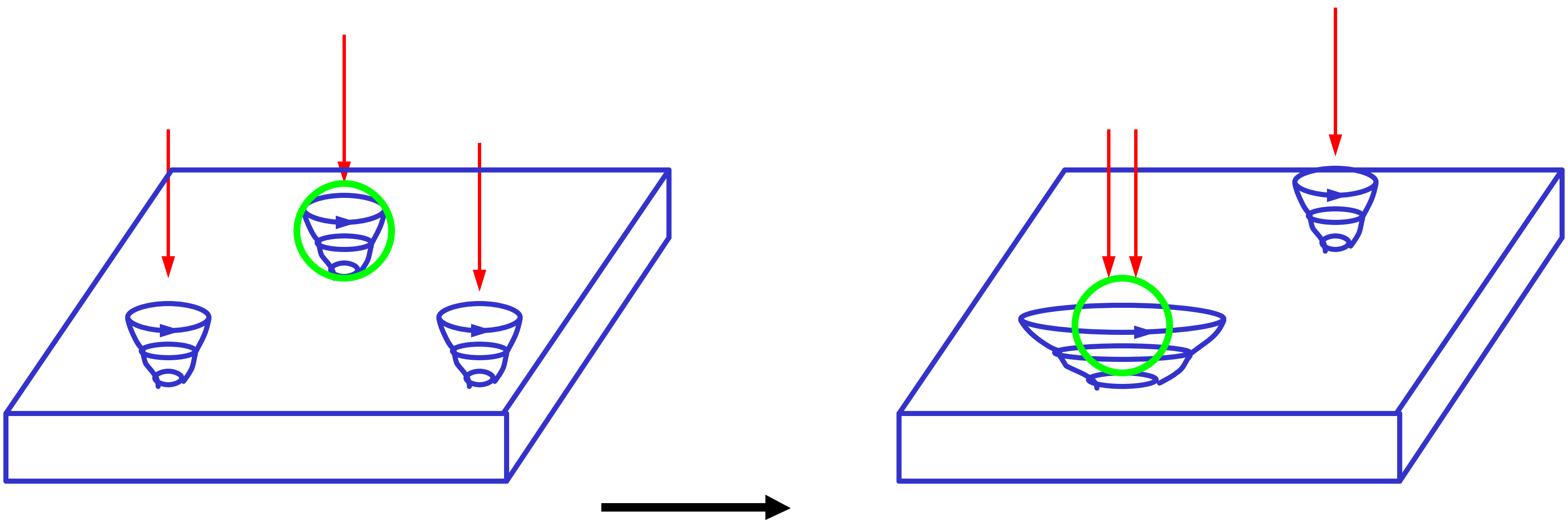

Lowers energy even more to superpose two vortices on electron

III. Quasiparticle charge and statistics

A. Vortex picture

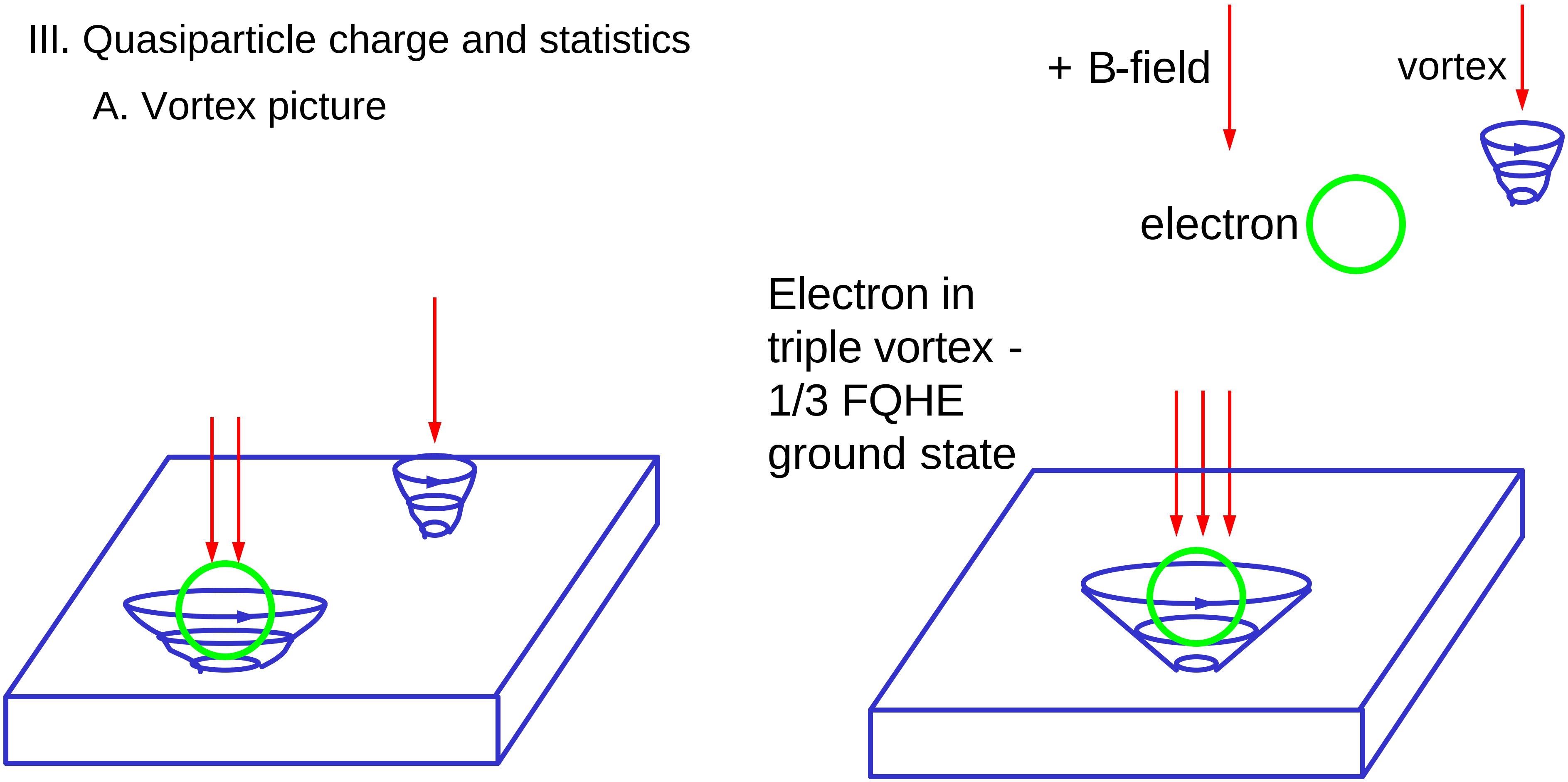

Superpose three vortices to further lower energy

Electron in triple vortex - 1/3 FQHE ground state

Bosonic ground state

III. Quasiparticle charge and statistics

A. Vortex picture

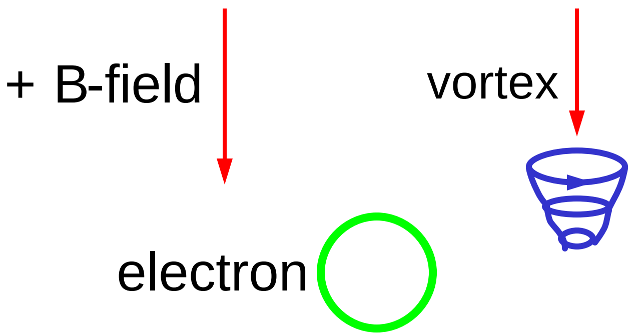

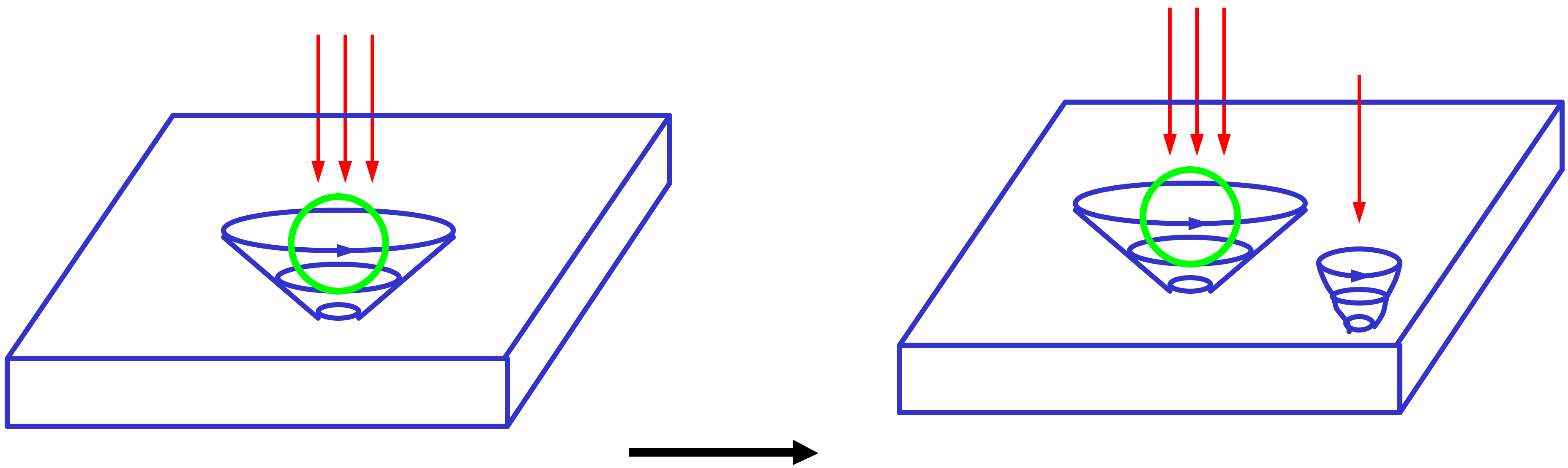

Apply more B-field: get another vortex of +1/3 charge

III. Quasiparticle charge and statistics

A. Vortex picture

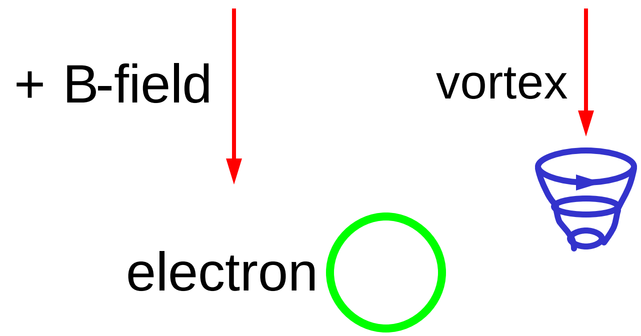

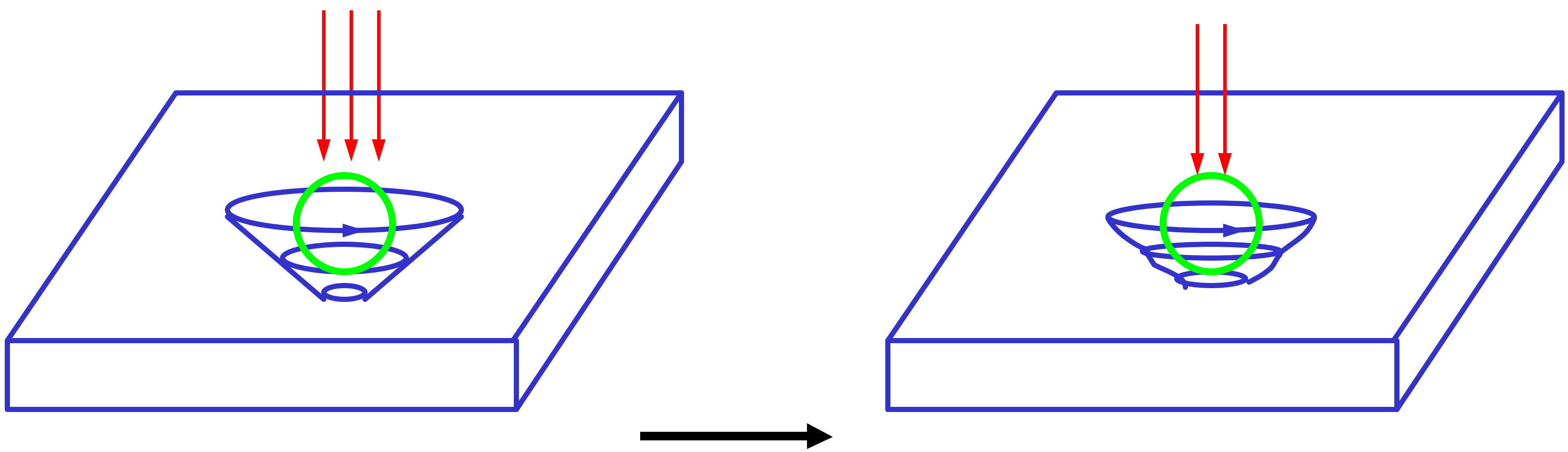

Decrease B-field: form a vortex/electron quasiparticle of -1/3 charge

III. Quasiparticle charge and statistics

A. Vortex picture

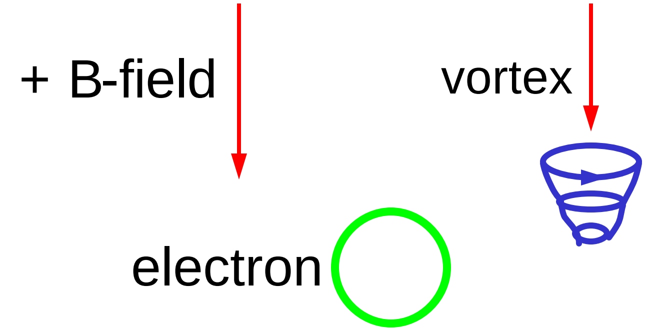

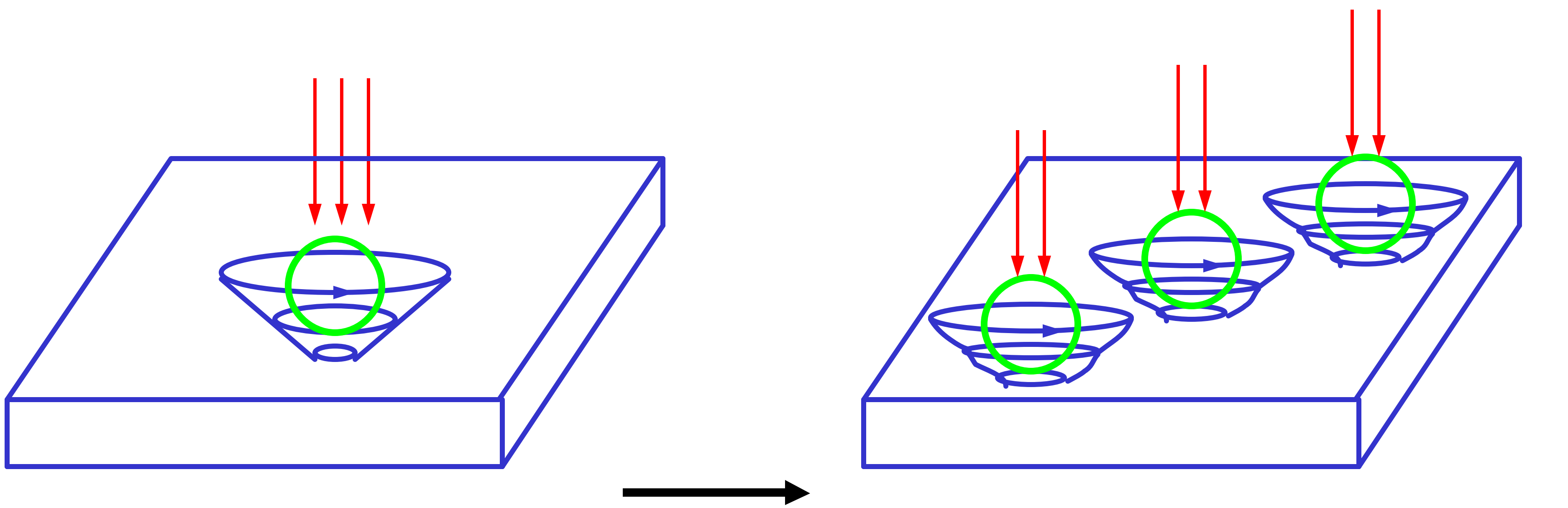

Add an electron: get three quasiparticles of -1/3 charge

Vortex picture

III. Quasiparticle charge and statistics

A. Vortex picture

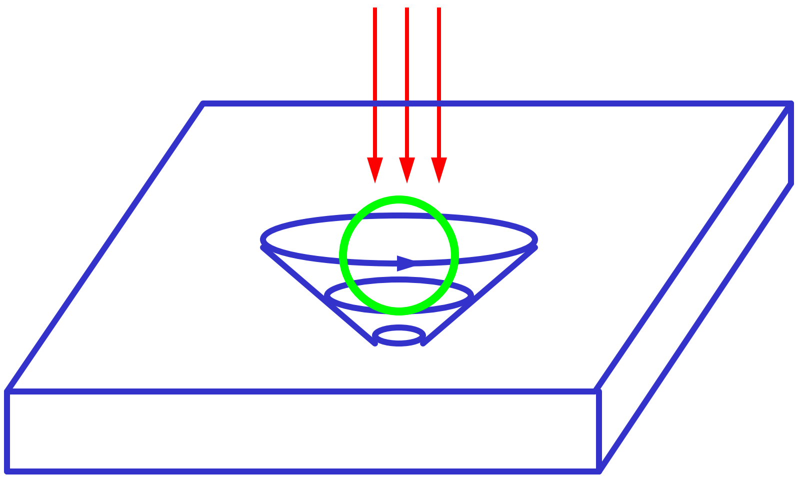

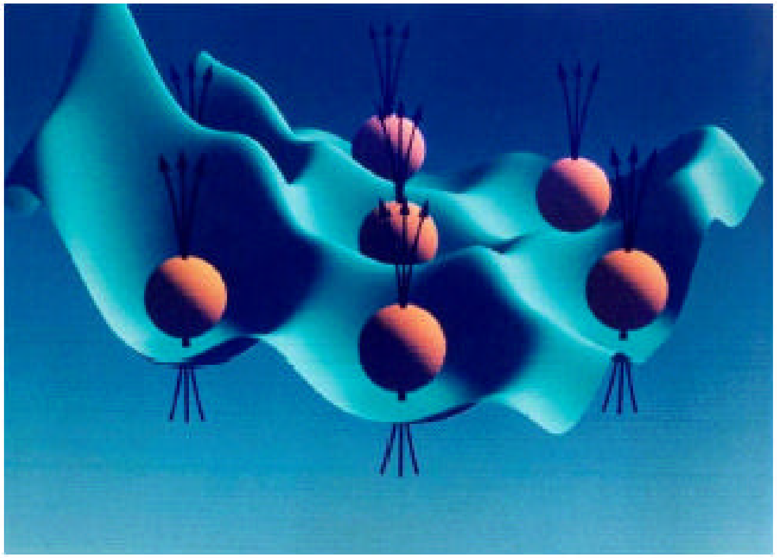

$$\Psi(z_1, z_2, \ldots, z_n) \sim \prod_{i<j} (z_i - z_j)^3$$

III. Quasiparticle charge and statistics

A. Vortex picture

Composite bosons

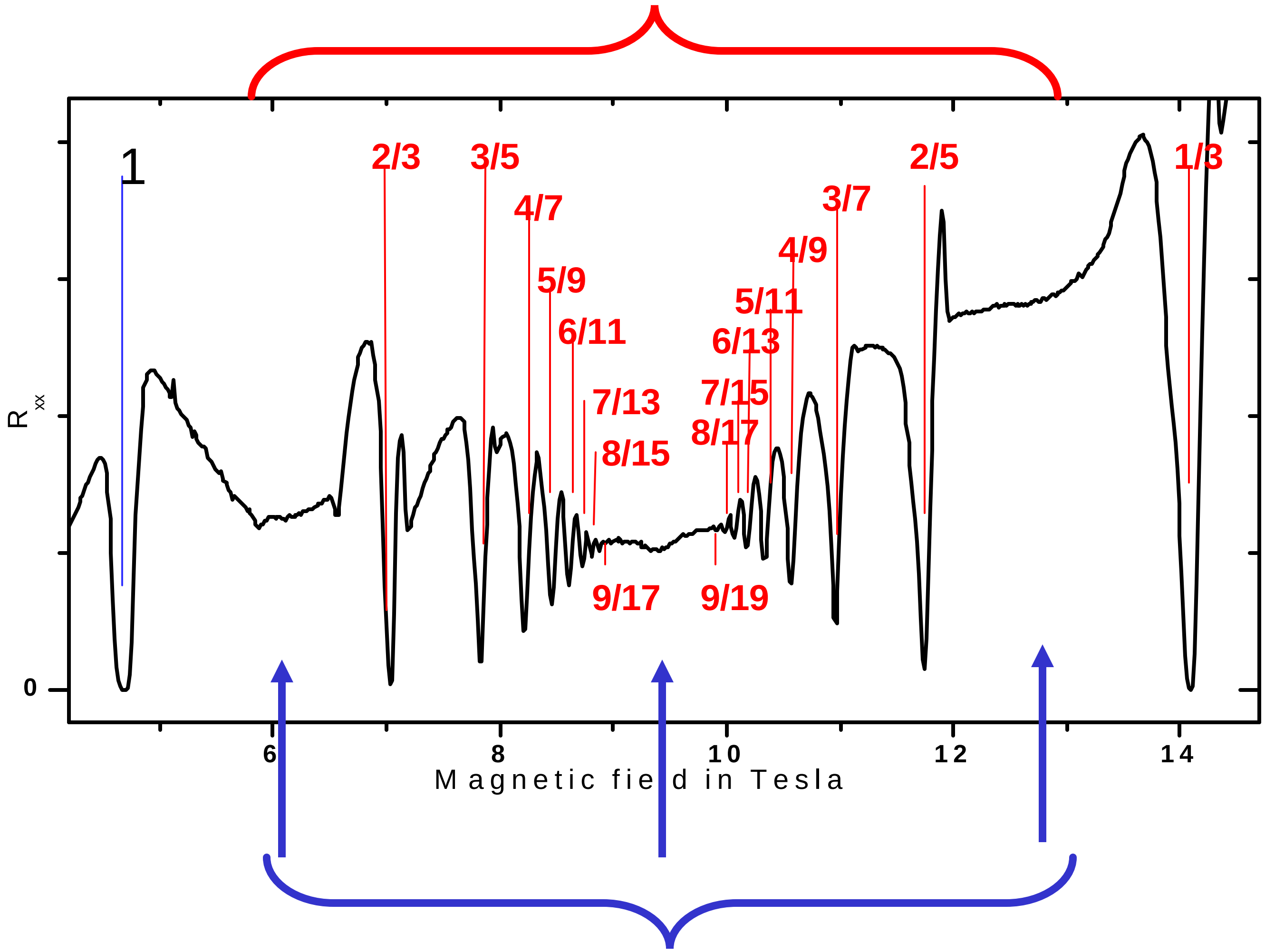

Composite fermions

With a change in B-field quasiparticle population changes

III. Quasiparticle charge and statistics

B. Fractional charge measurement

Fractional charge and the fractional quantum Hall states:

- fractional quantum Hall states are incompressible quantum liquids

- The ground states at odd-denominator filling factors are bose condensates of bosonic quasiparticles or fermionic composite particles in filled Landau levels

- the charge carrying excitations are other quasiparticles

- there is a finite energy required to produce these charge carrying excitations

- this gap energy must be determined by the interaction or Coulomb energy

- the nature of the excitations, or quasiparticles, implies a distinct duality between charge and magnetic field

- **Can this fractional charge be measured?**

III. Quasiparticle charge and statistics

B. Fractional charge measurement

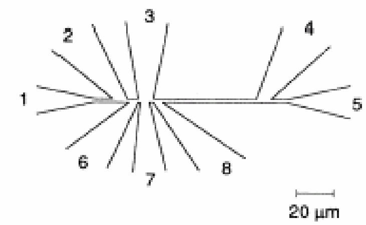

FIG. 1. Sample geometry and probe assignment. The width of the central narrow channel is 2.5 μm.

Three sets of measurements – All point out the difficulties of examining these condensed states and their excitations

a) Narrow channel resistance fluctuations
b) Current around an anti-dot
c) Shot noise from a fractional quantum Hall state

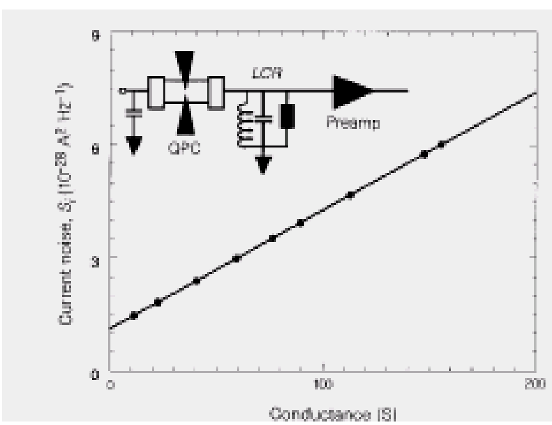

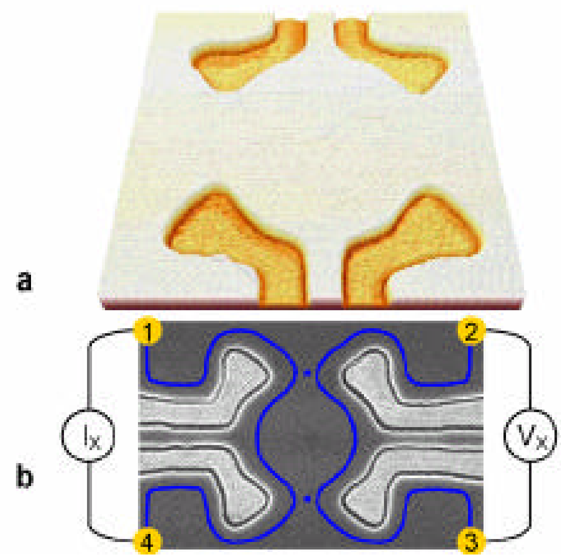

III. Quasiparticle charge and statistics

B. Fractional charge measurement

a) Narrow channel fluctuations

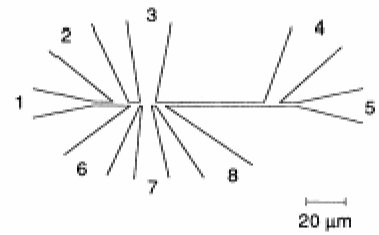

FIG. 1. Sample geometry and probe assignment. The width of the central narrow channel is 2.5 μm.

FQHE in a narrow (2?m wide) channel:
Etched defined channels

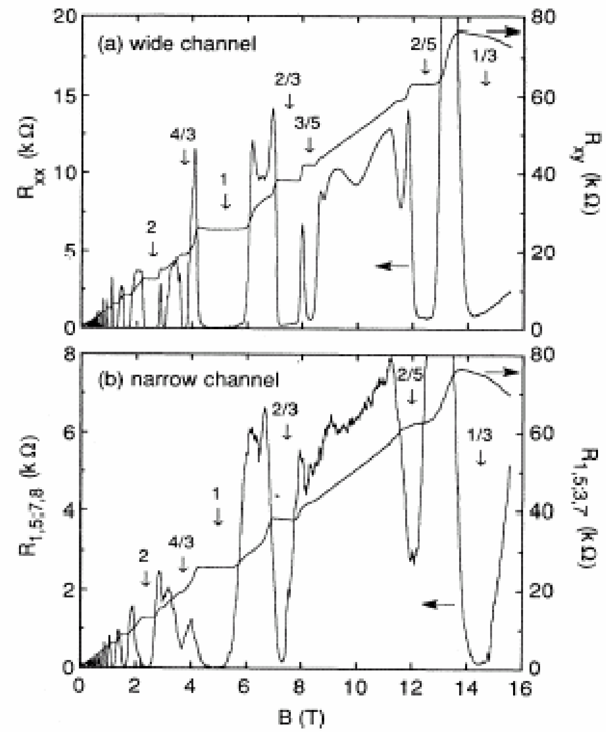

Resistance fluctuations in the integral- and fractional-quantum-Hall-effect regimes

J. A. Simmons,* S. W. Hwang, D. C. Tsui, H. P. Wei, L. W. Engel, and M. Shayegan
Department of Electrical Engineering, Princeton University, Princeton, New Jersey 08544

(Received 22 April 1991)

We report on our measurements of resistance fluctuations as a function of magnetic field B in an $Al_xGa_{1-x}As/GaAs$ heterostructure of etched width $w=2.5$ μm in the integral- and fractional-quantum-Hall-effect regimes. High-frequency fluctuations are observed near the longitudinal resistance (R_{xx}) minima for $\nu=1$, 2, 3, 4, and $\frac{1}{3}$. The quasiperiods $\Delta B(\nu=\text{integer})$ of the fluctuations for integer ν are all ~ 0.016 T, while for $\nu=\frac{1}{3}$, the quasiperiod $\Delta B(\nu=\frac{1}{3})$ is ~ 0.05 T, or a factor of 3 larger. The fluctuations at integer ν are consistent with inter-edge-state tunneling via magnetically bound states encircling a potential hill of a diameter roughly equal to the conducting width of the channel. A similar model, with the difference that the tunneling is by quasiparticles of fractional charge $e^*=e/q$, predicts a scaling of the quasiperiod as $\Delta B(\nu=1/q)=q\,\Delta B(\nu=\text{integer})$. Interpreted in terms of this model, the data provide direct evidence of the existence of quasiparticles of charge $e^*=e/3$ in the $\nu=\frac{1}{3}$ fractional quantum Hall effect. For both $\nu=\frac{1}{3}$ and $\nu=$ integer, the individual fluctuation patterns for different pairs of voltage probes are strongly correlated only if the pairs share a length of the channel, indicating that the source of the fluctuations is local, as predicted by the model. A Coulomb blockade as the origin of the fluctuations is ruled out by the fact that for $\nu=1$ and 2 the fluctuation amplitudes saturate at temperatures $T_c(\nu=1)\simeq 66$ mK and $T_c(\nu=2)\simeq 121$ mK, and also saturate at currents $I_c(\nu=1)\simeq 0.5$ nA and $I_c(\nu=2)\simeq 1.7$–3.0 nA. These results indicate that for integer ν, the bound-state-energy spacing $\Delta\varepsilon(\nu)$ scales as ν or B^{-1}, inconsistent with a Coulomb blockade.

FIG. 2. Longitudinal and Hall resistances at 25 mK, plotted at the same field scale (a) for the 300-μm-wide Hall bar, and (b) for the 2.5-μm-wide Hall bar, measured as $R_{1,5;7,8}$ and $R_{1,5;3,7}$. For the narrow channel the robustness of the fractional and higher integer states is greatly reduced, and resistance fluctuations are present.

PRL '89

III. Quasiparticle charge and statistics

B. Fractional charge measurement

a) Narrow channel fluctuations

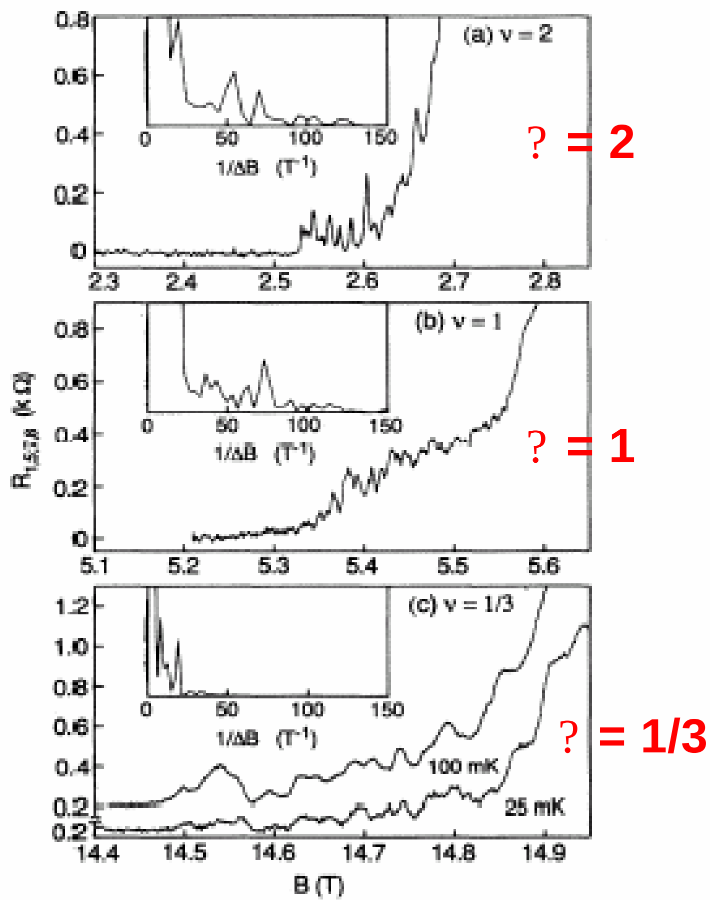

FIG. 4. $R_{1,5;7,8}$ near the high-B sides of R_{xx} minima for (a) $\nu=2$ at 25 mK, (b) $\nu=1$ at 25 mK, and (c) $\nu=\frac{1}{3}$ at 25 and 100 mK, all plotted with the same field scale. Insets: Fourier power spectra of the fluctuation regions for each ν.

Oscillations are observed in longitudinal resistivity near the minima of filling factors ? = 2, 1, and 1/3

III. Quasiparticle charge and statistics

B. Fractional charge measurement

a) Narrow channel fluctuations

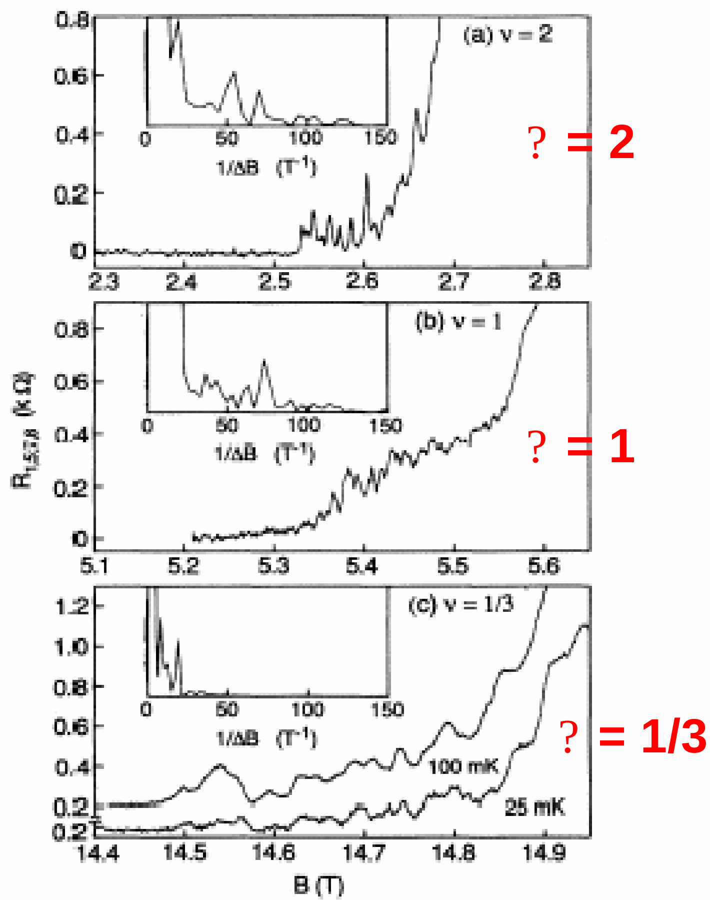

FIG. 4. $R_{1,5;7,8}$ near the high-B sides of R_{xx} minima for (a) $\nu=2$ at 25 mK, (b) $\nu=1$ at 25 mK, and (c) $\nu=\frac{1}{3}$ at 25 and 100 mK, all plotted with the same field scale. Insets: Fourier power spectra of the fluctuation regions for each ν.

Oscillations are observed in longitudinal resistivity near the minima of filling factors ? = 2, 1, and 1/3

Claim is that in certain channel positions impurities exist that can act as tunneling sites for current from one side of the channel to the other

III. Quasiparticle charge and statistics

B. Fractional charge measurement

a) Narrow channel fluctuations

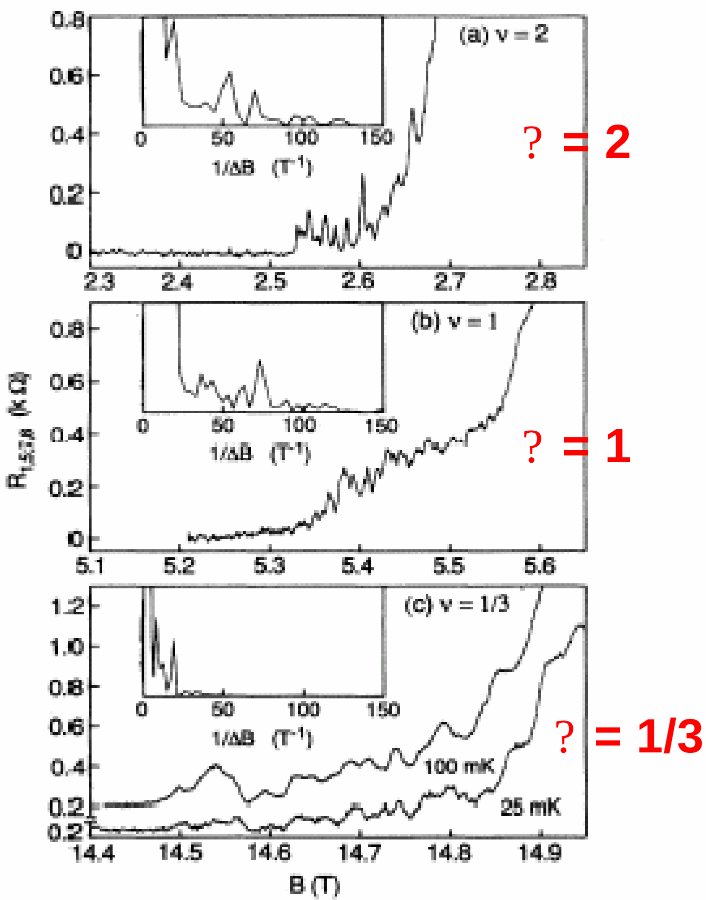

FIG. 4. $R_{1,5;7,8}$ near the high-B sides of R_{xx} minima for (a) $\nu=2$ at 25 mK, (b) $\nu=1$ at 25 mK, and (c) $\nu=\frac{1}{3}$ at 25 and 100 mK, all plotted with the same field scale. Insets: Fourier power spectra of the fluctuation regions for each ν.

Oscillations are observed in longitudinal resistivity near the minima of filling factors ? = 2, 1, and 1/3

Claim is that in certain channel positions impurities exist that can act as tuneling sites for current from one side of the channel to the other

Fluctuations seen in the same channel segment on thermal cycling

III. Quasiparticle charge and statistics

B. Fractional charge measurement

a) Narrow channel fluctuations

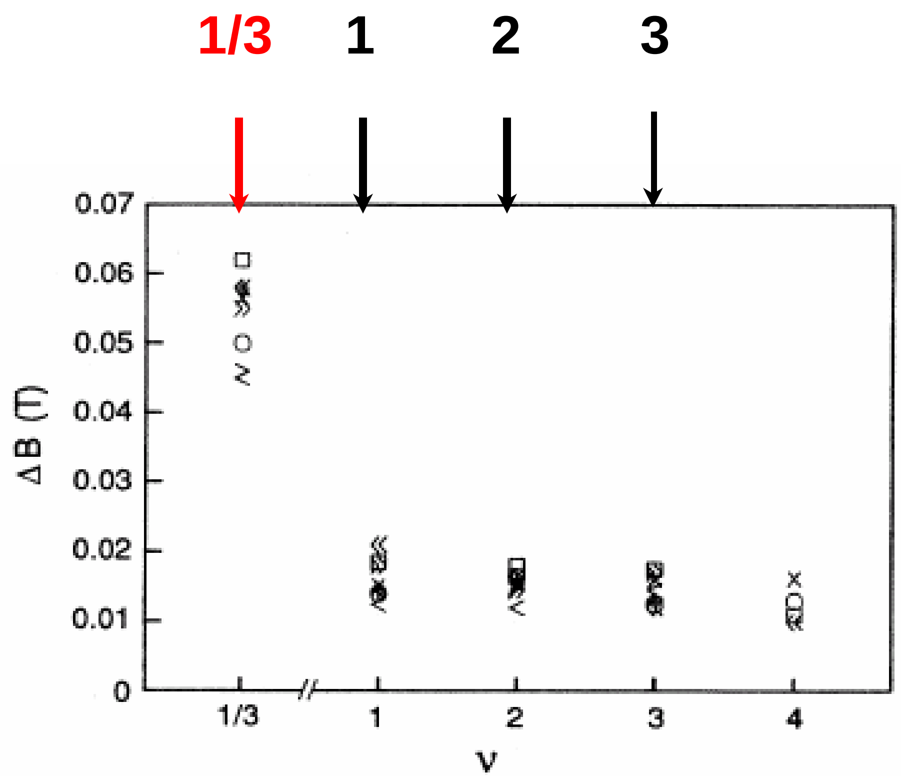

FIG. 5. Data on quasiperiods of resistance fluctuations at 25 mK on the high-B sides of R_{xx} minima for $\nu=1, 2, 3, 4$, and $\frac{1}{3}$: from first T cycle, $R_{1,5;7,8}$ (○); and from the second T cycle, $R_{1,5;7,8}$ (□), $R_{2,5;7,8}$ (>>), $R_{1,5;6,7}$ (×), $R_{2,5;6,7}$ (+), $R_{1,5;3,4}$ (>), $R_{2,5;3,4}$ (<), and $R_{1,5;2,3}$ (<<). Uncertainties are all ~25%. Points for $\nu=\frac{1}{3}$, 1, and 2 represent Fourier power spectra; $\nu=3$ and 4 are estimates by eye.

The oscillation periods are different:

? = 4,3,2, and 1 are one third that of the oscillation period at
? = 1/3

III. Quasiparticle charge and statistics

B. Fractional charge measurement

a) Narrow channel fluctuations

1) Accidental occurrence of scattering site in channel
2) Site can support a magnetically bound state
3) Quasiparticles can tunnel from one edge, traverse the bound state site, and tunnel to other edge
4) Bound-state Bohr-Sommerfeld quantization condition: N flux quanta (h/e) enclosed
5) Transport through the bound state is resonant, with resistance period given by

Mechanism:

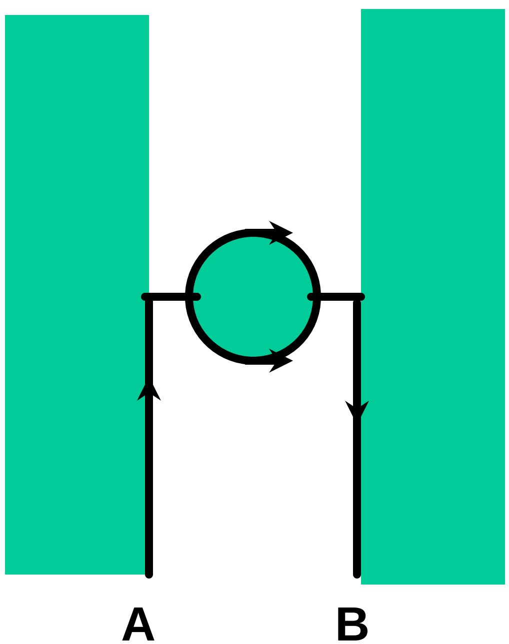

Jain and Kivelson

$$\Delta B = \frac{h}{e}\left(\pi r^2 + \frac{r h^2 n_{2D}}{m^* e E_r(\mu_c)}\right)^{-1}$$

Aharanov-Bohm term

Changing energy of Landau level

Resistance
$R_{xx} = [R/(1-R)]h/e^2$
With R the probability of scattering from one edge to the other

If area of bound site is a, flux quantum is ?, then oscillation period occurs for

(? B/?)a=1 period: ?=h/e*; ? ? e*a/h=1 period
for e*=e, ? B_1, and for e*=e/3, ? B_2,
Then ? B_2=3? B_1

III. Quasiparticle charge and statistics

B. Fractional charge measurement

a) Narrow channel fluctuations

Magnetically bound-state

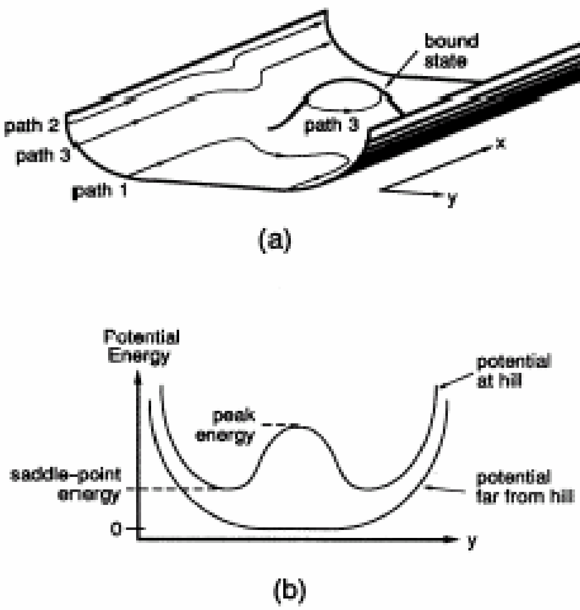

FIG. 10. Geometry treated by Jain and Kivelson, that of a potential hill in the center of a narrow channel. (a) Perspective view of the potential as a function of x and y, showing the three types of edge states formed at three different values of μ. Path (1) corresponds to perfect reflection, path (2) to perfect transmission, and path (3) to the intermediate case, with a magnetically bound state formed around the potential hill. (b) The potential as a function of y, both at the potential hill and far from the potential hill.

Bound states and Fermi level

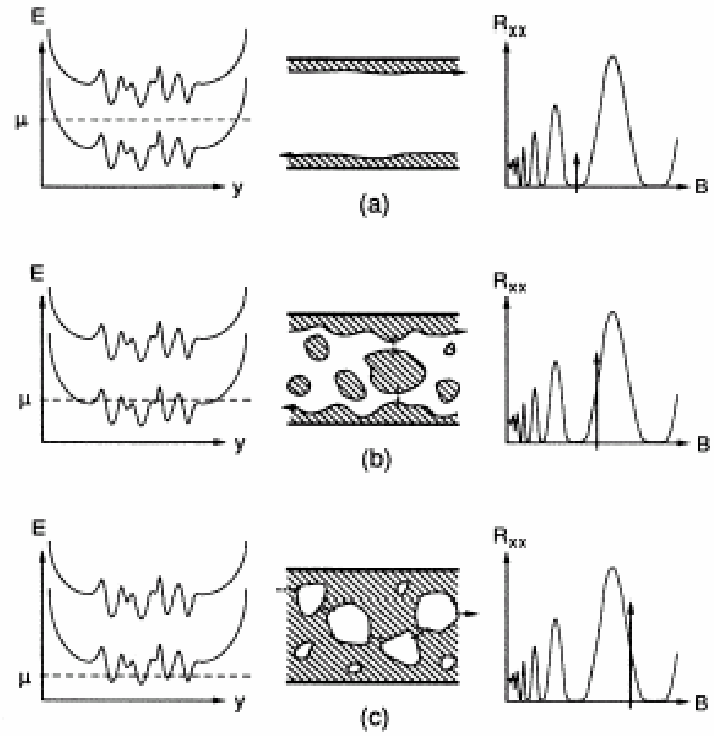

FIG. 11. Illustration of edge state configurations as a function of μ. The left column of figures shows the relative energies of μ and two Landau levels; the center column the corresponding edge state configurations (where shaded regions represent energies above μ and dashed lines represent tunneling paths); and the right column the corresponding values of B. In (a) μ lies well between two Landau levels, corresponding to well-separated edge states and B in an R_{xx} minimum. In (b) μ is lower in energy, corresponding to islands in the Fermi sea and B at the high-B side of an R_{xx} minimum. In (c) μ is lower yet in energy, corresponding to Fermi lakes on insulating land, and B at the low-B side of an R_{xx} minimum. Transport in (c) occurs by tunneling along the length of the channel.

Simmons PRB '91

III. Quasiparticle charge and statistics

B. Fractional charge measurement

a) Narrow channel fluctuations

1) Accidental occurance of scattering site in channel
2) Site can support a magnetically bound state
3) Quasiparticles can tunnel from one edge, traverse the bound state site, and tunnel to other edge
4) Bound-state Bohr-Sommerfeld quantization condition: Nh/e flux quanta enclosed
5) Transport through the bound state is resonant, with resistance period given by

$$\Delta B = \frac{h}{e}\left[\pi r^2 + \frac{r h^2 n_{2D}}{m^* e E_r(\mu_c)}\right]^{-1}$$

Mechanism:

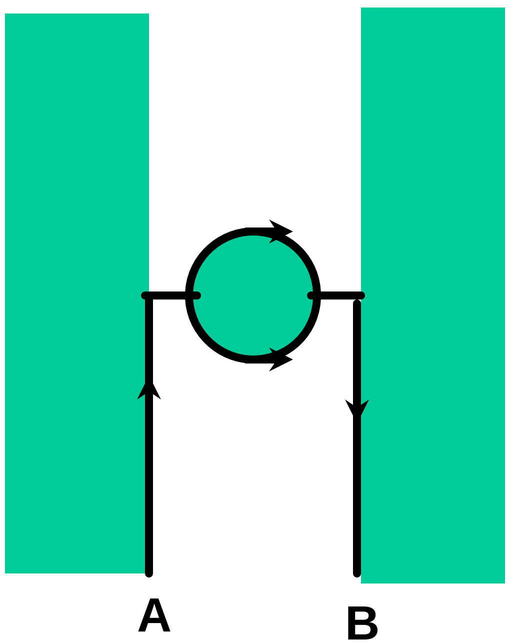

Resistance
$R_{xx} = [R/(1-R)]h/e^2$
With R the probability of scattering from one edge to the other

ALSO, if $E_r = 10^5$ V/m and $\Delta B \simeq 0.016$ T

we obtain $r \simeq 0.4\ \mu\text{m}$

~ right for the channel dimensions

Jain and Kivelson

III. Quasiparticle charge and statistics

B. Fractional charge measuremer

a) Narrow channel fluctuations

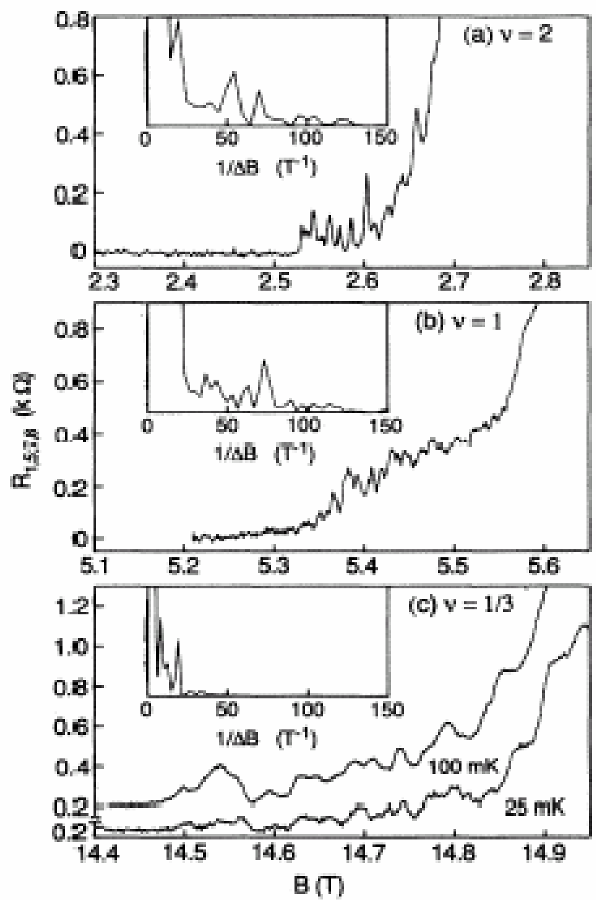

FIG. 4. $R_{1,5;7,8}$ near the high-B sides of R_{xx} minima for (a) $\nu=2$ at 25 mK, (b) $\nu=1$ at 25 mK, and (c) $\nu=\frac{1}{3}$ at 25 and 100 mK, all plotted with the same field scale. Insets: Fourier power spectra of the fluctuation regions for each ν.

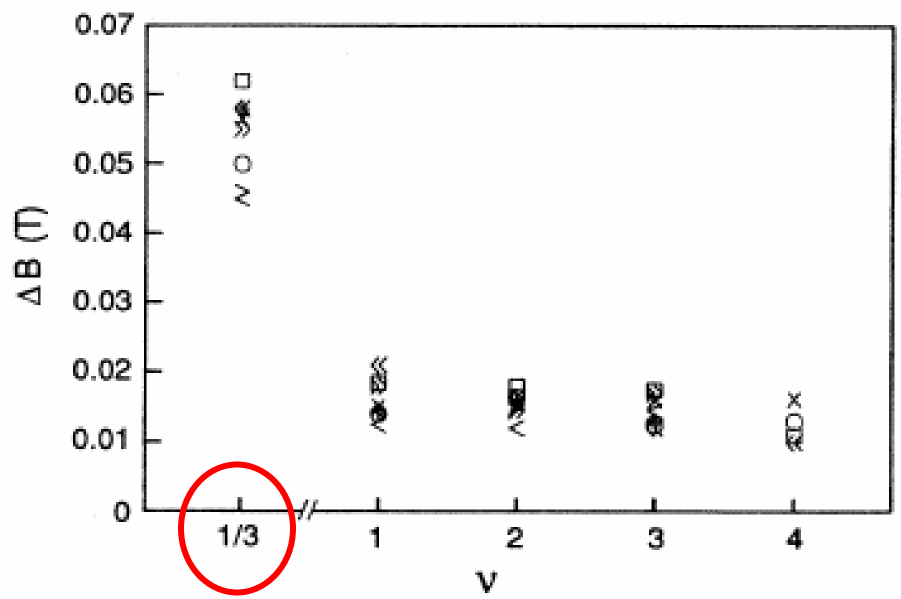

Is this:

a) Tunneling through bound states in channel, which gives charge of quasiparticles, or

b) Claim that Coulomb blockade present, which does not give charge of quasiparticles?

unanswered

III. Quasiparticle charge and statistics

B. Fractional charge measurement

$$\frac{h}{e}=\Delta B\frac{d(B\pi r^2)}{dB}=\Delta B\left[\pi r^2+2\pi rB\left[\frac{\partial r}{\partial \nu}\right]_\mu\frac{d\nu}{dB}\right], \qquad (2)$$

The first term is the usual Aharanov-Bohm term; the second is due to the changing energy of the Landau level. Assuming that μ is constant, $(\partial r/\partial \nu)_\mu=\hbar\omega_c/eE_r(\mu)=-\hbar B/m^*E_r(\mu)$, where $\hbar\omega_c$ is the Landau-level energy spacing and $E_r(\mu)$ is the radial electric field of the potential hill at the bound state. Here

$d\nu/dB$ is just $-(n_{2D}h)/eB^2$. We then have

$$\Delta B=\frac{h}{e}\left[\pi r^2+\frac{rh^2n_{2D}}{m^*eE_r(\mu)}\right]^{-1}.$$

fractional statistics.[36] Lee has recently made two important points with regard to our work. First, he maintains that the existence of quasiparticles of charge $e^*=e/3$ implies that ΔB would remain the same for $\nu=\frac{1}{3}$ as for ν=integer, but that the energy spacing $\Delta\varepsilon(\nu=\frac{1}{3})$ is only $\frac{1}{9}$ that of $\Delta\varepsilon(\nu=1)$. Thus he attributes our observation of $\Delta B(\nu=\frac{1}{3})=3\,\Delta B(\nu=\text{integer})$ to finite-temperature effects. Further experiments, either utilizing a back gate to vary μ, or conducting a more thorough comparison of the temperature dependences of the fluctuations at $\nu=\frac{1}{3}$ and at ν=integer, are needed to adjudicate the issue. Second, Lee suggests that the observed resistance fluctuations may actually be due to the Coulomb blockade effect.[37] In the next section we describe a third series of

III. Quasiparticle charge and statistics

B. Fractional charge measurement

b) Antidot “interferometer”

Given these findings using an “accidental” bound state in the narrow channel,

an artificial bound state or antidot was produced.

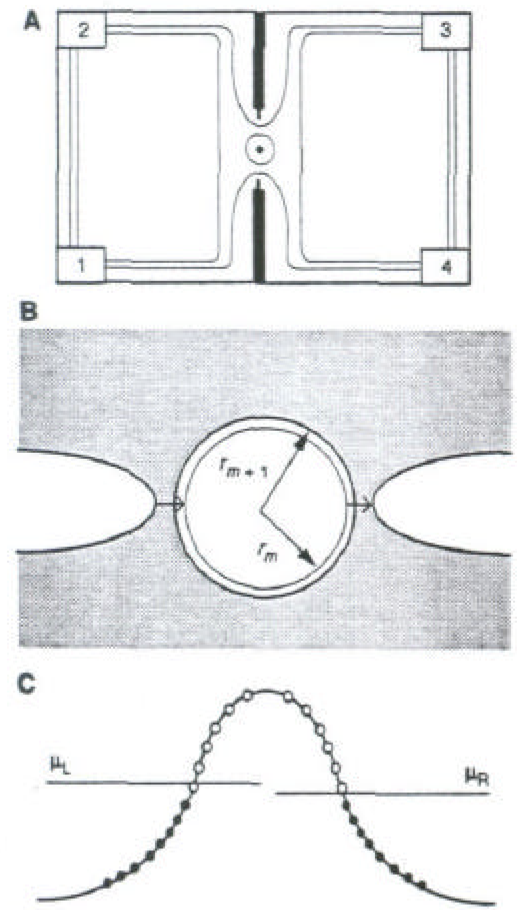

Fig. 1. (**A**) Illustration of the sample; numbered rectangles are ohmic contacts, black areas are front gates in etch trenches, and lines are edge channels. The back gate extends over the entire sample area on the opposite side of the substrate. (**B**) Near the antidot (potential hill), quasi-particle states are quantized: only two are shown: the highest occupied (m + 1)st and the lowest unoccupied mth. The gray area represents QH condensate at ν; the two solid lines are the edge channels around the front gates. (**C**) Potential profile near the antidot. Open circles are unoccupied states, and closed circles are occupied states; subscripts L and R signify left and right.

Goldman Science ‘95

III. Quasiparticle charge and statistics

B. Fractional charge measurement

b) Antidot “interferometer”

mechanism proposed with the antidot

Mechanism:

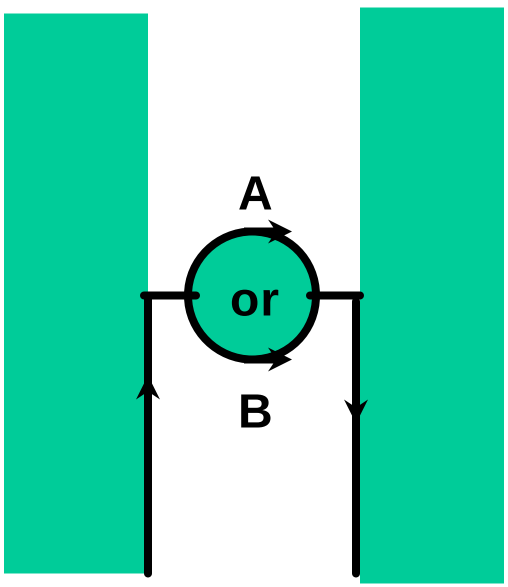

- planned occurance of scattering site in channel
- Quasiparticles can tunnel from one edge, traverse the bound state site, and tunnel to other edge
- Either path A or B can be traversed: interference leads to periodic oscillations

If area of bound site is a, flux quantum is ?,
then oscillation period occurs for

(? B/?)a=1 period: ?=h/e*; ? ? e*a/h=1 period

for e*=e, ? B_1

for e*=e/3, ? B_2,

Then ? B_2=3? B_1

Aharanov-Bohm oscillations produce channel fluctuations

Is a about right for the bound state size?

? B_1 = 0.05T, ? = 4x10^{-3} T-? m^2, then

a ~ 0.3 ? m x 0.3 ? m

III. Quasiparticle charge and statistics

B. Fractional charge measurement

b) Charging an antidot

Oscillations observed and related to quasiparticle interference

If area of bound site is a, flux quantum is ?, then oscillation period occurs for

(?B/?)a=1 period: ?=h/e*; ??e*a/h=1 period

for e*=e, $?B_1$

for e*=e/3, $?B_2$,

Then $?B_2=3?B_1$

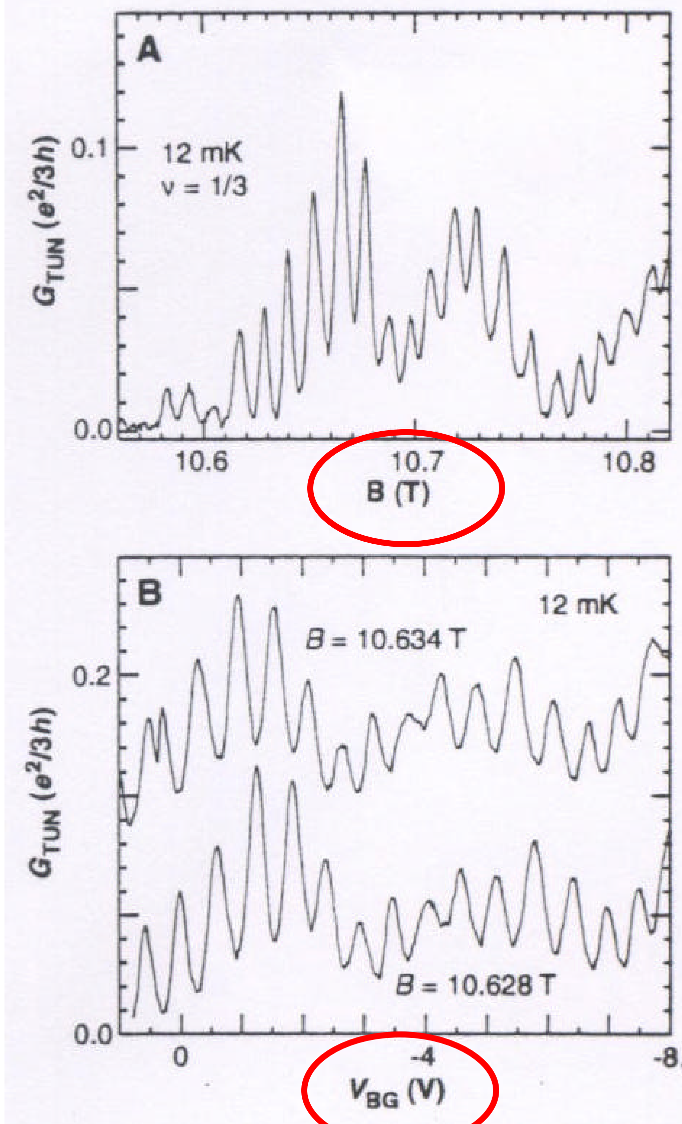

Fig. 4. The RT conductance of quasi-electrons at ν = 1/3 (in the bulk, ν_B = 3/7). (**A**) V_{BG} = 0. (**B**) The upper trace has a conductance minimum at V_{BG} = 0 (offset vertically by 0.08 $e^2/3h$); the lower trace has a conductance maximum at V_{BG} = 0.

III. Quasiparticle charge and statistics

B. Fractional charge measurement

b) Antidot “interferometer”

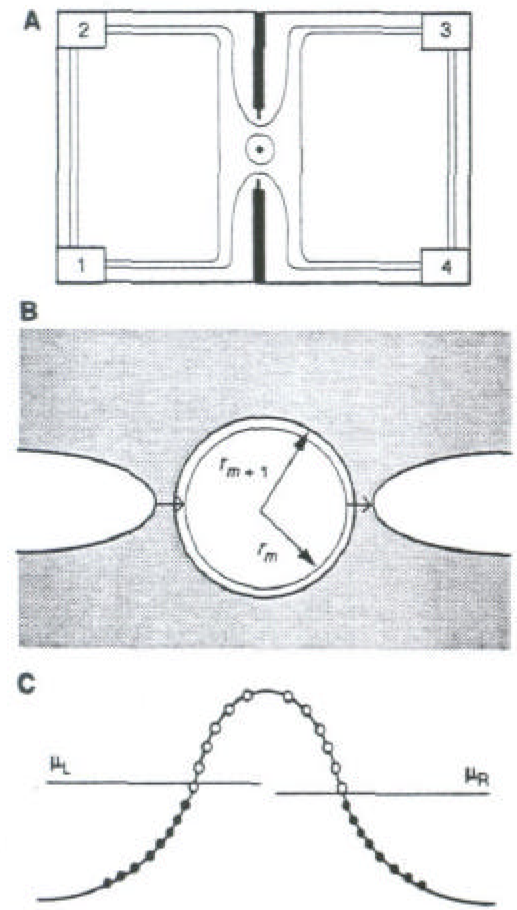

Fig. 1. (**A**) Illustration of the sample; numbered rectangles are ohmic contacts, black areas are front gates in etch trenches, and lines are edge channels. The back gate extends over the entire sample area on the opposite side of the substrate. (**B**) Near the antidot (potential hill), quasi-particle states are quantized: only two are shown: the highest occupied $(m + 1)$st and the lowest unoccupied mth. The gray area represents QH condensate at ν; the two solid lines are the edge channels around the front gates. (**C**) Potential profile near the antidot. Open circles are unoccupied states, and closed circles are occupied states; subscripts L and R signify left and right.

Goldman Science ‘95

Is there another explanation:

Can the tunneling correspond to resonant transport around the antidot so that oscillations exist only due to the overall filling factor?

NOT AN INTERFERENCE EFFECT

III. Quasiparticle charge and statistics

B. Fractional charge measurement

b) “antidot charge interferometer”

Further refinements of this
device have occurred

Direct observation of fractional statistics in two dimensions

Fernando E. Camino, Wei Zhou & Vladimir J. Goldman
Department of Physics, Stony Brook University, Stony Brook, New York 11794-3800, USA

Goldman,
Cond-mat/0502406

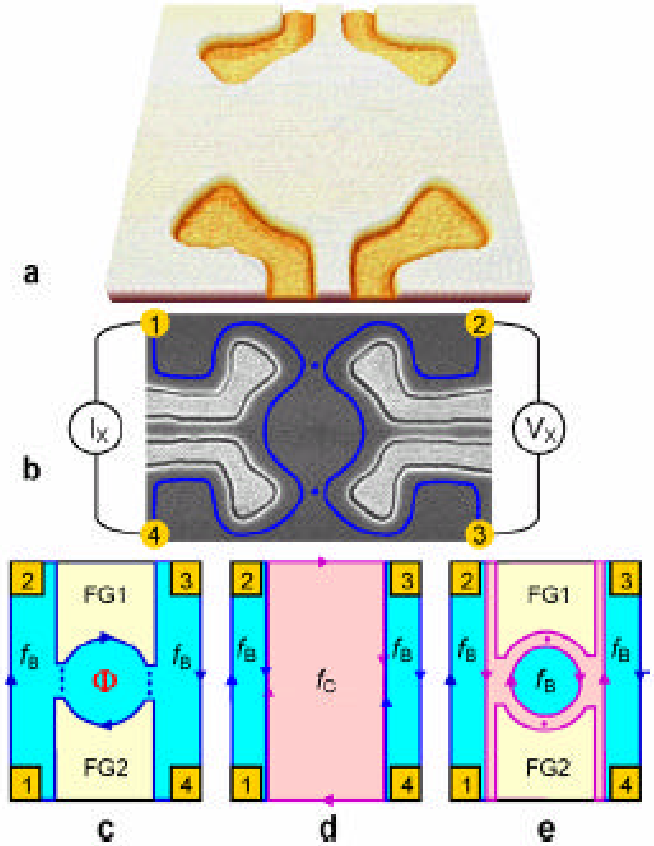

Figure 2 The quasiparticle interferometer samples. **a** and **b** are atomic force and scanning electron micrographs of a typical device. Four Au/Ti front gates (FG) in shallow etch trenches define the central island of 2D electrons of lithographic radius $R \approx 1{,}050$ nm. The front gates are used for fine-tuning the two wide constrictions. The backgate (not shown) extends over the entire sample on the opposite side of the insulating GaAs substrate. **c,** Schematic of the sample when magnetic field is such that there is only one QH filling f throughout the sample: f_C in the constrictions is equal to f_B in the 2D bulk and in the island. The numbered rectangles are Ohmic contacts. The chiral edge channels follow equipotentials at the periphery of the undepleted 2D electrons; tunneling paths are shown by dots. A closed edge channel path gives rise to Aharonov-Bohm oscillations in the conductance. **d,** A sample with two QH fillings exhibits quantized diagonal resistance $R_{XX} = (h/e^2)(1/f_C - 1/f_B)$, where $R_{XX} = V_{2\text{-}3}/I_{1\text{-}4}$. Observation of a quantized plateau in $R_{XX}(B)$ provides definitive values for both f_C and f_B. **e,** Schematic of the sample when magnetic field is such that $f_C < f_B$. The sample exhibits a quantized $R_{XX}(B)$ plateau, and, upon fine tuning of front gates, exhibits Aharonov-Bohm oscillations in conductance as a function of the flux enclosed by the *inner* island edge ring.

III. Quasiparticle charge and statistics

B. Fractional charge measurement

b) "antidot charge interferometer"

Different periods observed for FQHE states and IQHE states

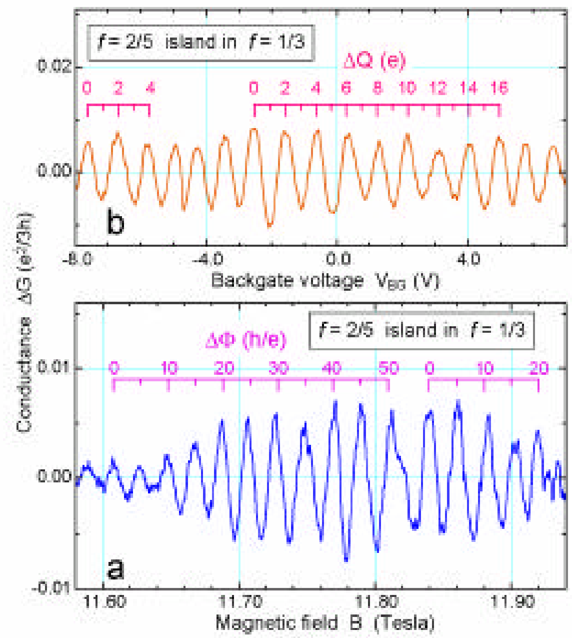

Figure 7 Interference of the inner ring $e/3$ Laughlin quasiparticles circling an island of the $f = 2/5$ FQH fluid. **a**, Magnetic flux through the island period of $\Delta\Phi = 5h/e$ corresponds to creation of ten $e/5$ quasiparticles in the island (one fundamental flux quantum h/e induces two quasiparticles in the $f = 2/5$ FQH fluid). Such "superperiod" of $\Delta\Phi > h/e$ has never been reported before. **b**, The backgate voltage period of $\Delta Q = 10(e/5) = 2e$ directly confirms that the $e/3$ quasiparticle consecutive orbits around the island are quantized by the condition requiring incremental addition of ten $e/5$ quasiparticles of the $f = 2/5$ fluid. These observations imply relative statistics of $\Theta_{2/5}^{1/3} = -1/15$, when a charge $e/3$, statistics $\Theta_{1/3} = 2/3$ quasiparticle encircles one $e/5$, $\Theta_{2/5} = 2/5$ quasiparticle of the $f = 2/5$ fluid.

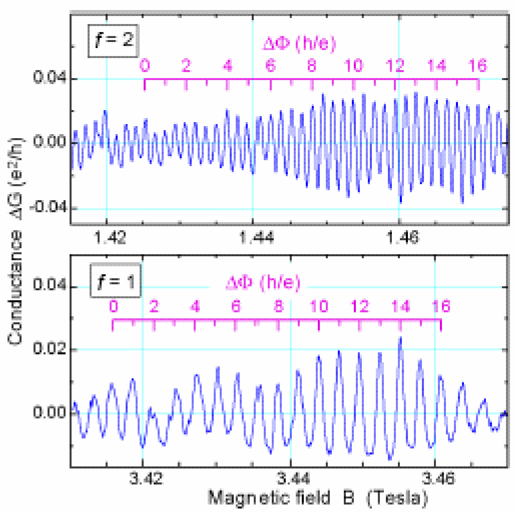

Figure 5 Interference of electrons in the outer ring of the device in the integer quantum Hall regime. Aharonov-Bohm type oscillations in conductance are observed when one ($f = 1$) and two ($f = 2$) Landau levels are filled. The corresponding flux period $\Delta\Phi = h/e$ gives the outer ring radius $r_O \approx 685$ nm.

III. Quasiparticle charge and statistics

B. Fractional charge measurement

b) “antidot charge interferometer”

Again, arguments made that resonant tunneling at **a, b** will be determined by the magnetic field values, density: Periodic oscillations just as observed

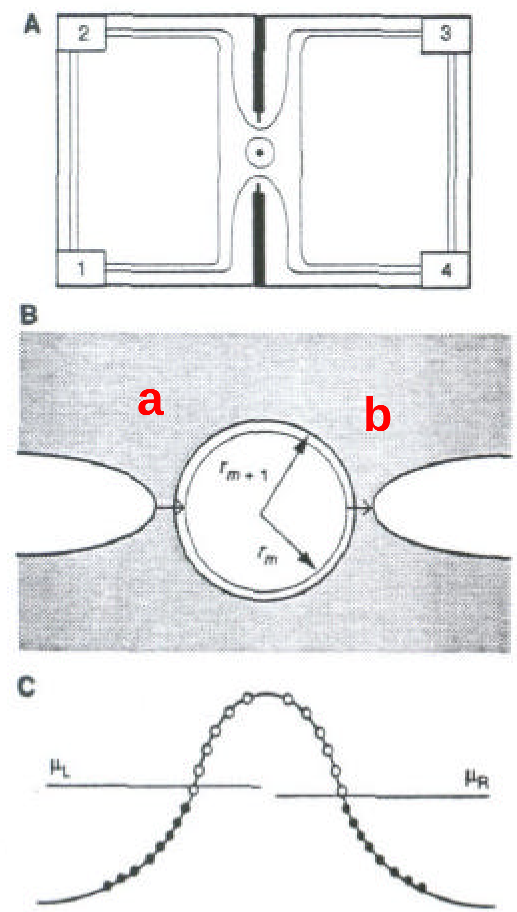

III. Quasiparticle charge and statistics

B) Fractional charge measurement so far:

- ✍ edge state tunneling to a central “defect”, natural or artificial

- ✍ tunneling to and from magnetically bound state exposes charge of quasiparticles?

- ✍ oscillation period ~ charge: period reflects the fractional charge?

- ✍ problem with both techniques:

a) could have charging of the island, which gives non-specific tunneling conductance oscillation period due to larger Hall voltage in 1/3 versus filling factor 1 case (i.e. does not imply fractional charge)

b) Resonant tunneling should give similar results

Not interference experiments?

III. Quasiparticle charge and statistics

C. Noise measurements and fractional charge

Different type of quasiparticle charge measurement

Direct observation of a fractional charge

R. de-Picciotto, M. Reznikov, M. Heiblum, V. Umansky, G. Bunin & D. Mahalu

Braun Center for Submicron Research, Department of Condensed Matter Physics, Weizmann Institute of Science, Rehovot 76100, Israel

Quantum shot noise results from the discreteness of the current-carrying charges and so is proportional to both the charge of the quasiparticles and the average current. Our measurements of quantum shot noise show unambiguously that current in a two-dimensional electron gas in the FQH regime is carried by fractional charges—*e*/3 in the present case—in agreement with Laughlin's prediction.

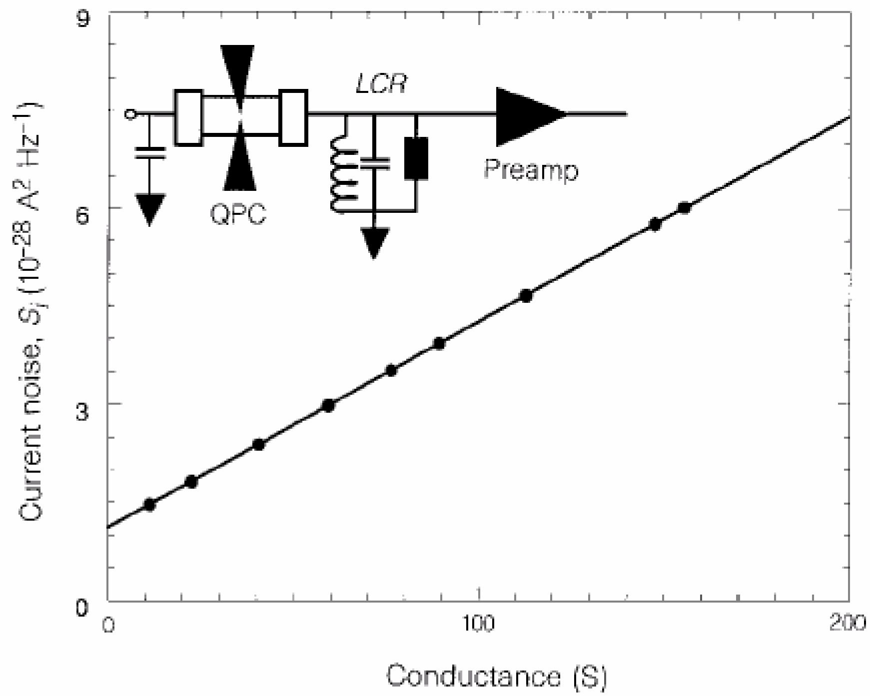

Figure 1 The total current noise inferred to the input of the preamplifier as a function of the input conductance at equilibrium (circles). The measured noise is a sum of thermal noise, $4K_BTG$ (leading to a straight line) and the constant noise of the amplifier. This measurement allows the determination of both the temperature of the 2DEG as 57mK and the amplifier's current noise as $S_i(G = 0) = 1.1 \times 10^{-28}\,\mathrm{A^2\,H_3^{-1}}$. Inset, the QPC embedded in the two-dimensional electron gas is shown to be connected to an *LCR* circuit at the input of a cryogenic preamplifier.

Nature '97

III. Quasiparticle charge and statistics

C. Noise measurements

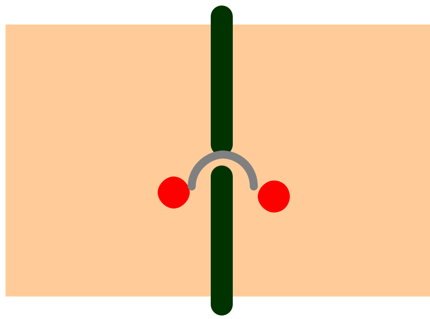

Compared to previous experiments less perturbation to 2D gas

Fractional quantum Hall liquids

Temporal Correlation of Electrons: Suppression of Shot Noise in a Ballistic Quantum Point Contact

M. Reznikov, M. Heiblum, Hadas Shtrikman, and D. Mahalu

Braun Center for Submicron Research, Department of Condensed Matter Physics, Weizmann Institute of Science, Rehovot 76100, Israel

(Received 13 February 1995)

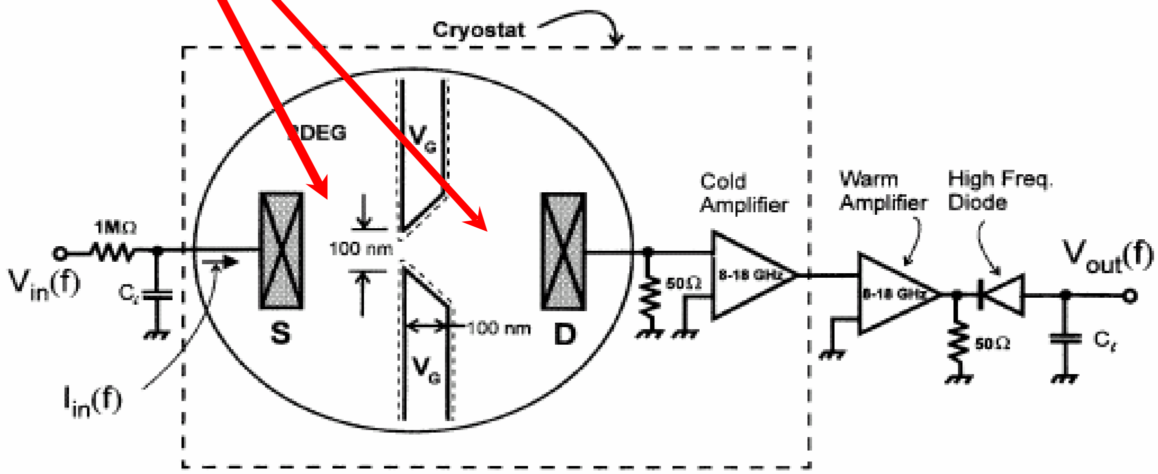

FIG. 1. The experimental setup. The voltage controls the number of 1D conducting channels in the QPC. The current, modulated at low frequency f, is provided to the QPC via a variable current source, with a voltage $V_{DS}(f)$ appearing across the QPC. A high frequency path to ground is provided via capacitor C_i. The current and its high frequency fluctuations are fed into a low noise cooled amplifier with a power gain of 10^3 in the band 8–18 GHz. Another "warm amplifier" follows—terminated by a high frequency diode and load capacitor C_l, providing the low frequency output $V_{\rm out}(f) \propto \langle(\Delta i)^2\rangle_{10\,\rm GHz}$.

III. Quasiparticle charge and statistics

C. Noise measurements

Direct observation of a fractional charge

R. de-Picciotto, M. Reznikov, M. Heiblum, V. Umansky, G. Bunin & D. Mahalu

Braun Center for Submicron Research, Department of Condensed Matter Physics, Weizmann Institute of Science, Rehovot 76100, Israel

Quantum shot noise results from the discreteness of the current-carrying charges and so is proportional to both the charge of the quasiparticles and the average current. Our measurements of quantum shot noise show unambiguously that current in a two-dimensional electron gas in the FQH regime is carried by fractional charges—$e/3$ in the present case—in agreement with Laughlin's prediction.

Measured quantum shot noise as a function of current through QPC: transmission ~ .8

subsequent theoretical works[13–15] predicted that quantum shot noise, S_i, generated by weak backscattering of the current, at fractional filling factors $\nu = 1/q$ and at zero temperature, should be proportional to the quasiparticle's charge $Q = e/q$ and to the back-scattered current I_B:

$$S_i = 2QI_B \qquad (1)$$

$$S_i = 2g_0 t(1-t)\left[QV\coth\left(\frac{QV}{2k_B T}\right) - 2k_B T\right] + 4k_B T g_0 t$$

S~ (e/q) I_B

and finite temperature corrections

III. Quasiparticle charge and statistics

C. Noise measurements

Quantum shot noise as expected for no B-field, 1/3 FQHE state

No B -field

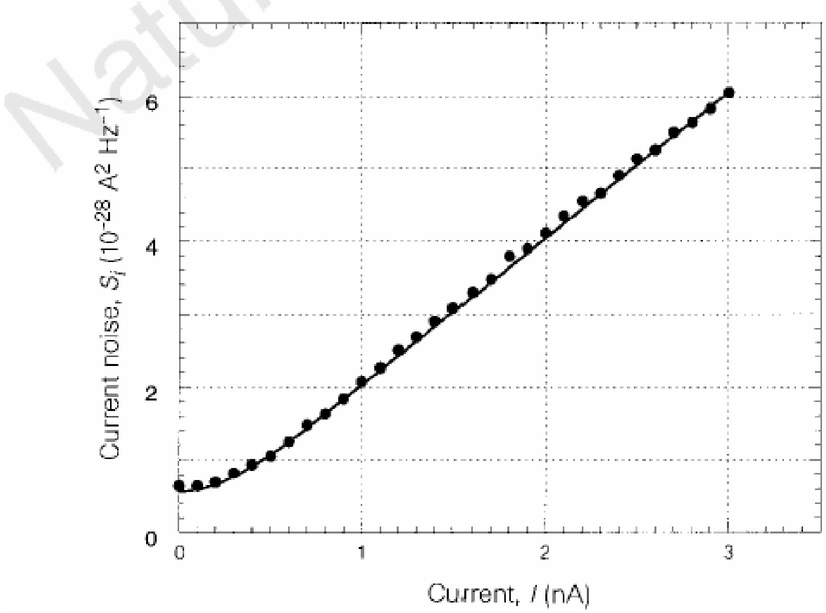

Figure 2 Quantum shot noise as a function of direct current, I, through the QPC without an applied magnetic field (circles). The solid line is equation (2) with the temperature (57 mK) deduced from Fig. 1. The transmission, t, is 0.37.

??= 1/3

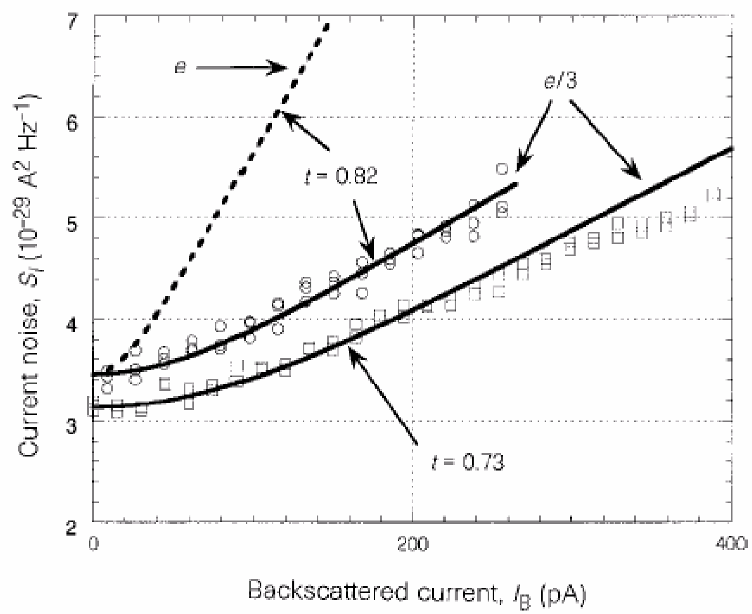

Figure 3 Quantum shot noise as a function of the backscattered current, I_B, in the FQH regime at $\nu = \frac{1}{3}$ for two different transmission coefficients through the QPC (circles and squares). The solid lines correspond to equation (2) with a charge $Q = e/3$ and the appropriate t. For comparison the expected behaviour of the noise for $Q = e$ and $t = 0.82$ is shown by the broken line.

III. Quasiparticle charge and statistics

C. Noise measurements

??**= 2/5:** expected that charge is e/5

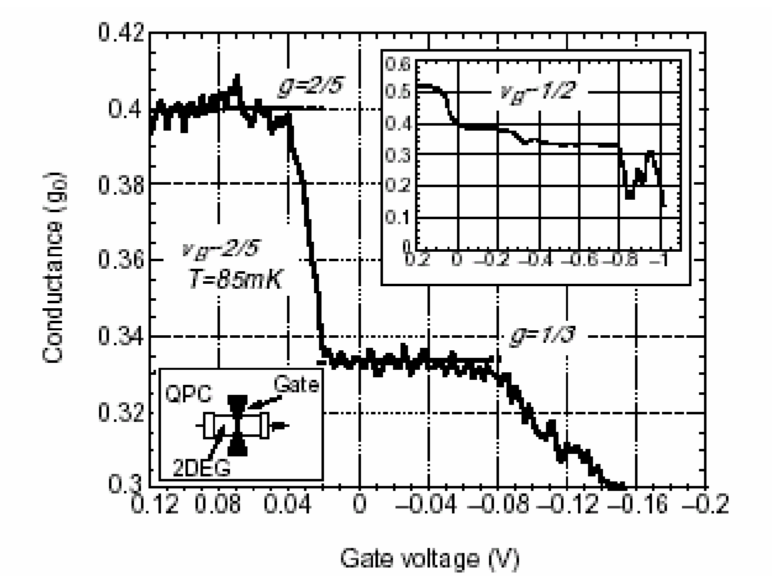

Observation of quasiparticles with one-fifth of an electron's charge

M. Reznikov*†, R. de Picciotto*†, T. G. Griffiths*, M. Heiblum* & V. Umansky*

* Braun Center for Submicron Research, Department of Condensed Matter Physics, Weizmann Institute of Science, Rehovot 76100, Israel

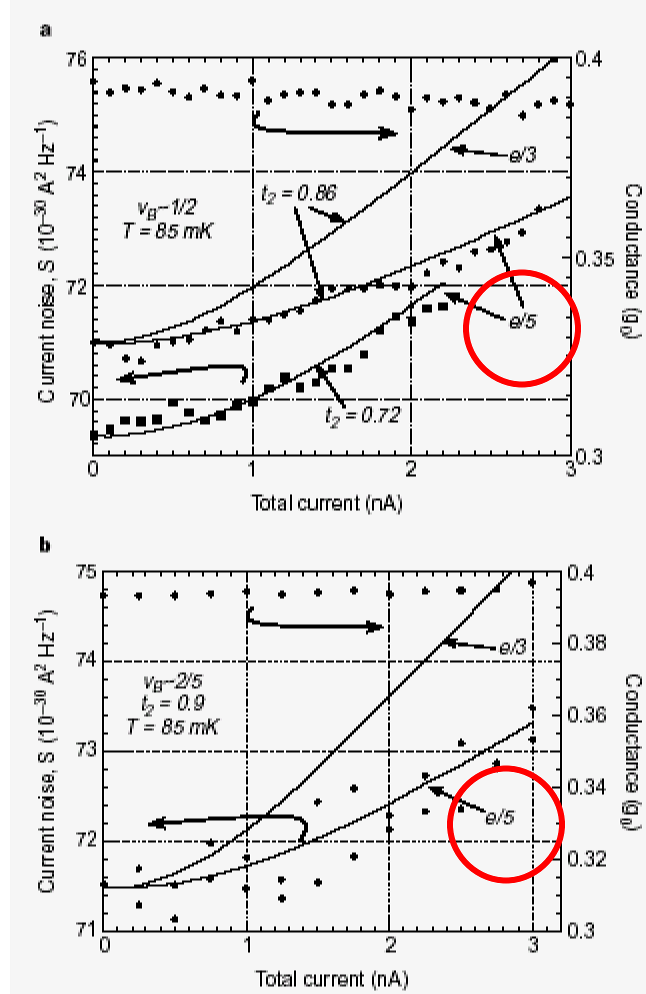

Figure 3 Measured noise of quasiparticles in the second composite fermion (CF) channel. The first CF channel (the '1/3' channel) is fully transmitted and does not produce noise (as seen Fig. 2 inset). **a**, Spectral density of current fluctuations against the total average current for transmission $t_2 = 0.86$ and $t_2 = 0.72$ at bulk filling factor $\nu_B = 1/2$ (filled circles, left-hand vertical axis). Solid lines are given by equation (2) assuming a charge $q = e/3$ and $q = e/5$ and $T = 85$ mK – as indicated. The sample's differential conductance, for transmission $t_2 = 0.86$ is also shown (filled diamonds, right-hand vertical axis). Note that the differential conductance, and hence the deduced transmission, are rather constant over the full range of the measurement. **b**, Similar noise and conductance data for $t_2 = 0.9$ and bulk filling factor $\nu_B = 2/5$. We note that there are no fitting parameters in the theoretical curves, as the transmission coefficient t_2 and the temperature of the electrons T are both measured independently[4,9].

III. Quasiparticle charge and statistics

C. Noise measurements

✍noise power appears to support fractional charge at 1/3 state

✍Also true at 2/5

✍details of densities at QPC open issue: **shot noise measurements have the advantage that a minimal perturbation to the 2D system is imposed**

How can one test the statistics of a system?

III. Quasiparticle charge and statistics

D. Statistical tests

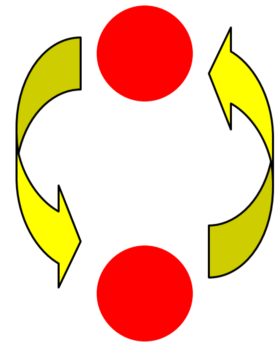

Electron phase change ?

Is it possible to experimentally test the statistics of a quasiparticle system?

Presently under consideration are two avenues

1) Mach-Zehnder **interferometry**

2) Hanbury Brown Twiss

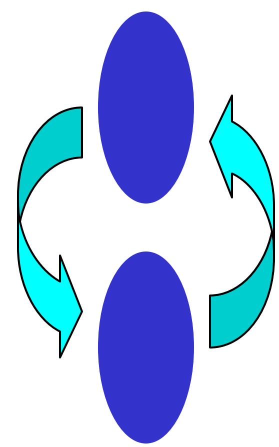

Quasiparticle phase change ???

III. Quasiparticle charge and statistics

D. Statistical tests

More controlled interference experiment

An electronic Mach–Zehnder interferometer

Yang Ji, Yunchul Chung, D. Sprinzak, M. Heiblum, D. Mahalu & Hadas Shtrikman

Braun Center for Submicron Research, Department of Condensed Matter Physics, Weizmann Institute of Science, Rehovot 76100, Israel

Double-slit electron interferometers fabricated in high mobility two-dimensional electron gases are powerful tools for studying coherent wave-like phenomena in mesoscopic systems[1–6]. However, they suffer from low visibility of the interference patterns due to the many channels present in each slit, and from poor sensitivity to small currents due to their open geometry[3–5,7]. Moreover, these interferometers do not function in high magnetic fields—such as those required to enter the quantum Hall effect regime[8]—as the field destroys the symmetry between left and right slits. Here we report the fabrication and operation of a single-channel, two-path electron interferometer that functions in a high magnetic field. This device is the first electronic analogue of the optical Mach–Zehnder interferometer[9], and opens the way to measuring interference of quasiparticles with fractional charges. On the basis of measurements of single edge state and closed geometry transport in the quantum Hall effect regime, we find that the interferometer is highly sensitive and exhibits very high visibility (62%). However, the interference pattern decays precipitously with increasing electron temperature or energy. Although the origin of this dephasing is unclear, we show, via shot-noise measurements, that it is not a decoherence process that results from inelastic scattering events.

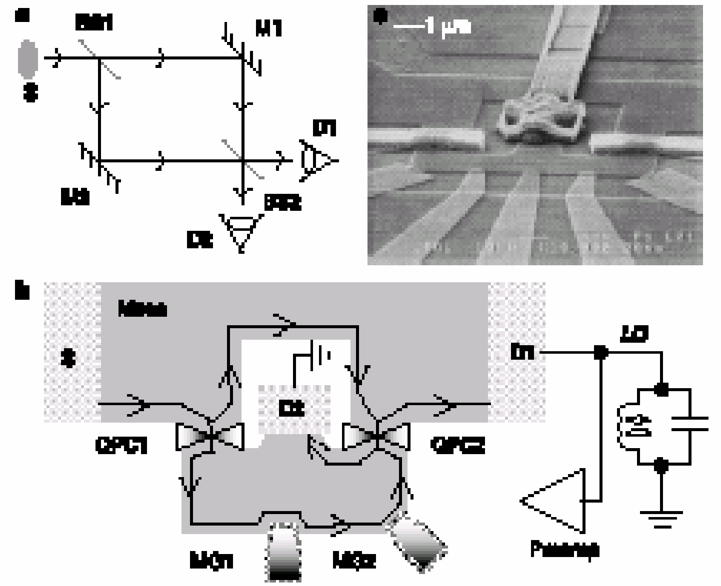

Figure 1 The configuration and operation of an optical Mach–Zehnder interferometer, and its realization with electrons. **a**, An optical Mach–Zehnder interferometer. D1 and D2 are detectors, BS1 and BS2 are beam splitters, and M1 and M2 are mirrors. With 0 (π) phase difference between the two paths, D1 measures maximum (zero) signal and D2 zero (maximum) signal. The sum of the signals in both detectors is constant and equal to the input signal. **b**, The electronic Mach–Zehnder interferometer and the measurement system. Edge states are formed in a high, perpendicular, magnetic field. The incoming edge state from S is split by QPC1 (quantum point contact 1) to two paths; one moves along the inner edge, and the other along the outer edge, of the device. The two paths meet again at QPC2, interfere, and result in two complementary currents in D1 and in D2. By changing the contours of the outer edge state and thus the enclosed area between the two paths, the modulation gates (MGs) tune the phase difference between the two paths via the Aharonov–Bohm effect. A high signal-to-noise-ratio measurement of the current in D1 is performed at 1.4 MHz with a cold *LC* resonant circuit as a band-pass filter followed by a cold, low-noise, preamplifier. **c**, Scanning electron micrograph of the device. A centrally located small ohmic contact ($3 \times 3\,\mu m^2$), serving as D2, is connected to the outside circuit by a long, metallic, air bridge. Two smaller metallic air bridges bring the voltage to the inner gates of QPC1 and QPC2—both serve as beam splitters for edge states. The five metallic gates (at the lower part of the figure) are MGs.

III. Quasiparticle charge and statistics

D. Statistical tests

More controlled interference experiment

An electronic Mach–Zehnder interferometer

Yang Ji, Yunchul Chung, D. Sprinzak, M. Heiblum, D. Mahalu & Hadas Shtrikman

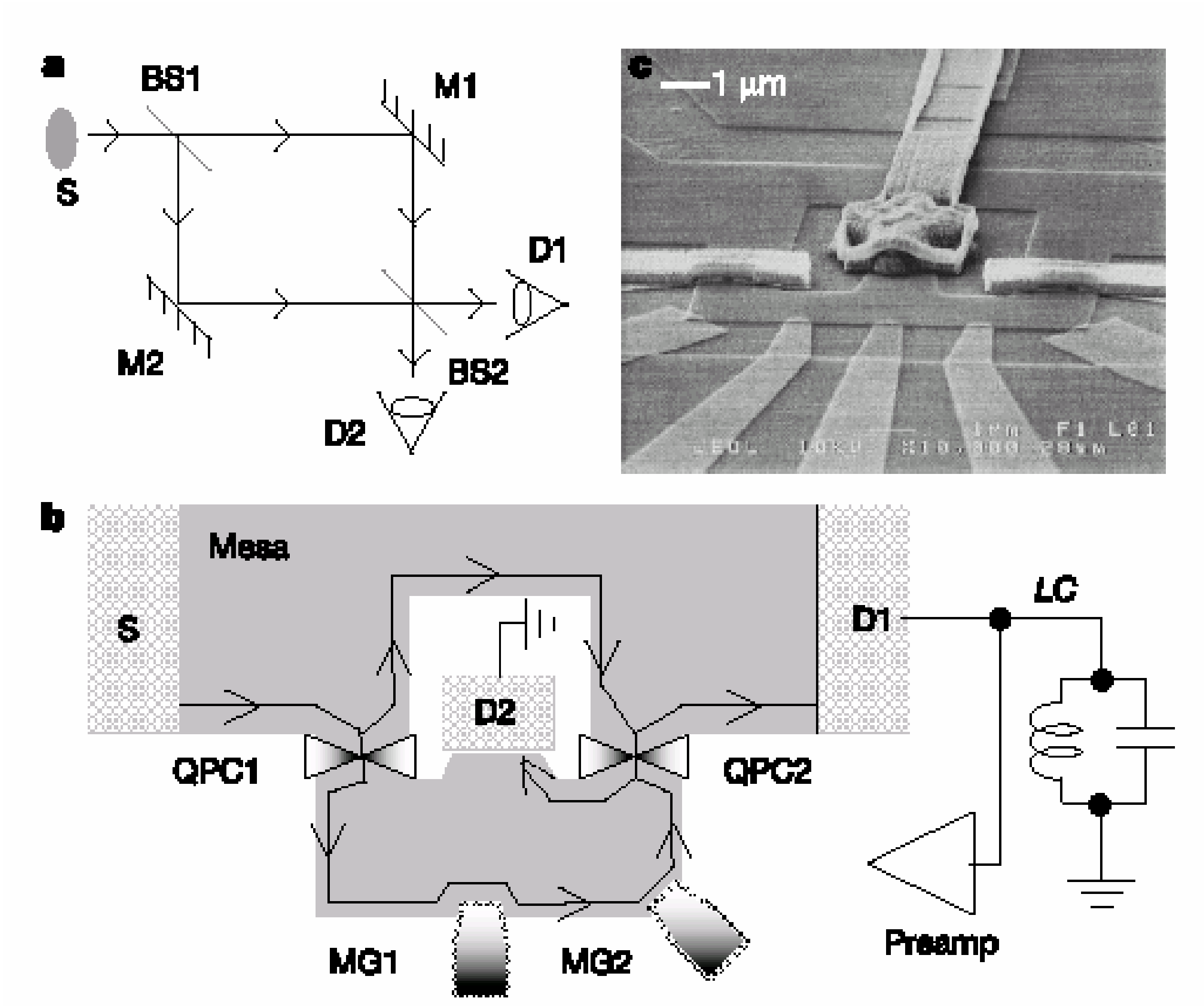

III. Quasiparticle charge and statistics

D. Statistical tests

Examining interference for electrons in the QHE regime

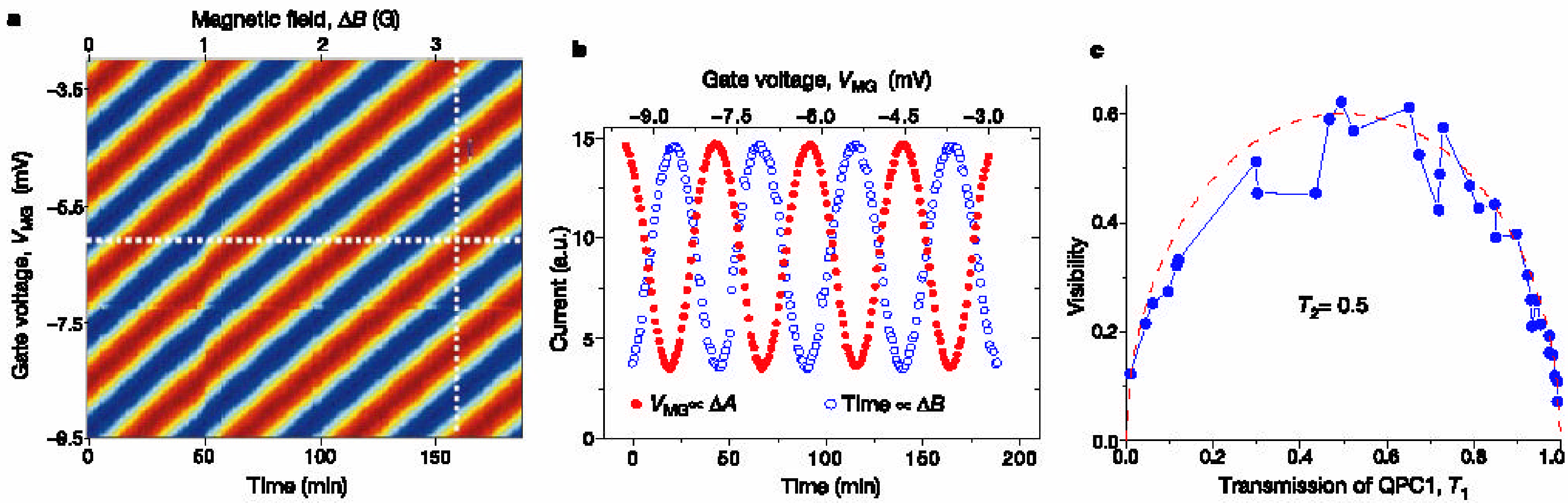

Figure 2 Interference pattern of electrons in a Mach–Zehnder interferometer and the dependence on transmission. **a**, Two-dimensional colour plot of the current collected by D1 as function of magnetic field and gate voltage at an electron temperature of ~20 mK. The magnet was set in its persistent current mode ($B \approx 5.5$ T at filling factor 1 in the bulk) with a decay rate of some 0.12 mT h^{-1}, hence time appears on the abscissa. The two QPCs were both set to transmission $T_1 = T_2 = 0.5$. Red (blue) stands for high (low) current. **b**, The current (a.u., arbitrary units) collected by D1 plotted as function of the voltage on a modulation gate, V_{MG} (red plot), and as function of the magnetic field, B (blue plot)—along the cuts shown in **a**. The visibility of the interference is 0.62. **c**, The visibility of the interference pattern (data points) as a function of the transmission probability T_1 of QPC1 when QPC2 is set to $T_2 = 0.5$. Red dashed line is a fit to the experimental data with visibility $2\eta\sqrt{T_1(1-T_1)}$. The normalization coefficient $\eta = 0.6$ accounts for possible decoherence and/or phase averaging.

III. Quasiparticle charge and statistics

D. Statistical tests

Promising possibilities: would be great system for examining fractional quantum Hall effects

However, new work has shown anomalous visibility effects

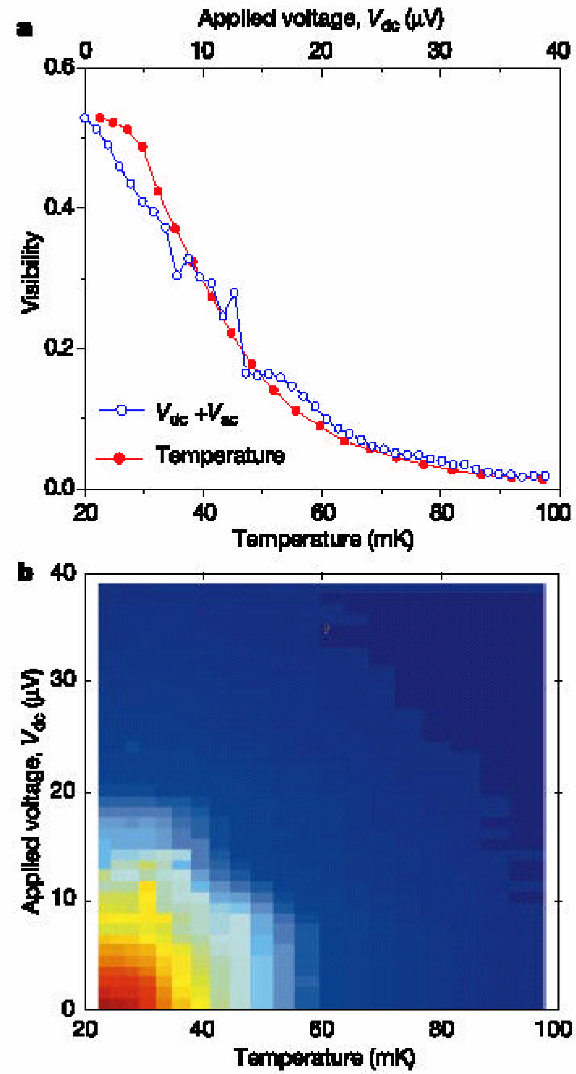

Figure 3 The dependence of the visibility of the interference pattern on temperature and applied voltage. **a**, Visibility as function of temperature at small excitation voltage for $V_{dc} = 0$ (red plot), and as function of V_{dc} with a small a.c. voltage V_{ac} superimposed on it at electron temperature 20 mK (blue plot). Both QPCs were set to $T_1 = T_2 = 0.5$. **b**, A two-dimensional colour plot of the visibility as function of temperature and applied d.c. voltage. Red (blue) stands for high (low) visibility.

III. Quasiparticle charge and statistics

D. Statistical tests

2) Hanbury Brown and Twiss

The Fermionic Hanbury Brown and Twiss Experiment

M. Henny,[1] S. Oberholzer,[1] C. Strunk,[1] T. Heinzel,[2] K. Ensslin,[2] M. Holland,[3] C. Schönenberger[1*]

A Hanbury Brown and Twiss experiment for a beam of electrons has been realized in a two-dimensional electron gas in the quantum Hall regime. A metallic split gate serves as a tunable beam splitter to partition the incident beam into transmitted and reflected partial beams. In the nonequilibrium case the fluctuations in the partial beams are shown to be fully anticorrelated, demonstrating that fermions exclude each other. In equilibrium, the cross-correlation of current fluctuations at two different contacts is also found to be negative and nonzero, provided that a direct transmission exists between the contacts.

correlations of current fluctuations may be used to establish statistics

Fig. 1. The particles in a beam of bosons obeying Bose-Einstein statistics tend to cluster (bunching). Consequently, a positive correlation is observed between two partial beams generated by a beam splitter. In contrast, in a degenerate beam of fermions the particles expel each other (antibunching) because a fermionic state can only be occupied once. Consequently, the partial beams are expected to be fully anticorrelated.

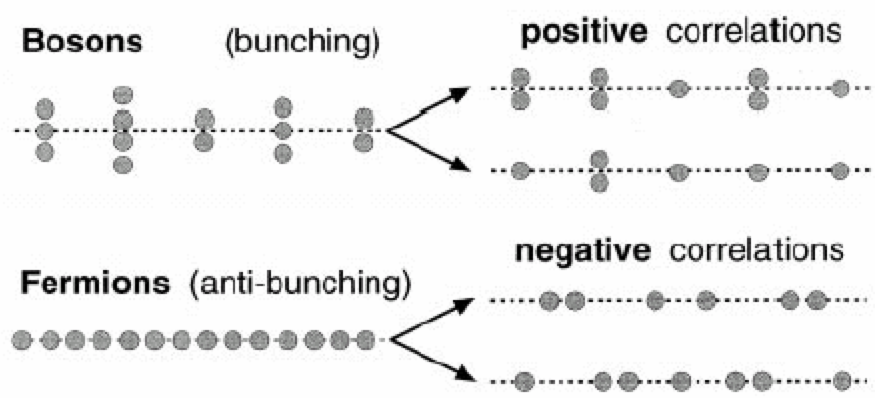

Science '99

III. Quasiparticle charge and statistics

D. Statistical tests

2) Hanbury Brown and Twiss

$$\langle \Delta I_\alpha \Delta I_\beta \rangle_s = \pm 2e|I|t(1-t)$$

$\alpha = \beta$ Autocorrelation

$\alpha \neq \beta$ crosscorrelation

Applied to edge state currents using QPC as splitter:

Fermionic anti-correlations demonstrated?

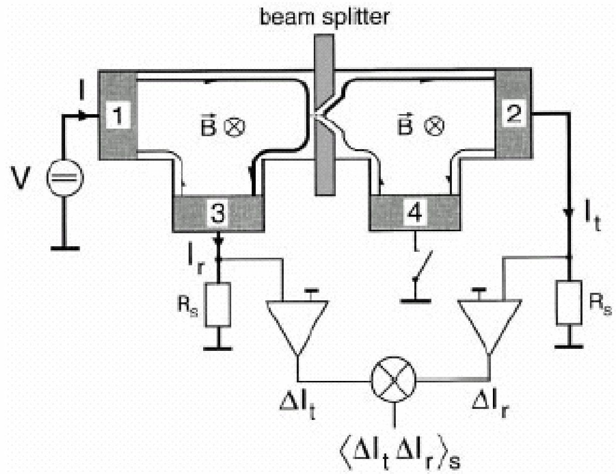

Fig. 2. Intensity correlation experiment for a degenerate beam of electrons realized in a semiconductor Hall bar connected to four electron reservoirs (dark shading). A metallic split gate (light shading) serves as a tunable beam splitter. The primary beam I originates from the electrons injected by the voltage source V connected to reservoir 1. These electrons move along the upper edge channel until reaching the gate, where they are either transmitted into contact 2 or reflected into 3. The time-dependent transmitted and reflected currents $I_{t,r}$ are converted to voltage signals by two 1-kilohm series resistors R_s and then amplified. Finally, an electronic correlator determines the spectral correlations $\langle \Delta I_t \Delta I_r \rangle_s$ of the fluctuations $\Delta I_{t,r}$ at a central frequency in the range of 100 kHz to 1 MHz (*11*).

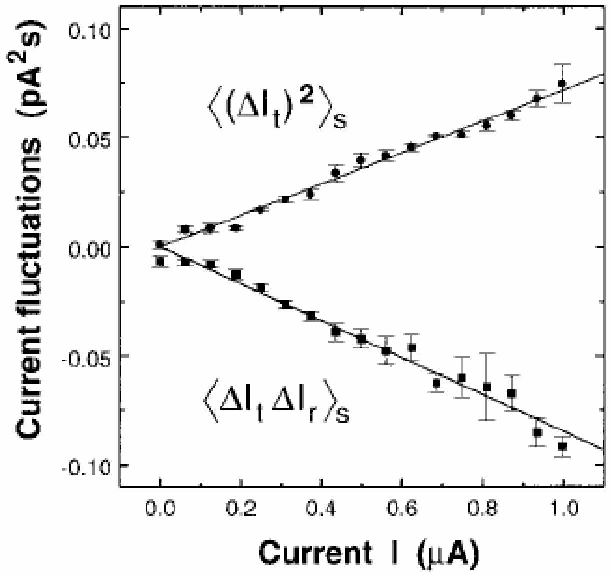

Fig. 3. Measured spectral densities of current-fluctuation correlations as a function of the current I of the incident beam at temperature $T = 2.5$ K and with the beam splitter adjusted to $t = 50\%$ transmission. $\langle (\Delta I_t)^2 \rangle_s$ denotes the autocorrelation in the transmitted channel and $\langle \Delta I_t \Delta I_r \rangle_s$ the cross-correlation between the transmitted and reflected channels. Current-independent fluctuations, such as thermal noise and residual amplifier noise, have been subtracted. From the experiment we deduce for the absolute slope $0.23 \cdot 2eI$ and $0.26 \cdot 2eI$ for the autocorrelation and cross-correlation, respectively. This is in good agreement with the expected prefactor given by $t(1-t) = 1/4$.

III. Quasiparticle charge and statistics:

A. vortex picture – magnetic field and charge contributions to quasiparticles

B. fractional charge measurements – indirect measures of charge with open questions

C. next step = statistical tests with quasiparticles - difficult to apply single particle (electron) methods to quasiparticles –

experimentally difficult to probe

We will see a particularly interesting statistical state in the higher Landau levels

Outline:

I. Introduction: materials, transport, Hall effects

II. Composite particles – FQHE, statistical transformations

III. Quasiparticle charge and statistics

IV. Higher Landau levels

  A. Overview
  B. 5/2 FQHE – the fraction that shouldn't be there
  C. 9/2 stripes and other things
  D. Higher Landau level experimental issues

V. Other parts of spectrum: non-equilibrium effects, electron solid?

VI. Multicomponent systems: Bilayers

IV. Higher Landau Levels

A. Overview:

Energy and length scales
(density $1 \times 10^{11} cm^{-2}$)
Compare LLL to HLL

	?=7/2	and	?=1/2
Coulomb energy	55 K		144 K
Spin gap	.35 K		2.4 K
Effective Fermi Wavevector	41 ?m^{-1}		110 ?m^{-1}

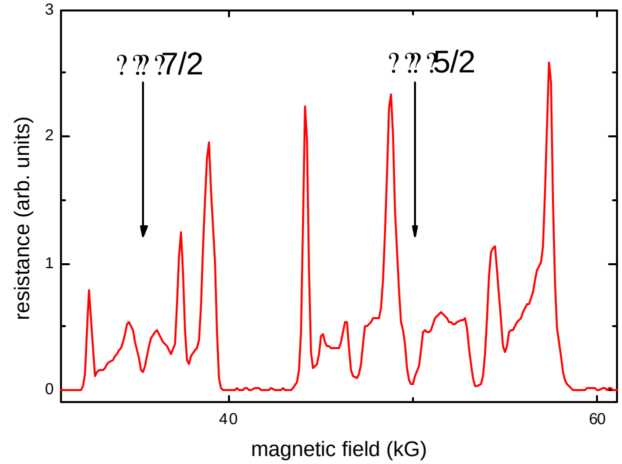

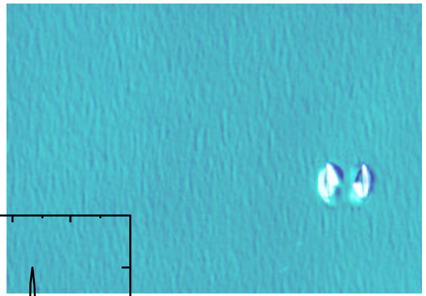

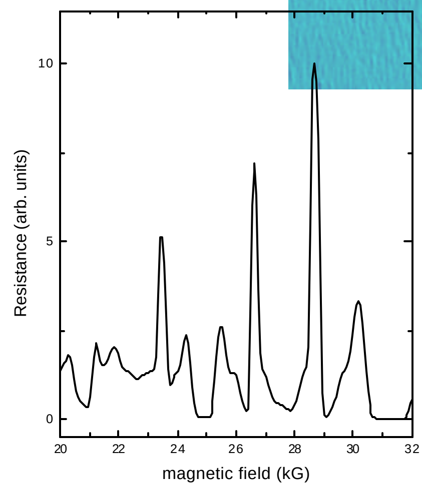

Effective interaction energy scale much lower at 7/2

IV. Higher Landau Levels

A. Overview:

Wavefunctions different in higher Landau levels

Different interactions energies:
Exchange plays an important role

Lowest:
N=0

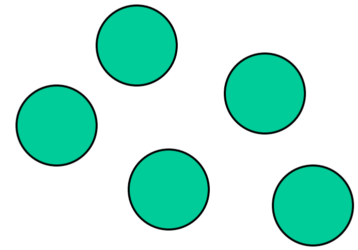

Second:
N=1

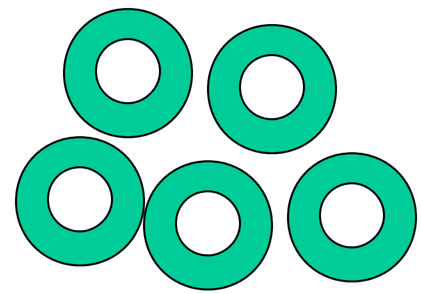

Third:
N=2

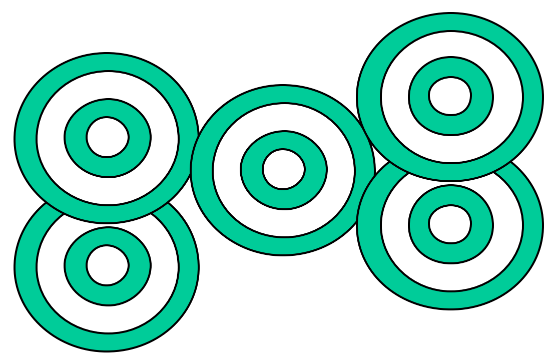

IV. Higher Landau Levels

A. Overview:

Wavefunctions different in higher Landau levels.
Also, filled inert lower Landau level leaves **fewer electrons in the higher LL for screening**

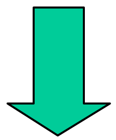

Disorder has more severe consequence on higher Landau level physics

IV. Higher Landau Levels

A. Overview:

Wavefunctions different in higher Landau levels. Also, filled inert lower Landau level leaves fewer electrons in the higher LL for screening

Disorder has more severe consequence on higher Landau level physics

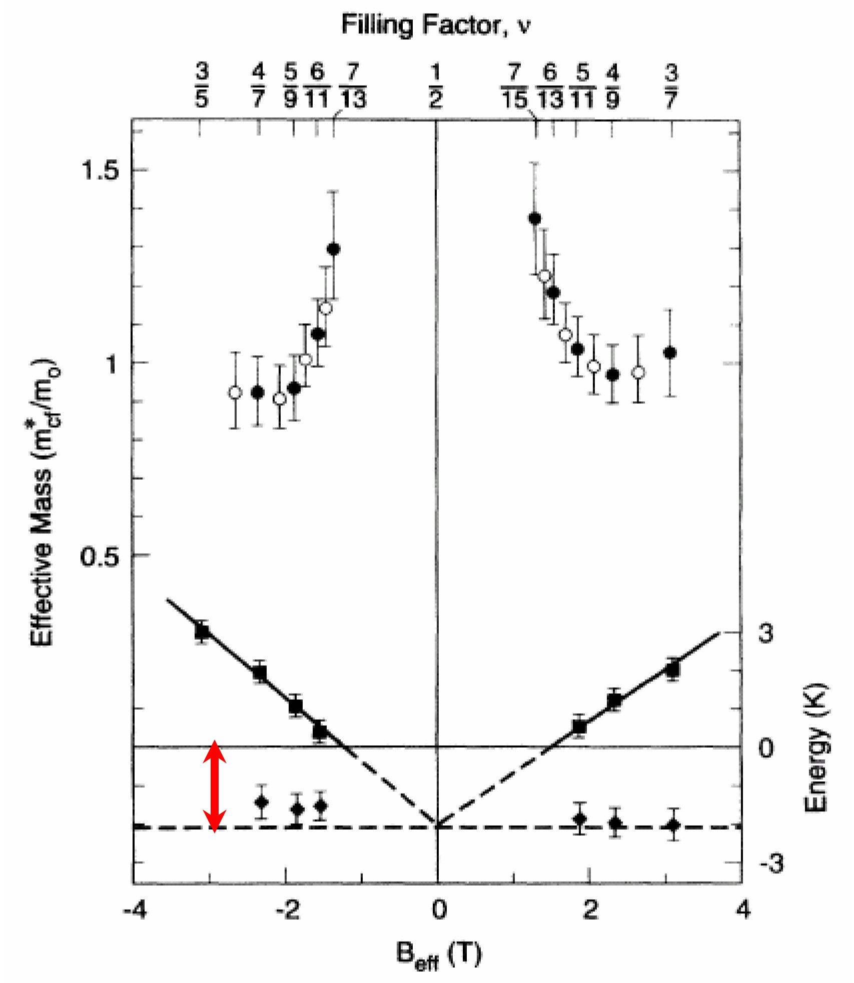

Large disorder diminution of gaps in lowest Landau level: ? ~ 2 K
Similar absolute gap reduction may apply in HLL for intrinsically smaller gaps

IV. Higher Landau Levels

A. Overview:

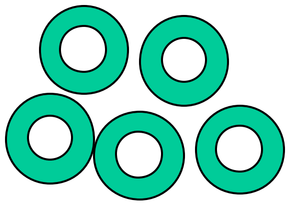

Wavefunctions different in
higher Landau levels
&
Lower effective density
&
Persistent disorder

Smaller energy scales, more difficult to examine correlation effects
Need lower temperatures and higher mobilities

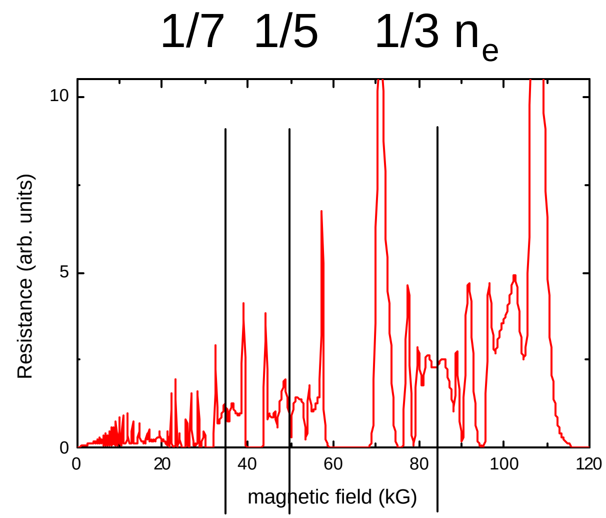

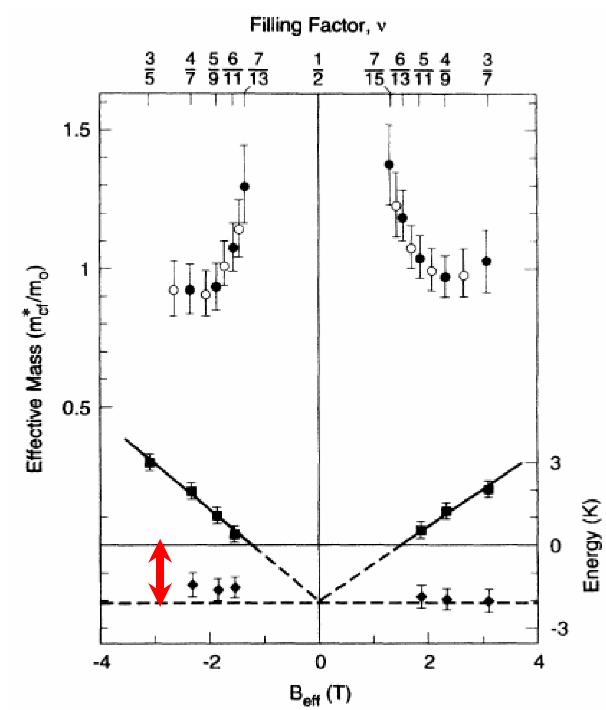

IV. Higher Landau Levels

B. 5/2 fractional quantum Hall effect:
the fraction that shouldn't be there

According to composite fermion theory it is expected that at filling factors 1/2, 3/2, 5/2, etc. we should see Fermi surfaces forming

This is true at 1/2 and 3/2, but **at 5/2 it was found that at low temperatures a quantum Hall state exists**

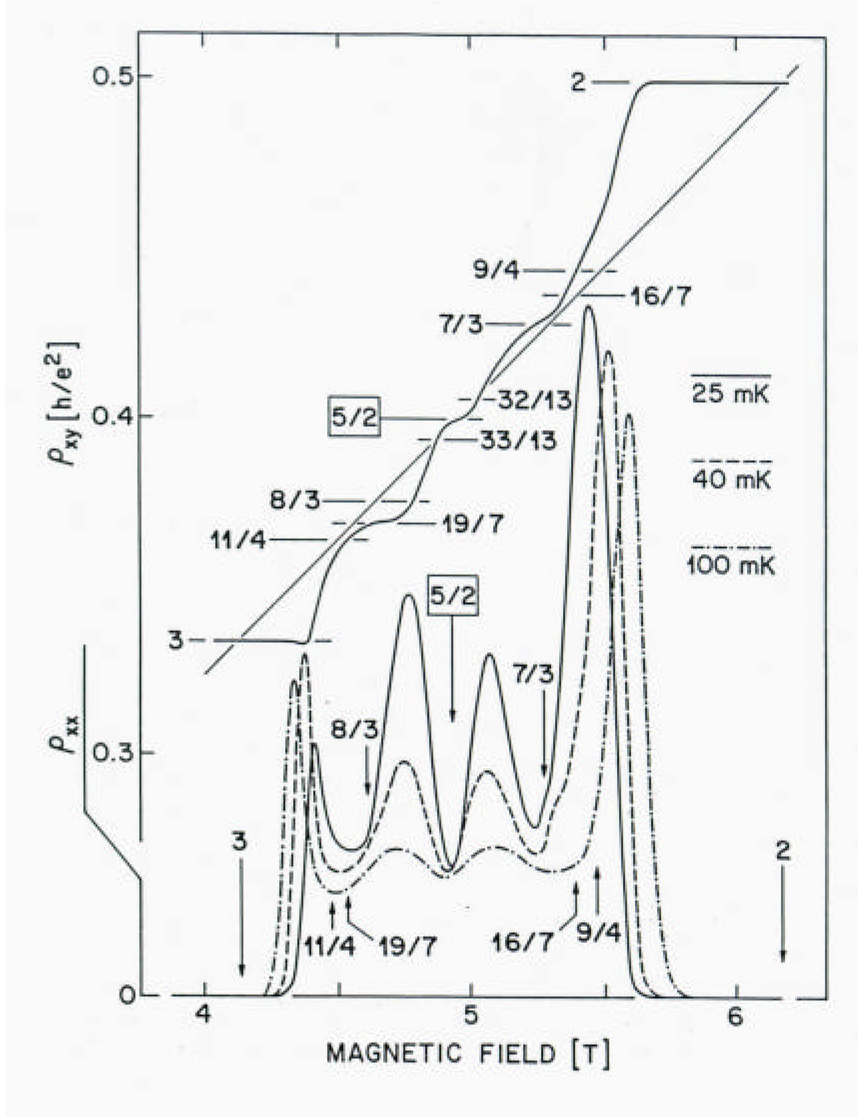

IV. Higher Landau Levels

B. 5/2 fractional quantum Hall effect:
the fraction that shouldn't be there

This is true at 1/2 and 3/2, but at 5/2 it was found that at low temperatures a quantum Hall state exists

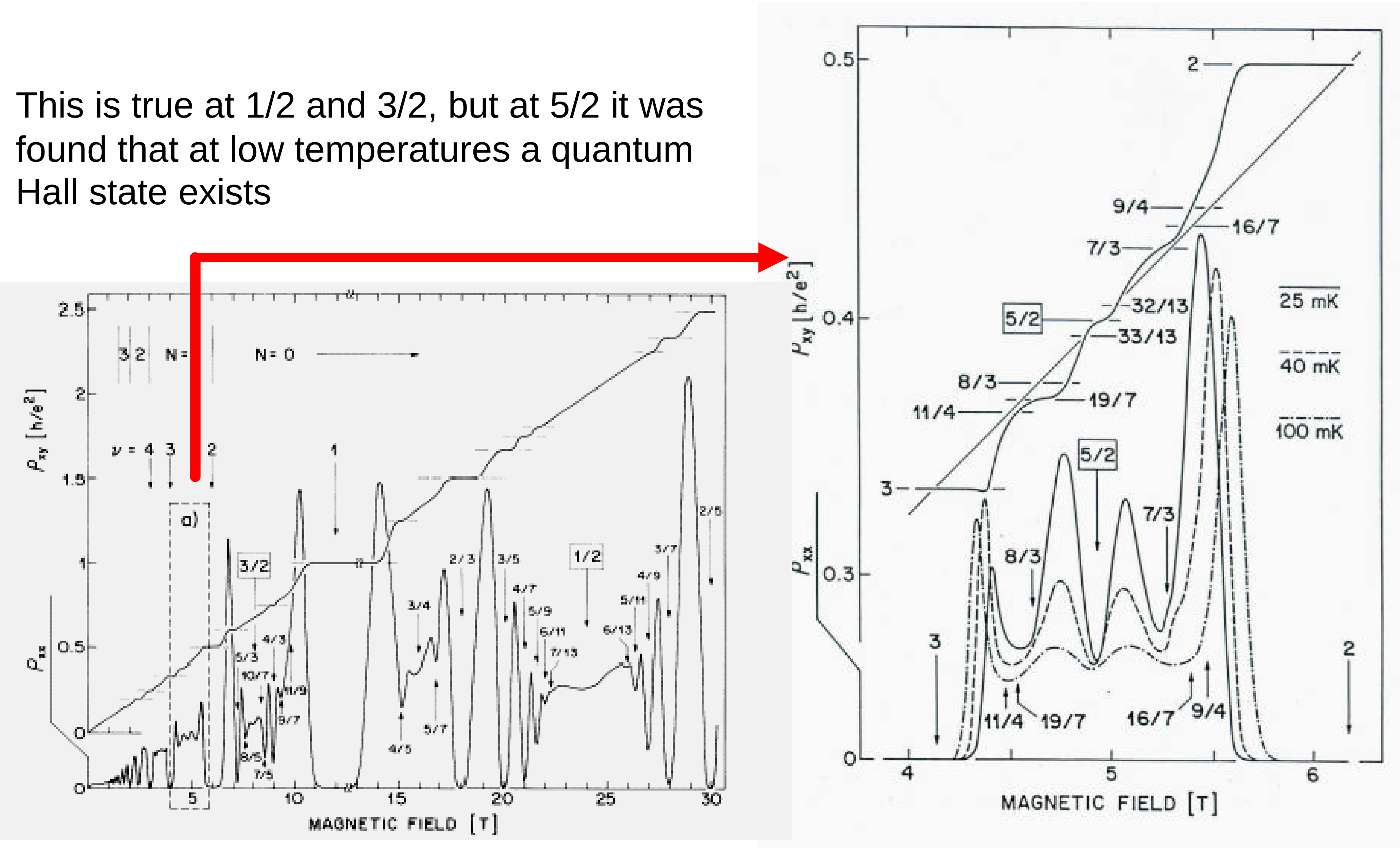

IV. Higher Landau Levels

B. 5/2 fractional quantum Hall effect:

Upon tilting the sample in the B-field, the new state disappears

Spin gap ~ total B-field

Orbital gaps ~ orthogonal B-field

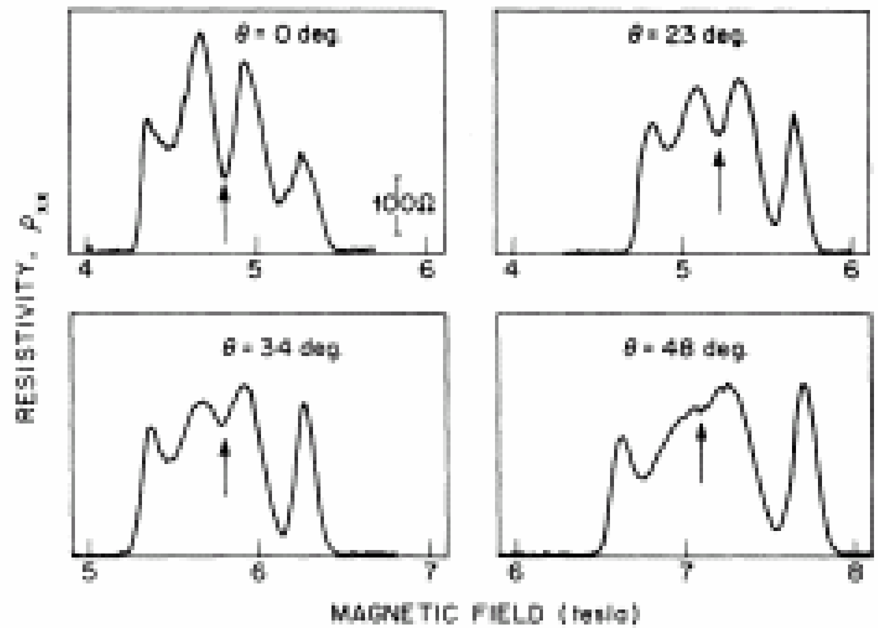

FIG. 1. Diagonal-resistivity ρ_{xx} data for various tilt angles θ at 25 mK. Arrows mark field positions of $\nu = \frac{5}{2}$ filling factor. Resistivity minima above and below the $\nu = \frac{5}{2}$ feature occur near $\nu = \frac{7}{3}$ and $\frac{8}{3}$, respectively.

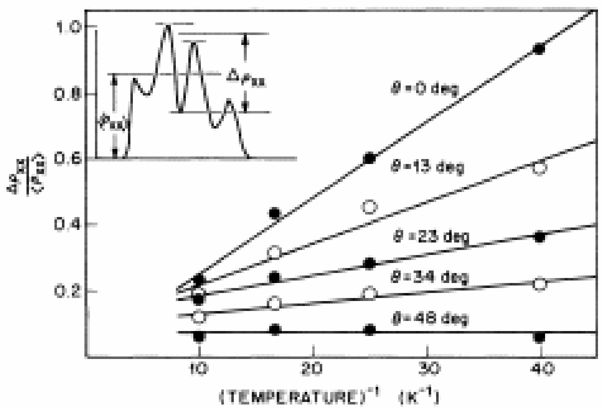

FIG. 2. Temperature dependence of the strength of the $\nu = \frac{5}{2}$ FQHE for various tilt angles. Inset: definition of the strength ratio $\Delta\rho_{xx}/\langle\rho_{xx}\rangle$.

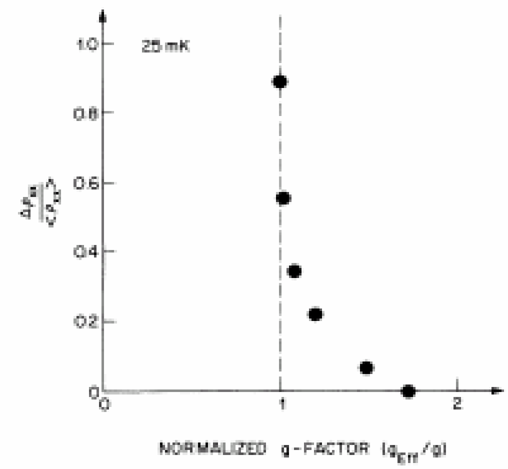

FIG. 3. Strength of the $\nu = \frac{5}{2}$ FQHE at 25 mK vs normalized g factor defined as $g_{eff}/g = 1/\cos\theta$. Vertical dashed line indicates perpendicular-field case.

IV. Higher Landau Levels

B. 5/2 fractional quantum Hall effect:

Two theoretical possibilities proposed:

1) Haldane-Rezayi: non-spin polarized state = d-wave pairing of composite fermions

2) Moore-Read: spin polarized state = p-wave pairing of composite fermions

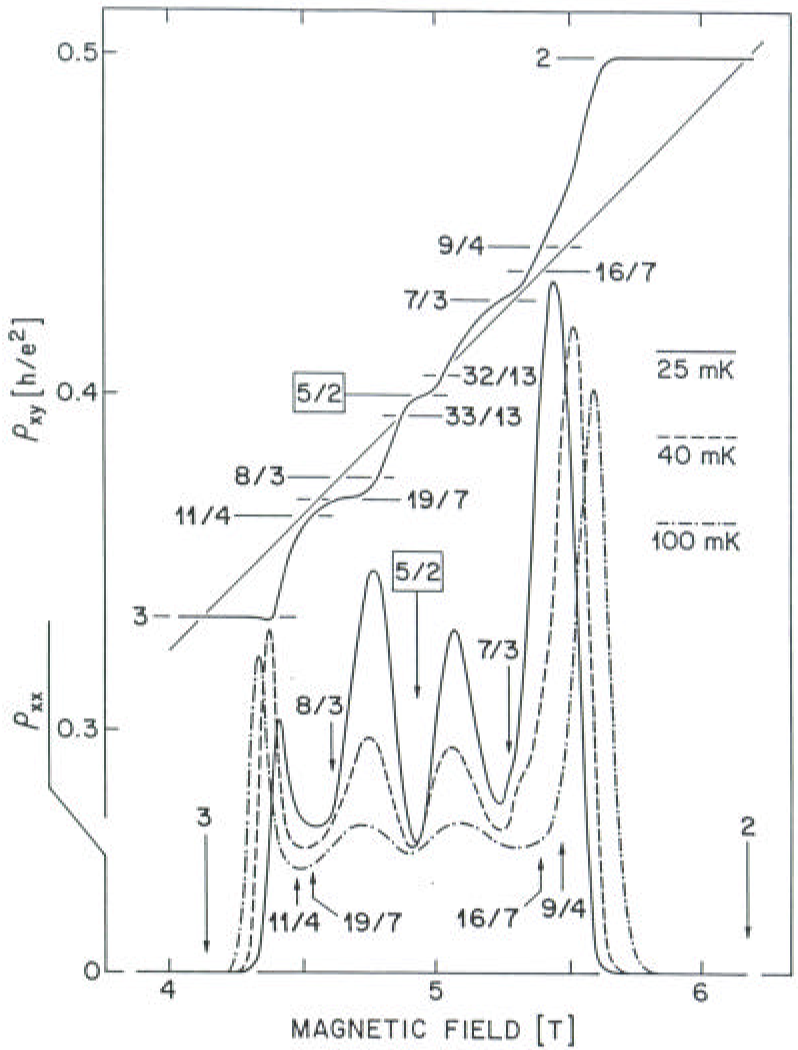

Tilted field results suggest that Haldane-Rezayi state is the likely candidate

IV. Higher Landau Levels

B. 5/2 fractional quantum Hall effect:

Much later, numerical studies by R. Morf indicated that
the p-wave state (spin polarized) is energetically favorable

? the system at high temperatures is a filled Fermi sea that condenses at low temps to the 5/2 FQHE

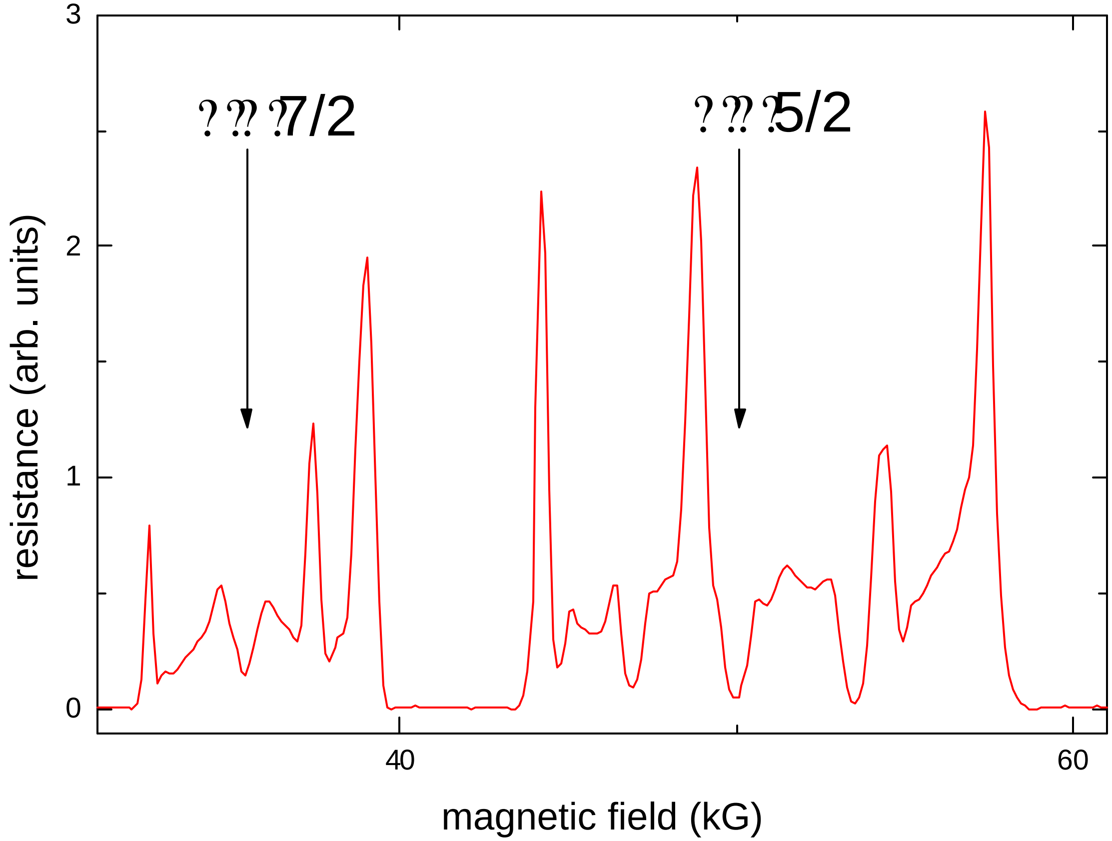

Experimentally samples improved significantly

IV. Higher Landau Levels

B. 5/2 fractional quantum Hall effect:

Examine this transition from fermionic to bosonic system: can the Fermi surface at 5/2 be observed

Sign of fermi surface formation is enhanced conductivity at even denominator filling factors observed using SAW

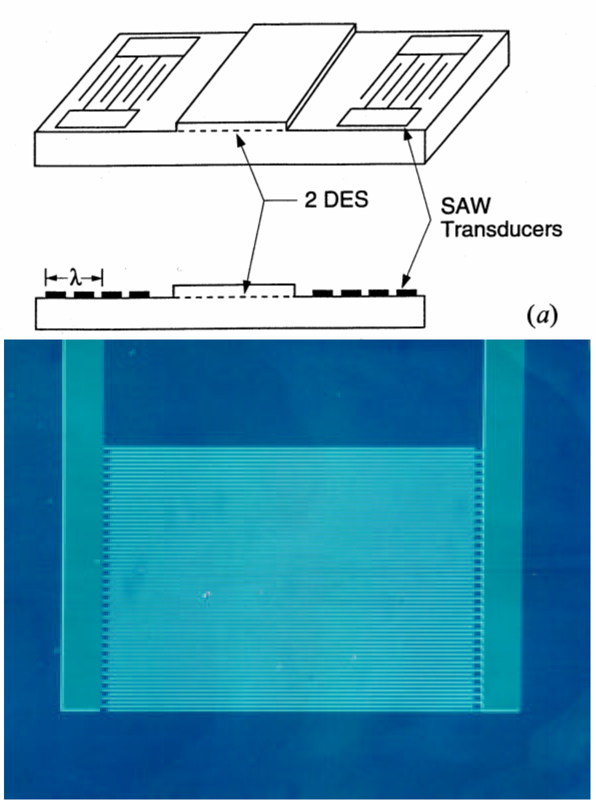

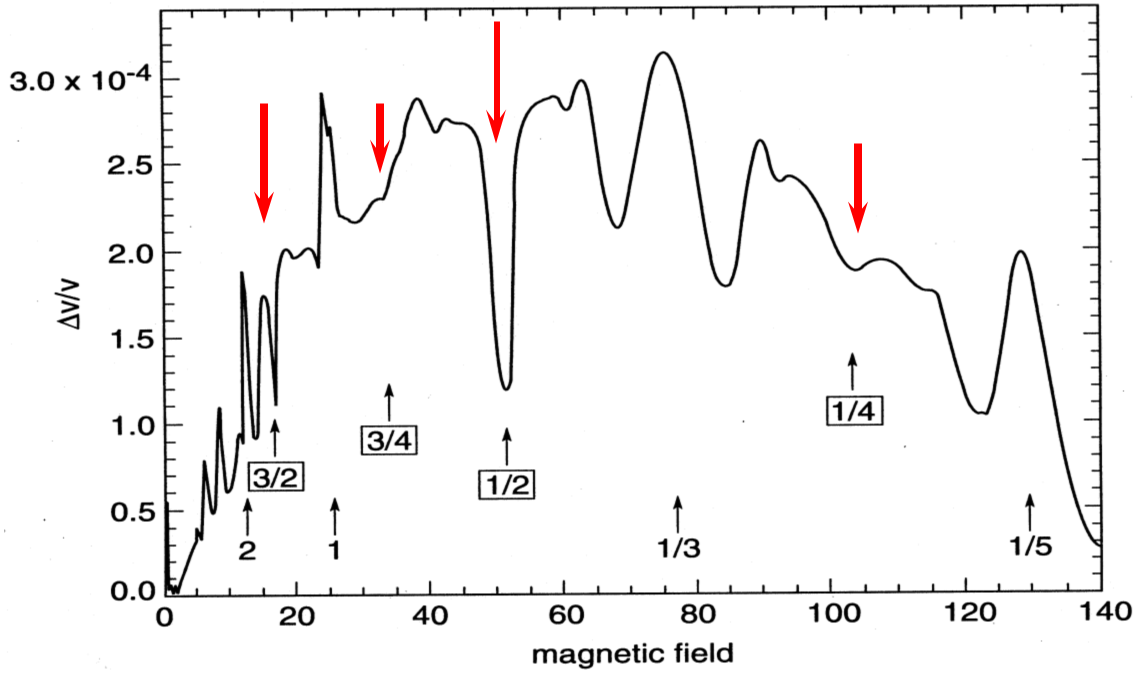

IV. Higher Landau Levels

B. 5/2 fractional quantum Hall effect:

SAW results for “low” mobility system

- small effect at 3/2
- no effect at 5/2

T=300mK

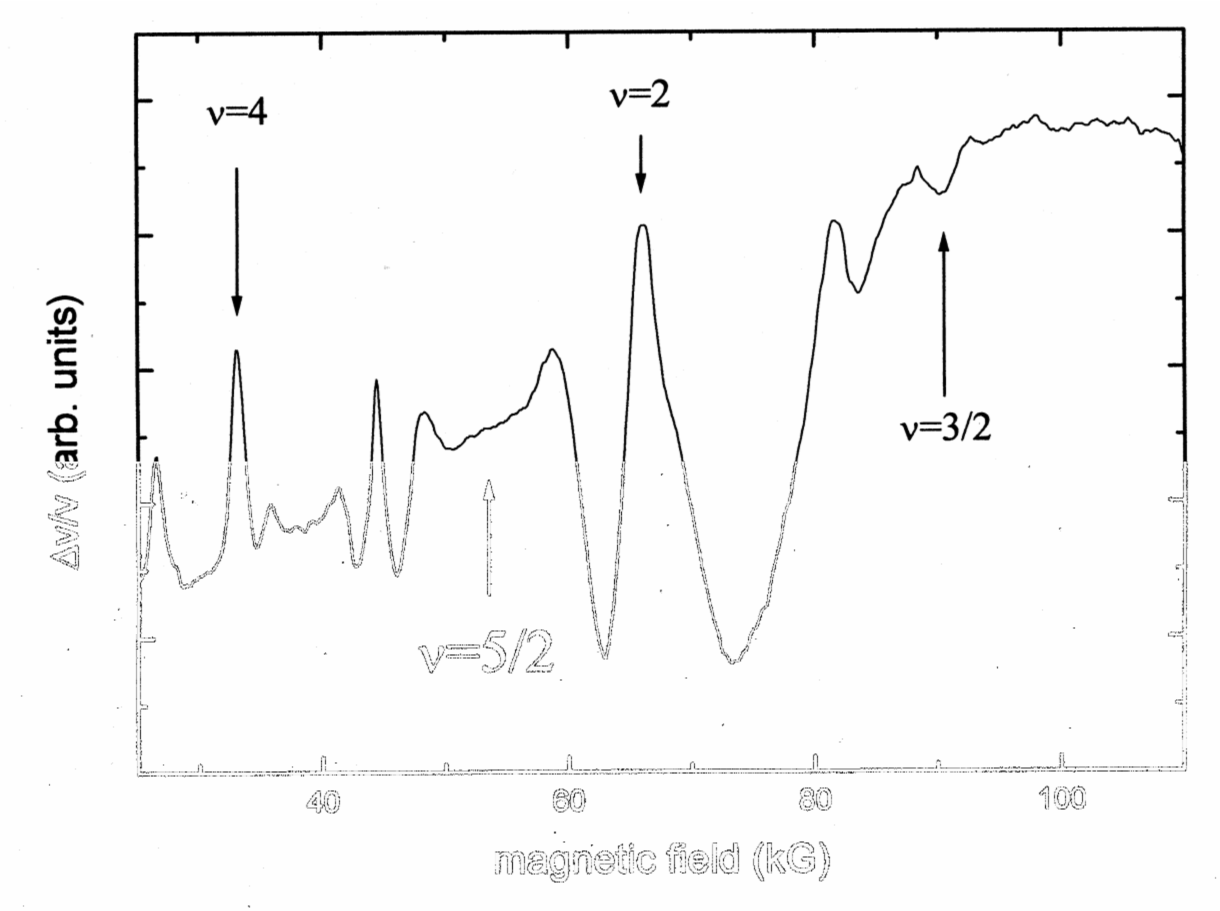

IV. Higher Landau Levels

B. 5/2 fractional quantum Hall effect:

enhanced conductivity
present at 5/2

SAW results for high mobility system:
? ?> 30 x 10^6 cm^2/V-sec

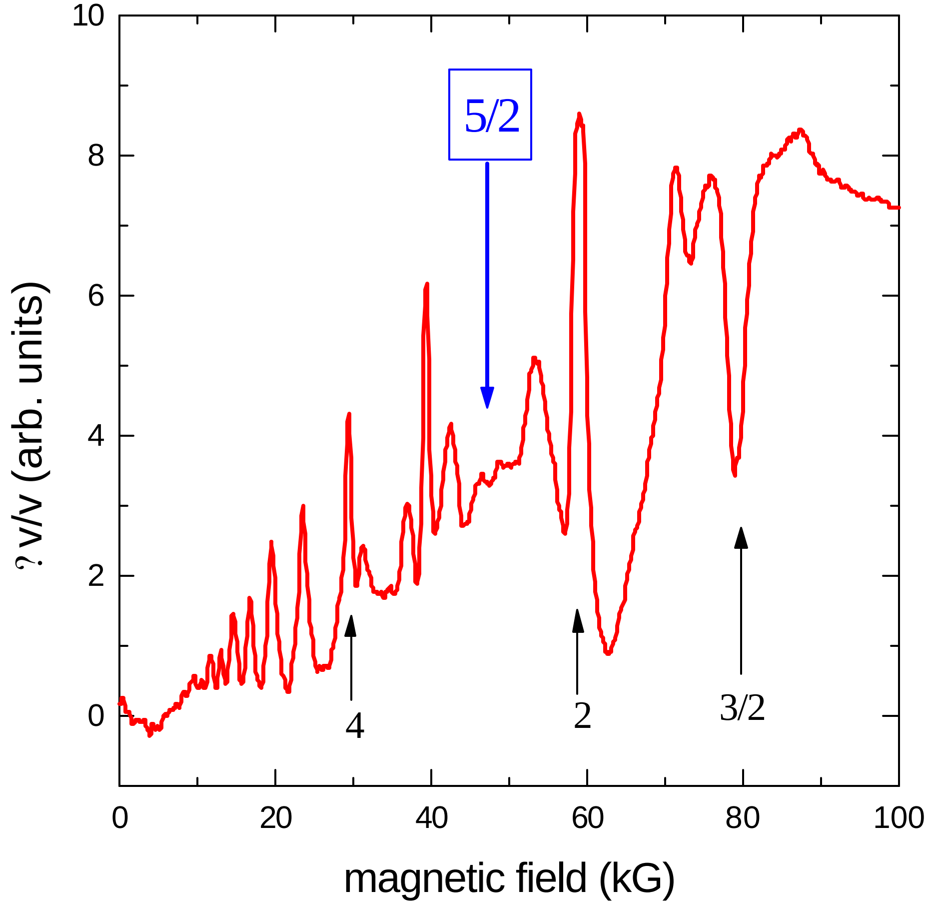

IV. Higher Landau Levels

B. 5/2 fractional quantum Hall effect:

T ~ 290 mK:enhanced conductivity at high T

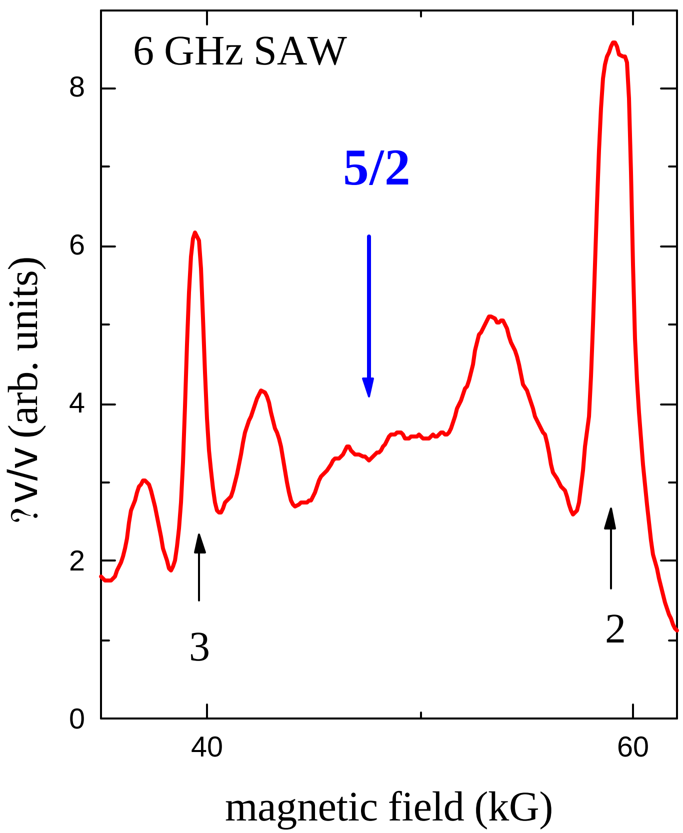

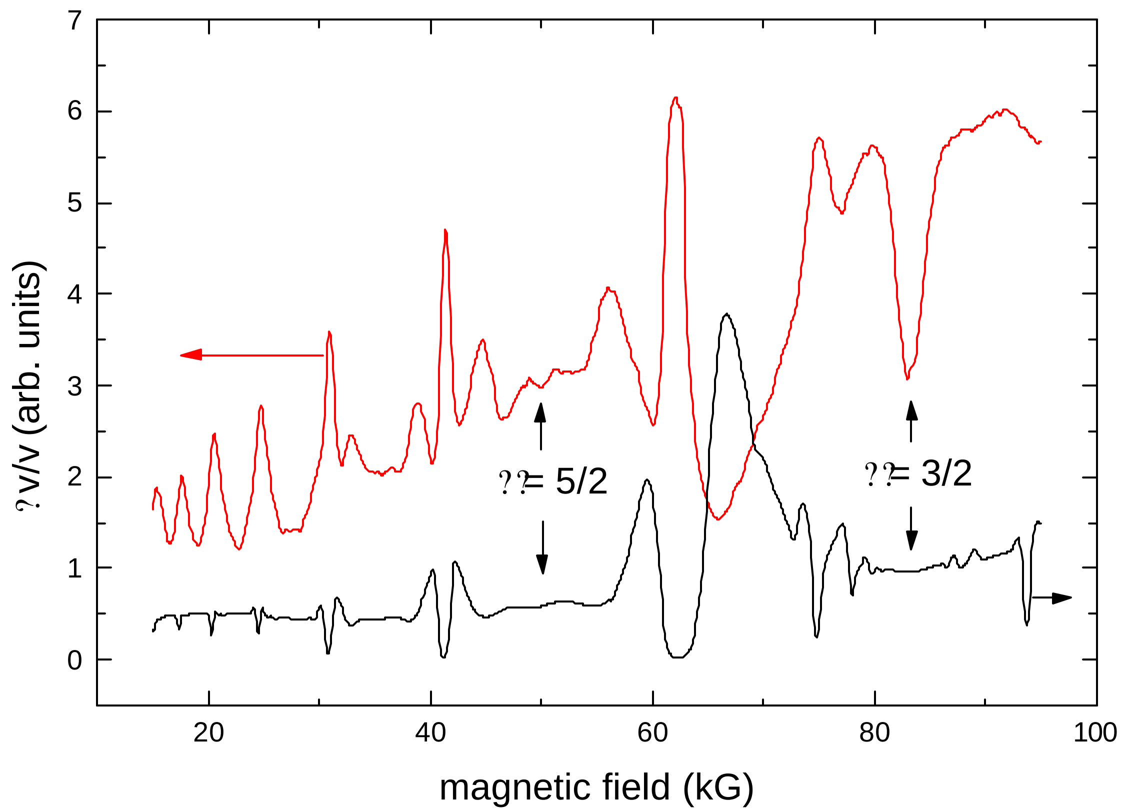

SAW results for high mobility system:
?? > 30 x 10^6 cm^2/V-sec

SAW response shows clear minimum at ? =5/2 for 6GHz, ? ~ 0.5 ?m

IV. Higher Landau Levels

B. 5/2 fractional quantum Hall effect:

SAW results for high mobility system:
? ?> 30 x 10^6 cm^2/V-sec

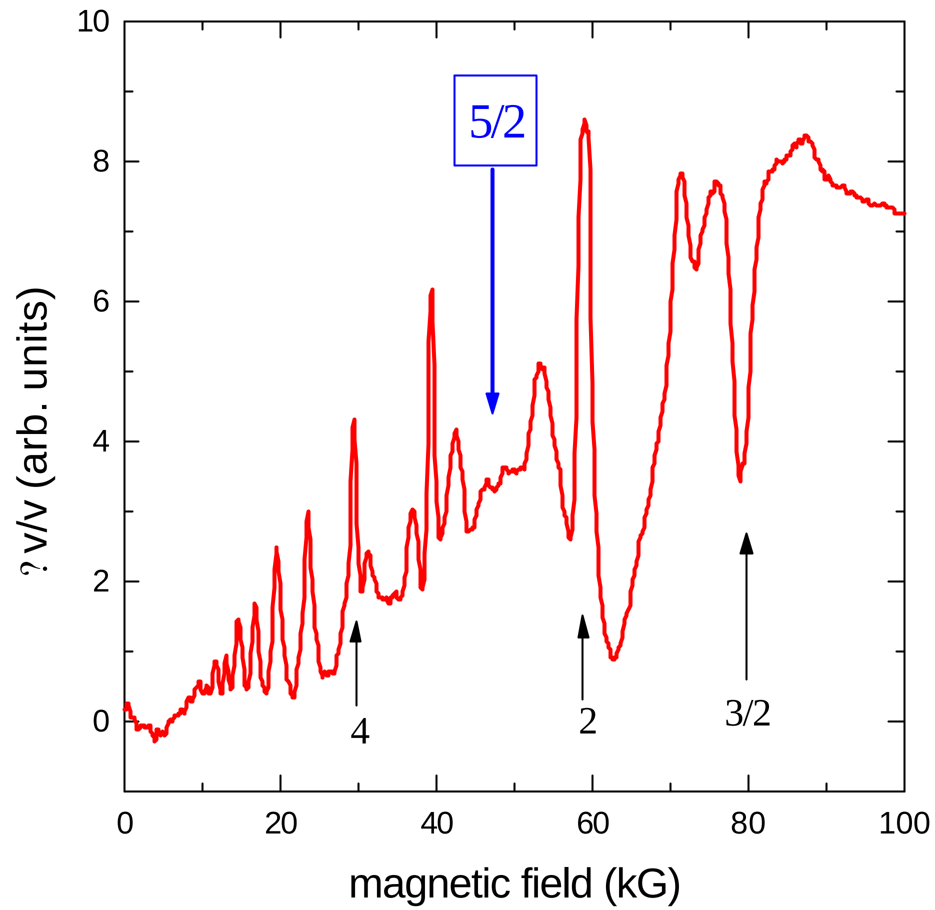

enhanced conductivity present at 5/2

No Hall plateau, & only weak ?$_{xx}$ minimum in d.c. transport at this temperature

IV. Higher Landau Levels

B. 5/2 fractional quantum Hall effect:

Larger minimum in SAW response at ? = 5/2 for 8 GHz

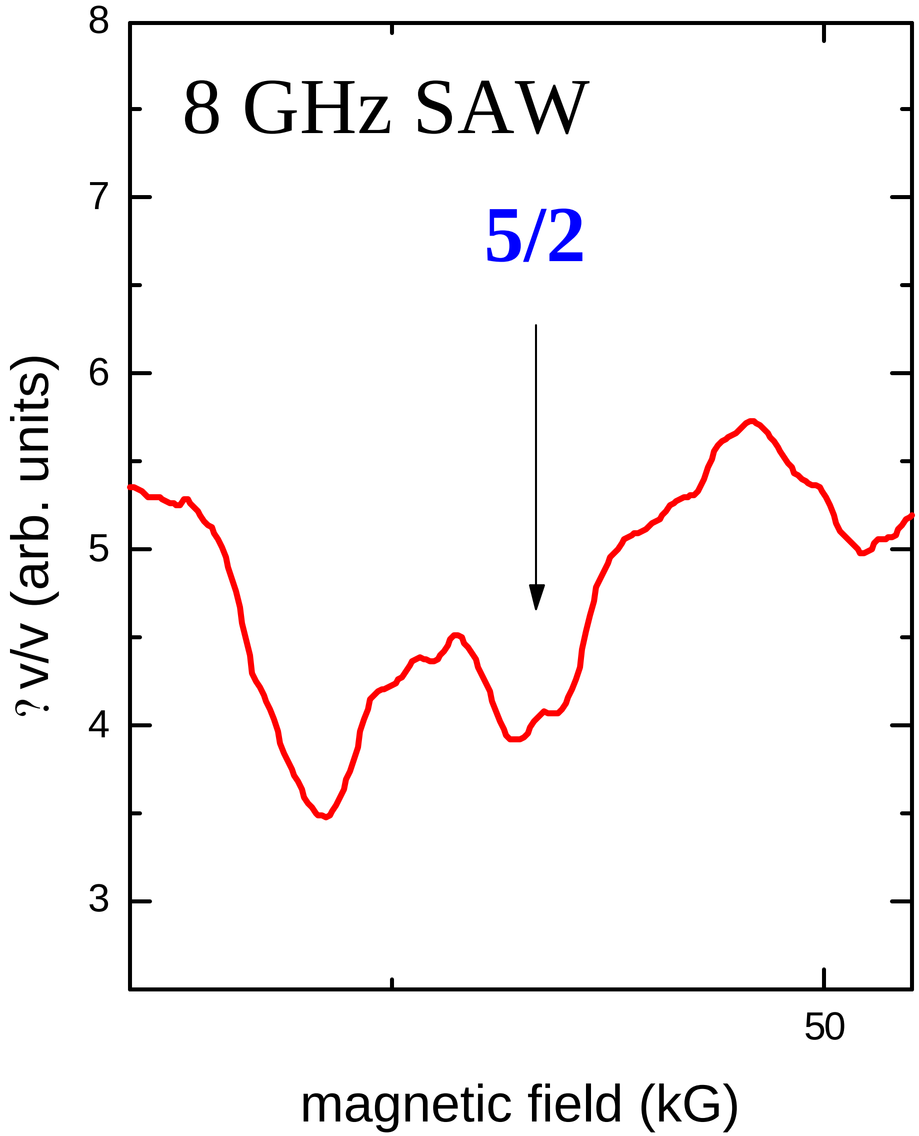

IV. Higher Landau Levels

B. 5/2 fractional quantum Hall effect:

just as for “1/2” composite particle, smaller SAW ? ?shows larger enhanced conductivity

Onset of 5/2 enhanced conductivity at SAW wavelength ~ 0.7 ? m ? composite particle mean-free-path << “1/2” composite particle

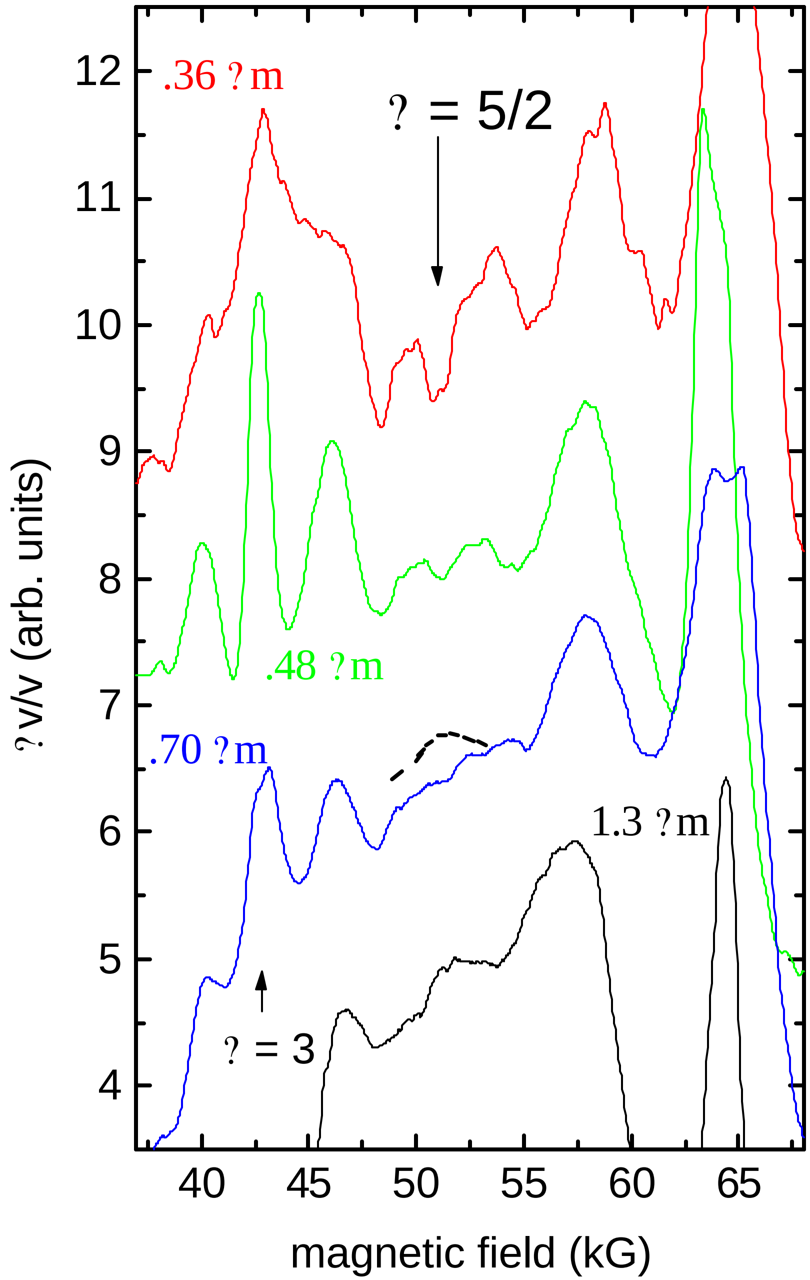

IV. Higher Landau Levels

B. 5/2 fractional quantum Hall effect:

use enhanced
conductivity width ? k_F

Width of enhanced conductivity can give Fermi wavevector k_F, from

?B ~ q(hk_F /?e) ,   and k_F = (4?n)$^{1/2}$,

where n is quasiparticle density of a given spin population filling up to k_F

compare to known total density to assess spin-polarization.

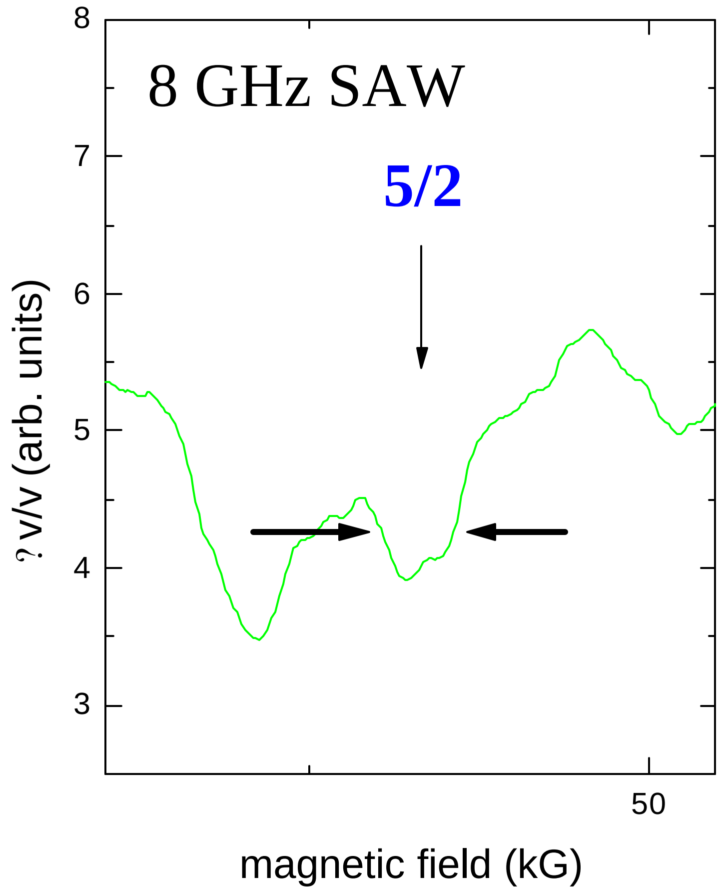

IV. Higher Landau Levels

B. 5/2 fractional quantum Hall effect:

Using appropriate quasiparticle density adjustments, comparing to 3/2 effect,

APPEARS TO BE SPIN POLARIZED

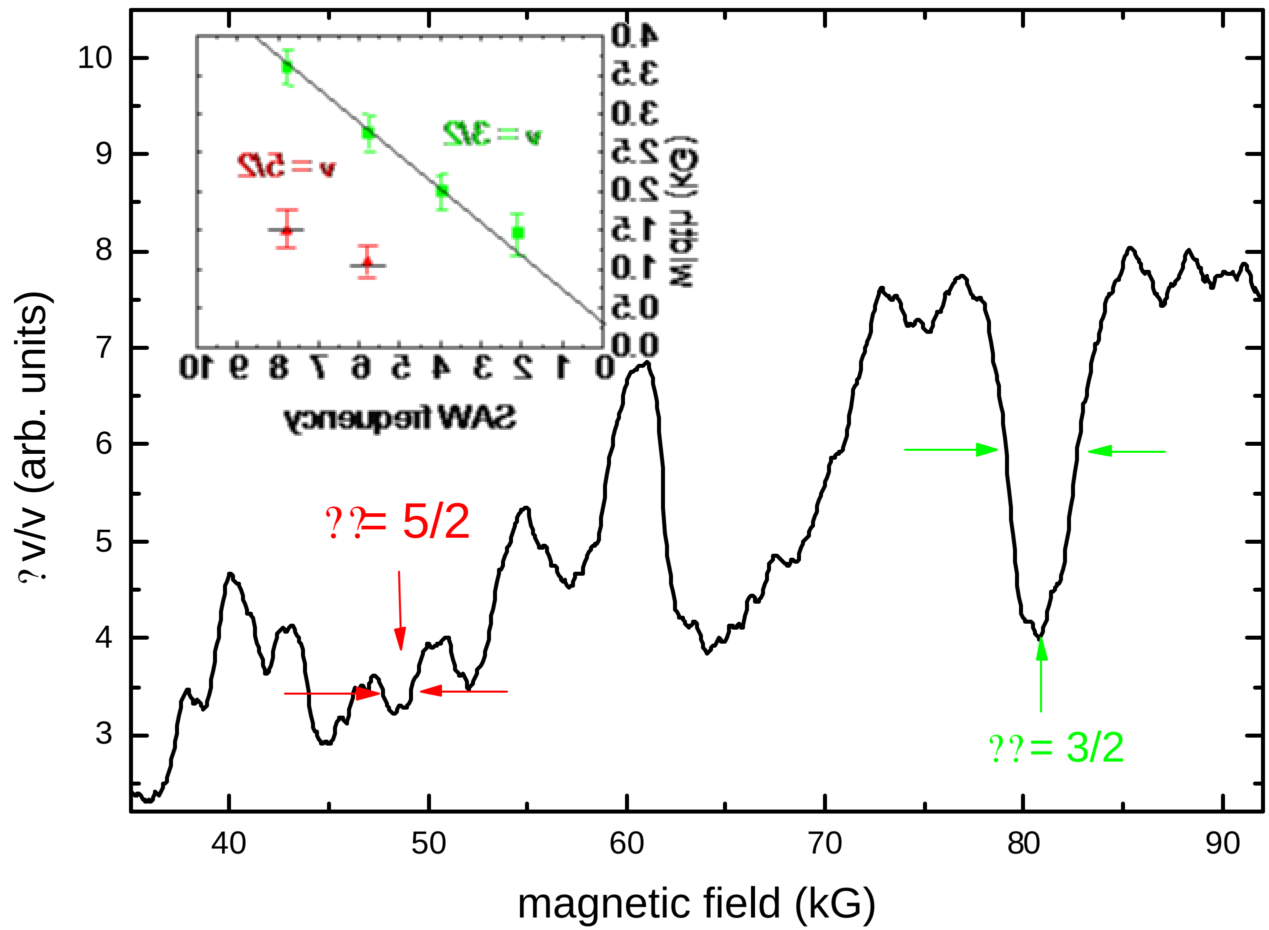

3/2 appears to be spin polarized in SAW resonances, but **not** in activation energy studies

IV. Higher Landau Levels

B. 5/2 fractional quantum Hall effect:

Composite fermion theory suggests that the system at high temperatures is a filled Fermi sea that condenses at low temps to the 5/2 FQHE

High temperatures → Low temperatures

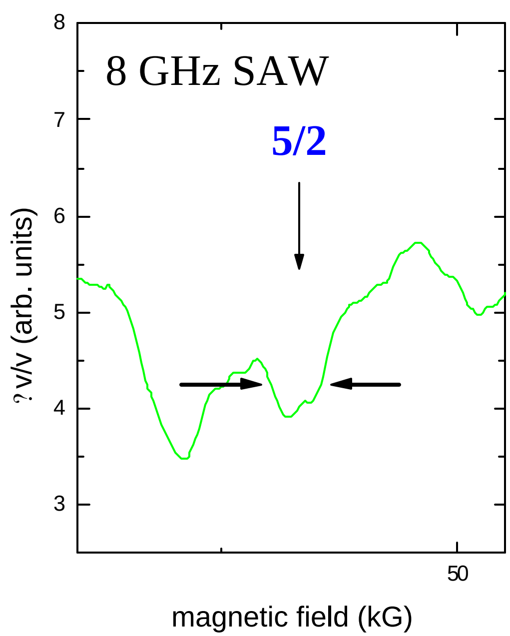

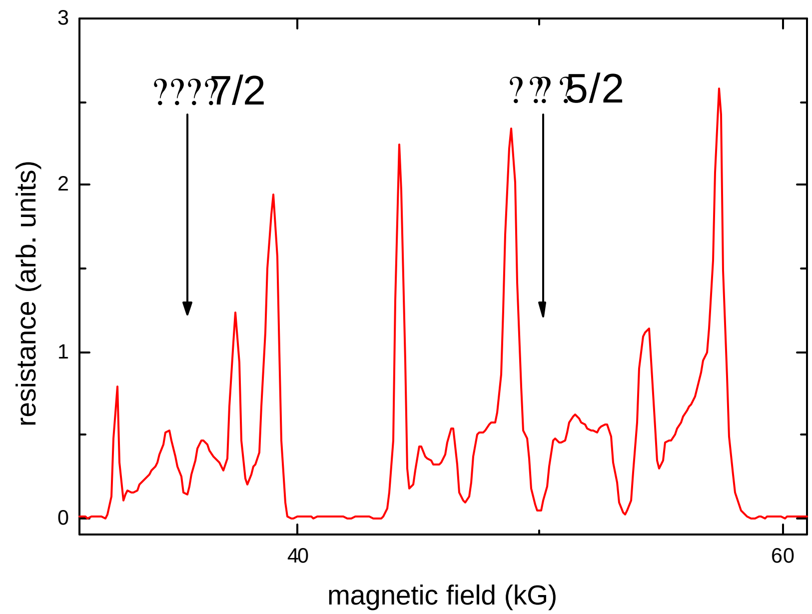

Fermi sea with Fermi surface effects → Quantum Hall state

IV. Higher Landau Levels

B. 5/2 fractional quantum Hall effect:

At 5/2 - pairing of composite fermions ??

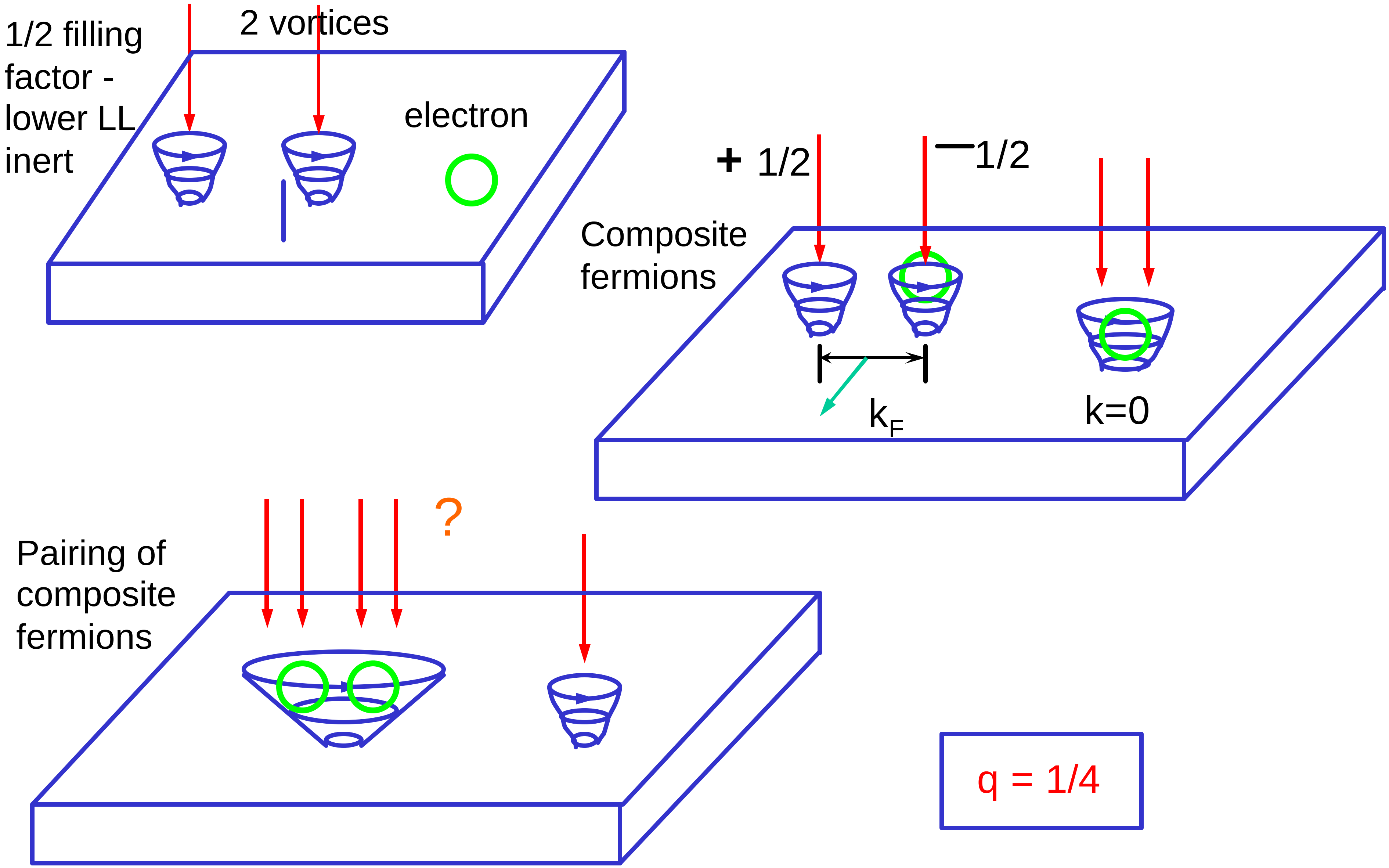

$q = 1/4$

IV. Higher Landau Levels

B. 5/2 fractional quantum Hall effect:

Even higher mobility samples
and even lower temperatures
show better 5/2

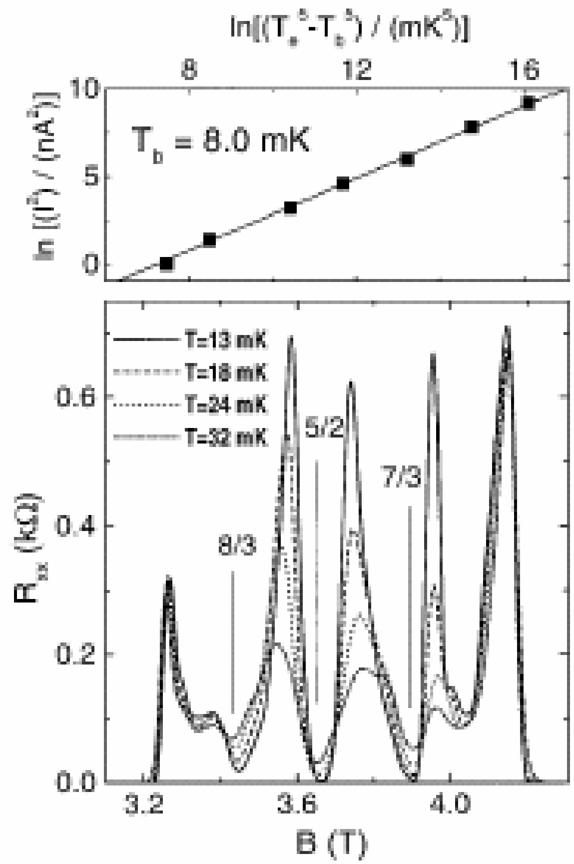

FIG. 2. Lower panel: The temperature evolution of R_{xx} between $\nu = 2$ and $\nu = 3$. Upper panel: $\ln(I^2)$ vs $\ln(T_e^5 - T_b^5)$. I is current in nA. T_e is electron temperature and T_b is bath temperature, in mK.

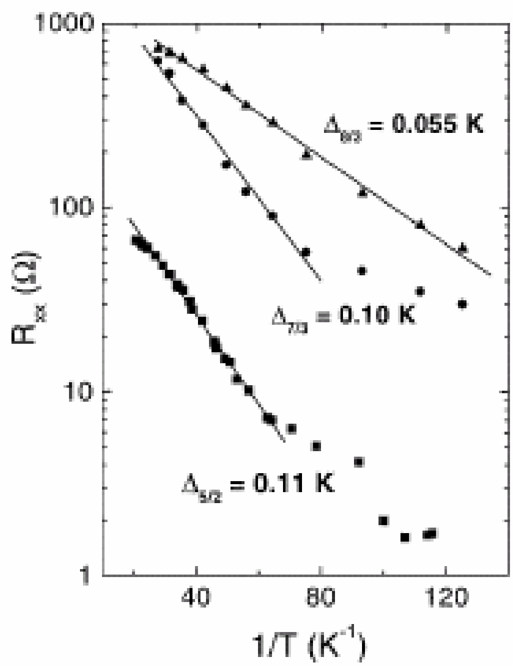

FIG. 3. Activation energy plots for R_{xx} at the $\nu = 5/2, 7/3$, and 8/3 minima for $8.0 < T_b < 50.0$ mK. The data for $\nu = 7/3$ and $\nu = 8/3$ are multiplied by 10 for clarity. Activation energy gaps, Δ_ν, are determined from the slope of the extended linear regions.

Activation energies still small:
? ~ 0.1K at 5/2

Pan PRL '99

IV. Higher Landau Levels

B. 5/2 fractional quantum Hall effect:

Vary density to see if spin transition present

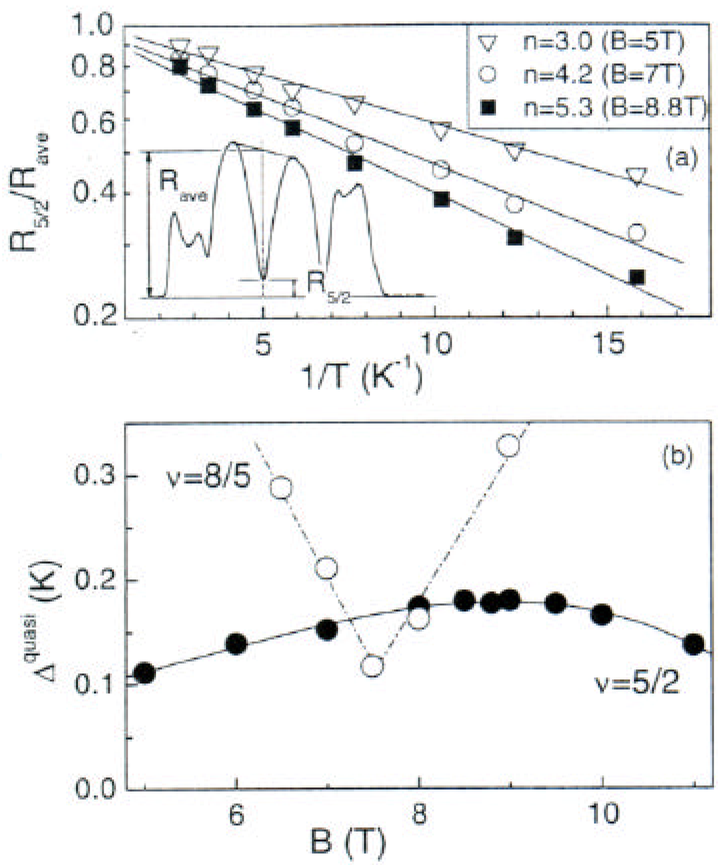

Fig. 3. (a) Arrhenius plot for $R_{5/2}/R_{ave}$ at three densities, in units of 10^{11} cm^{-2}. (b) (●) Smooth variation of quasi-energy gap of the $\nu = 5/2$ FQHE state as a function of magnetic field (i.e. electron-density). (○) Collapse of the $\nu = 8/5$ quasi-energy gap due to the well-documented transition in its spin-polarizations.

Large density variation,
but no transition
~ spin polarized ?

Pan PRL ‘02

IV. Higher Landau Levels

B. 5/2 fractional quantum Hall effect:

Even higher mobility samples and even lower temperatures show better 5/2

But, other complications in the higher Landau levels

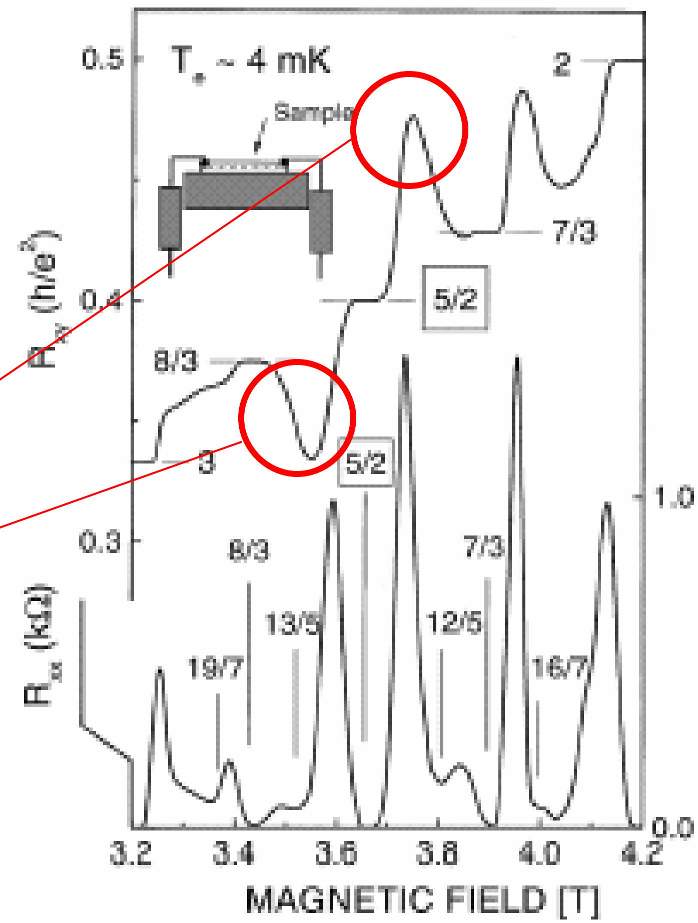

FIG. 1. Hall resistance R_{xy} and longitudinal resistance R_{xx} at an electron temperature $T_e \simeq 4.0$ mK. Vertical lines mark the Landau level filling factors. The inset shows a schematic of the sample with attached sintered silver heat exchangers (gray) to cool the 2DES.

Pan, PRL ‘99

IV. Higher Landau Levels

B. 5/2 fractional quantum Hall effect:

Summary:

5/2 unique state:

✍Fragile (low temps, high mobilities needed to observe)

✍tilted field reduces strength of effect

✍at high temperatures (>250mK) Fermi surface effects present

✍Fermi surface effects consistent with spin polarized system

FUTURE:

Statistics are different: QUASIPARTICLES SAID TO OBEY NON-ABELIAN STATISTICS

IV. Higher Landau Levels

B. 5/2 fractional quantum Hall effect:
FUTURE

Non-abelian statistics; what does this mean

FERMIONS

ABELIAN

BOSONS

"NON-ABELIONS"

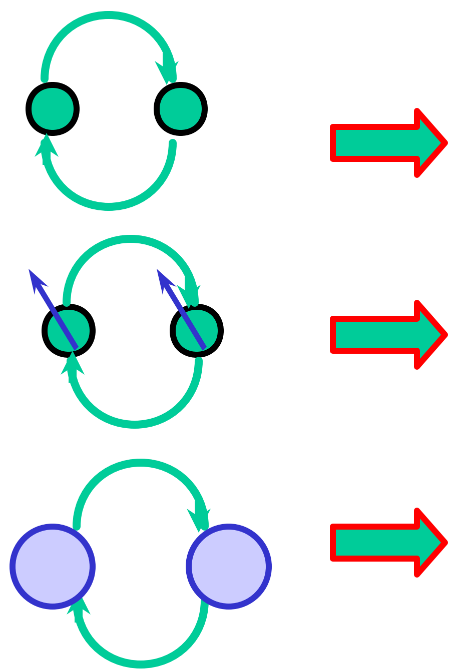

$e^{-i?}$

$e^{-i2?}$

$e^{?}$ + system rotation

Non-Abelions do not have the simple scalar phase change of Abelian system

Non-abelian statistics; how do you detect these statistics?

IV. Higher Landau Levels

C. 9/2: stripes and other things

After composite fermions in lowest Landau levels (N=0), and 5/2 state in second Landau level (N=1), what happens at lower B fields?

Recall that wavefunctions have more nodal structure for higher N

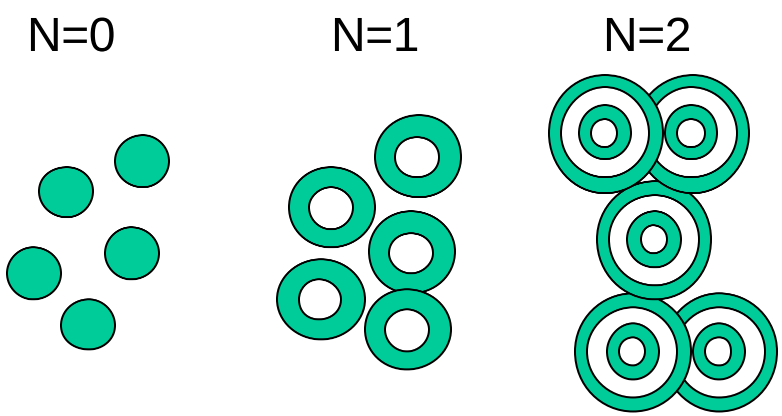

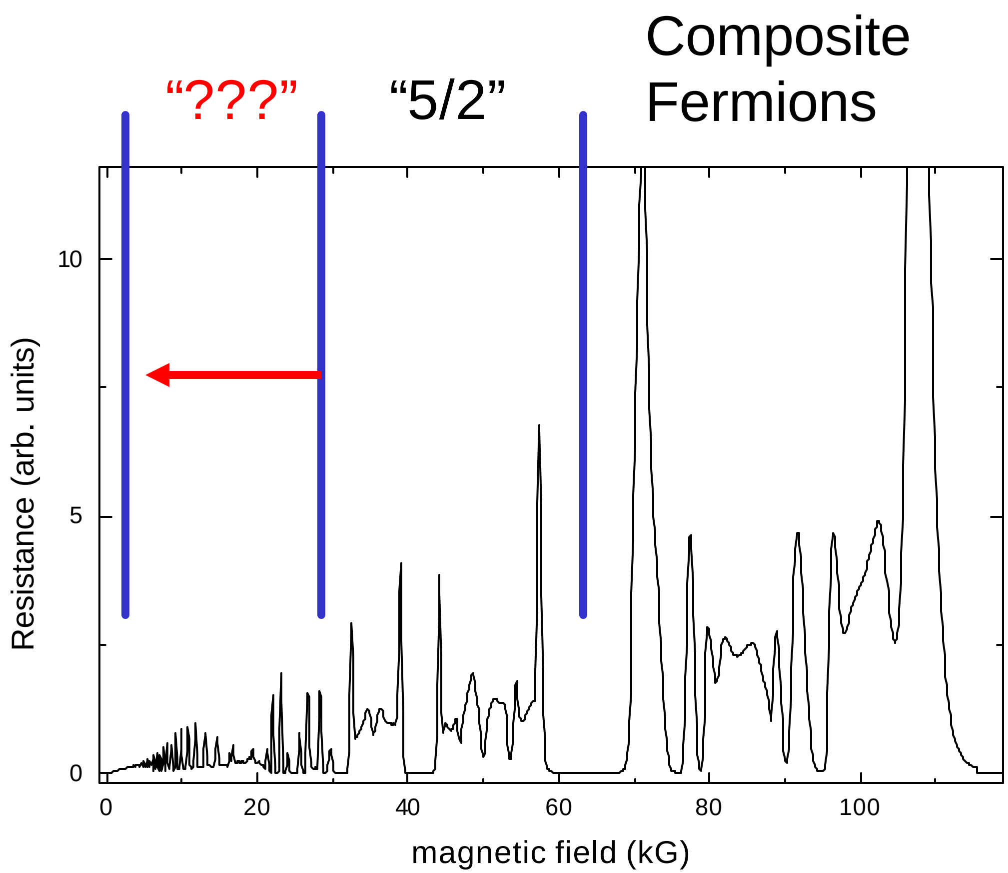

IV. Higher Landau Levels

C. 9/2: stripes and other things

Higher mobility samples show features in the low B-field range of resistivity between integer quantum Hall zeroes

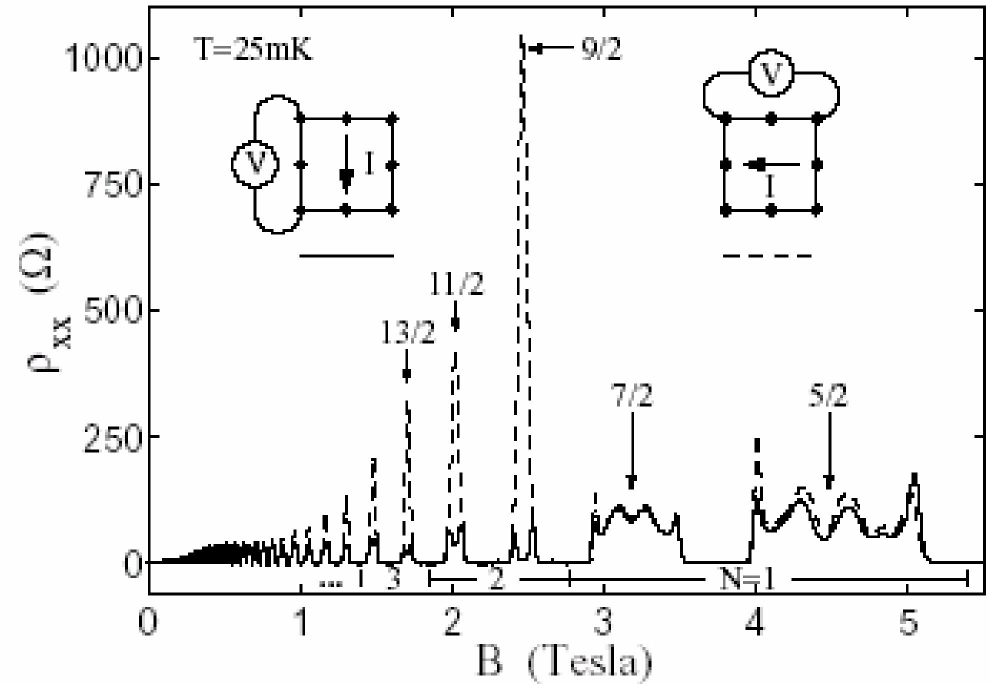

FIG. 3. Anisotropy of ρ_{xx} in sample A at $T = 25$ mK. The two traces result from simply changing the direction of current through the sample; the sample itself is *not* rotated.

Evidence for an Anisotropic State of Two-Dimensional Electrons in High Landau Levels

M. P. Lilly,[1] K. B. Cooper,[1] J. P. Eisenstein,[1] L. N. Pfeiffer,[2] and K. W. West[2]
[1]*California Institute of Technology, Pasadena, California 91125*
[2]*Bell Laboratories, Lucent Technologies, Murray Hill, New Jersey 07974*

(Received 19 August 1998)

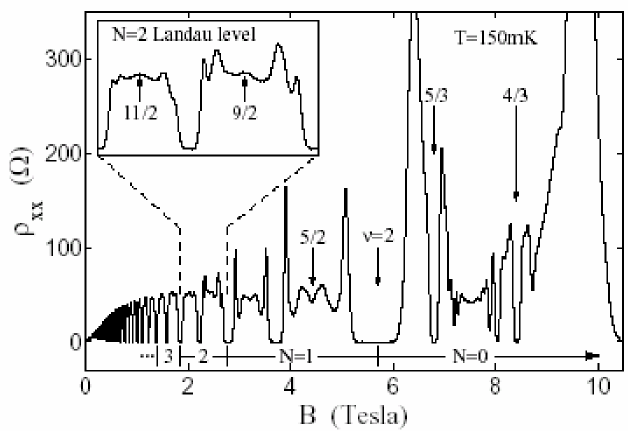

FIG. 1. Overview of diagonal resistivity in sample A at T = 150 mk. Structure in the $N = 2$ Landau level is expanded in the inset.

Lilly, PRL ‘99 also , Du PRL ‘99

IV. Higher Landau Levels

C. 9/2: stripes and other things

Higher mobility samples show features in the low B-field range of resistivity between integer quantum Hall zeroes:
Anisotropic transport

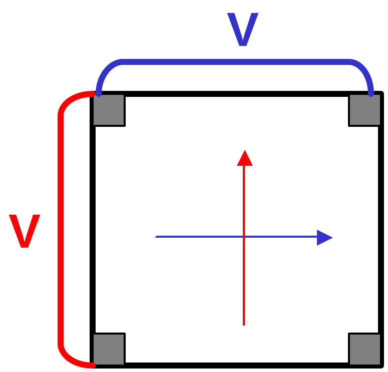

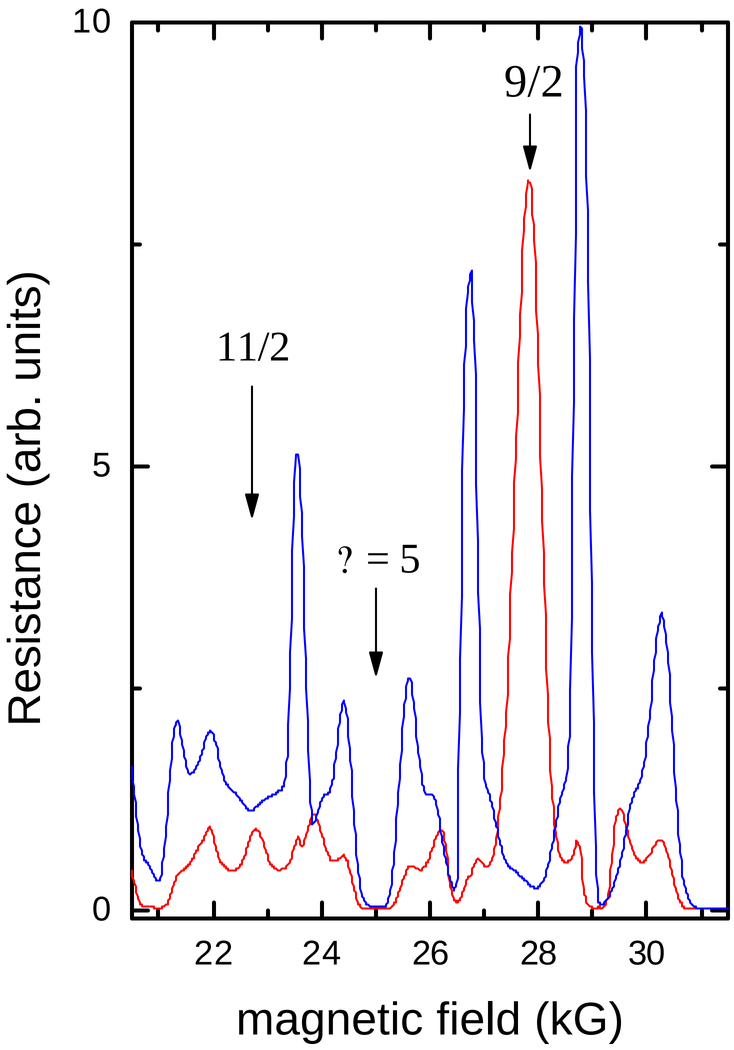

IV. Higher Landau Levels

C. 9/2: stripes and other things

Higher mobility samples show features in the low B-field range of resistivity between integer quantum Hall zeroes:
Anisotropic transport

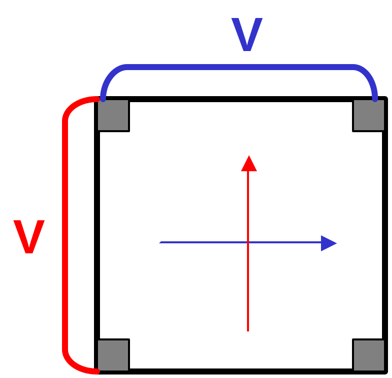

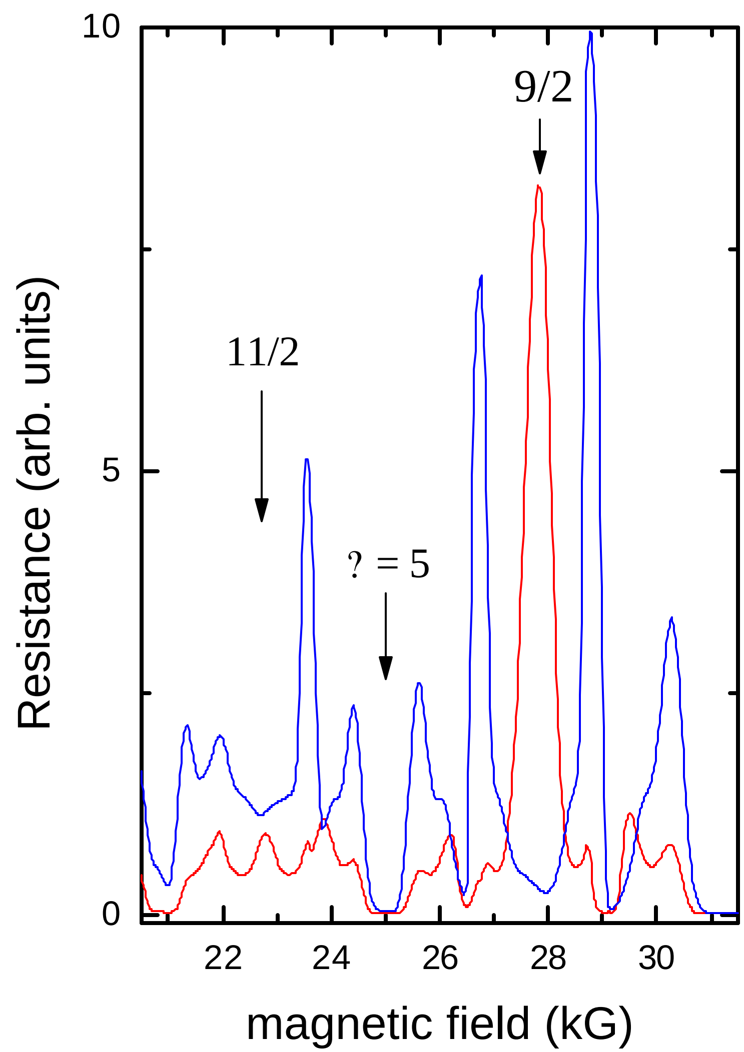

large resistance across 110,
small resistance along 110

IV. Higher Landau Levels

C. 9/2: stripes and other things

Koulakov, Fogler, and Shklovskii; Moessner and Chalker 1996

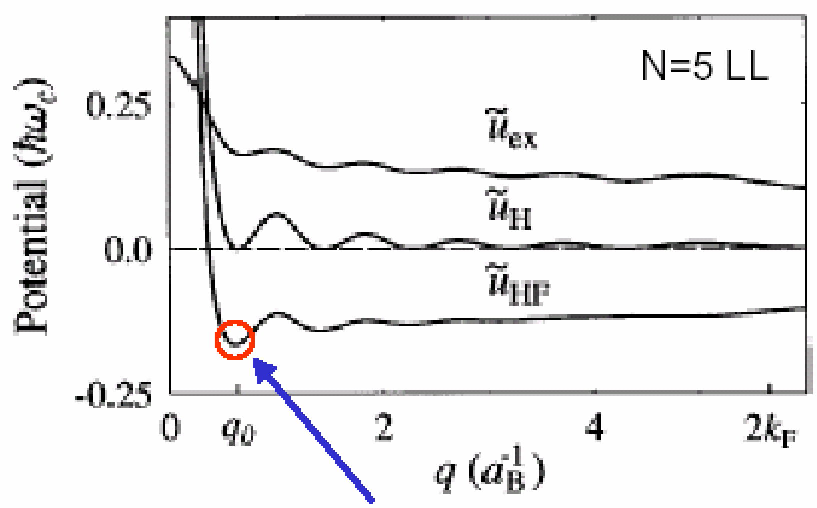

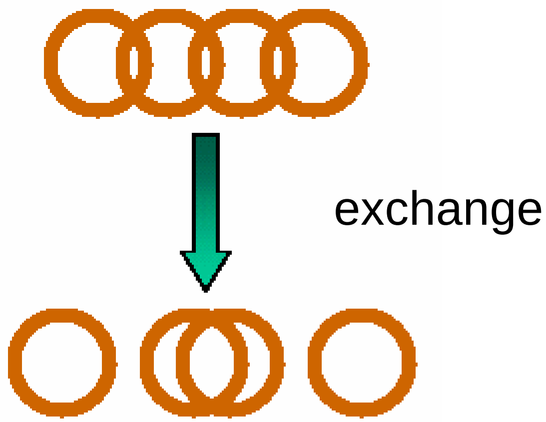

Theory: nodes in high Landau level wavefunctions important for the Coulomb repulsion between electrons. Exchange energy favors phase separation.

This phase separation manifests as charge density waves or stripes

IV. Higher Landau Levels

C. 9/2: stripes and other things

Theory indicates **stripes** at 9/2, 11/2,….

bubbles (incomplete stripes) at 4+1/4, 4+3/4,….

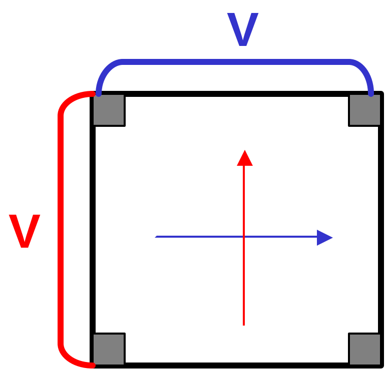

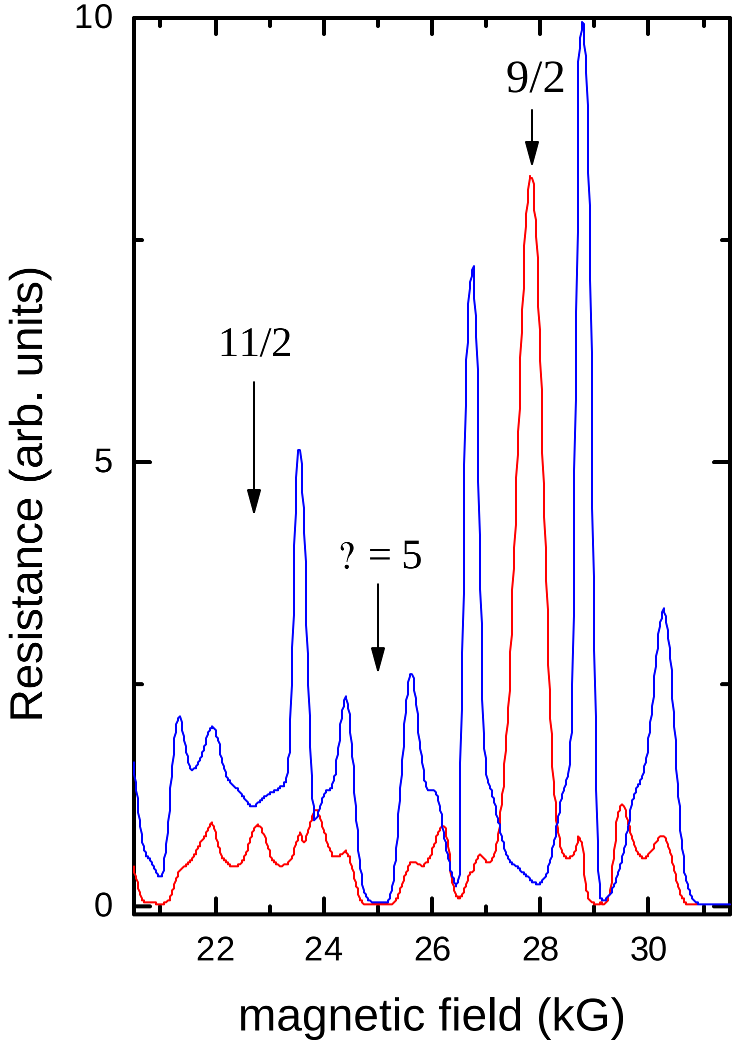

large resistance across 110, small resistance along 110

IV. Higher Landau Levels

C. 9/2: stripes and other things

Recently, Koulakov, Fogler, and Shklovskii [2] and subsequently Moessner and Chalker [3] have proposed that in a clean 2DEG in the $N = 2$ and higher LLs the uniform electron liquid may be unstable against the formation of charge density waves (CDW). They further suggest that near half filling of the LL the CDW is a unidirectional "stripe phase" having a wavelength of order the cyclotron radius. In this stripe phase the electron density in the uppermost LL alternates between zero and full filling. At $\nu = 9/2$ this implies there are stripes of the incompressible QHE states $\nu = 4$ and $\nu = 5$. While it is surely plausible that electrical transport in such a unidirectional phase would be anisotropic, it is not clear what would pin the stripes or why they are apparently coherent over the macroscopic size of our samples.

[2] A. A. Koulakov, M. M. Fogler, and B. I. Shklovskii, Phys. Rev. Lett. **76**, 499 (1996); Phys. Rev. B **54**, 1853 (1996); M. M. Fogler and A. A. Koulakov, Phys. Rev. B **55**, 9326 (1997).
[3] R. Moessner and J. T. Chalker, Phys. Rev. B **54**, 5006 (1996).

Charged density wave should show non-linear I-V

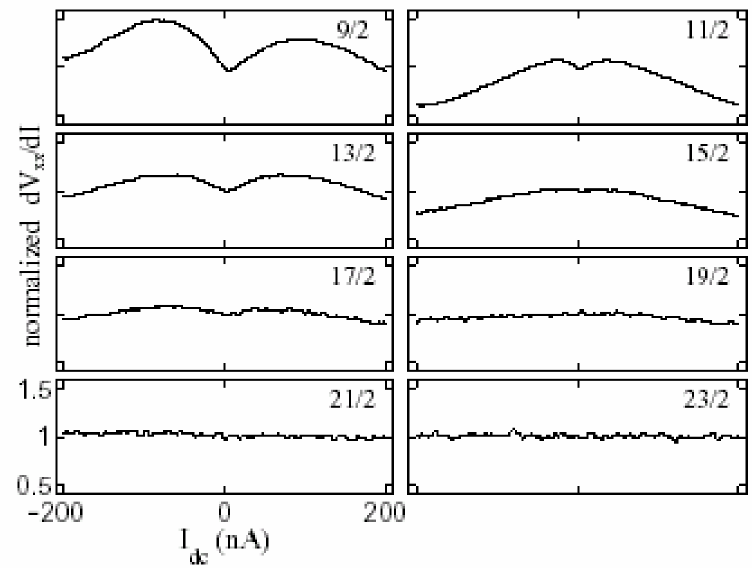

FIG. 5. Nonlinearity of differential resistivity dV_{xx}/dI in sample C at half filling of several high LLs at $T = 25$ mK. The resistivity is normalized by its value at $I_{dc} = 0$. In each panel I_{dc} runs from -200 to $+200$ nA and the normalized dV_{xx}/dI from 0.5 to 1.5.

Lilly, PRL '99

Theory had already suggested that a charged density wave or "striped phase" may exist in the higher Landau levels.

IV. Higher Landau Levels

C. 9/2: stripes and other things

Peaks in one direction, minima in the orthogonal direction

Low temperatures needed

High resistance for current across stripes, low resistance along stripes?

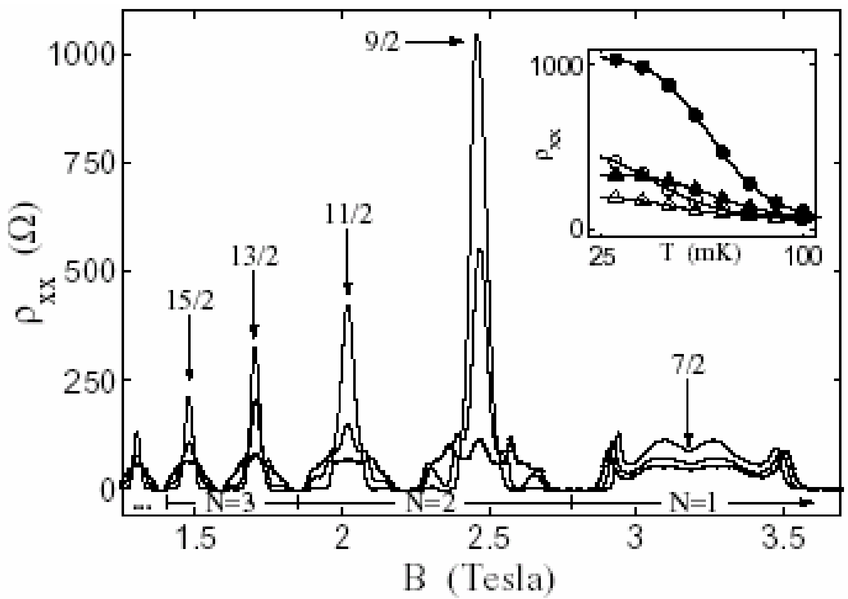

FIG. 2. Peaks in ρ_{xx} in sample A developing at low temperatures in high LLs (dotted line: $T = 100$ mK; thick line 65 mK; thin line: 25 mK). Inset: temperature dependence of peak height at $\nu = 9/2$ (closed circles), 11/2 (open circles), 13/2 (closed triangles), and 15/2 (open triangles).

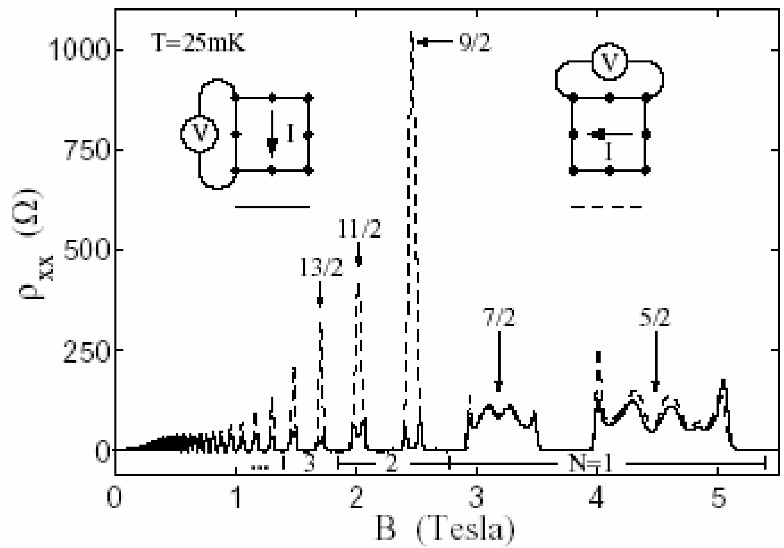

FIG. 3. Anisotropy of ρ_{xx} in sample A at $T = 25$ mK. The two traces result from simply changing the direction of current through the sample; the sample itself is *not* rotated.

Du et al PRL ‘99

IV. Higher Landau Levels

C. 9/2: stripes and other things

Two questions stand out
1) what are the current flow patterns, and
2) what establishes the anisotropy directions

Experiment**:** infer current flow by examining voltages at different spatial contact configurations

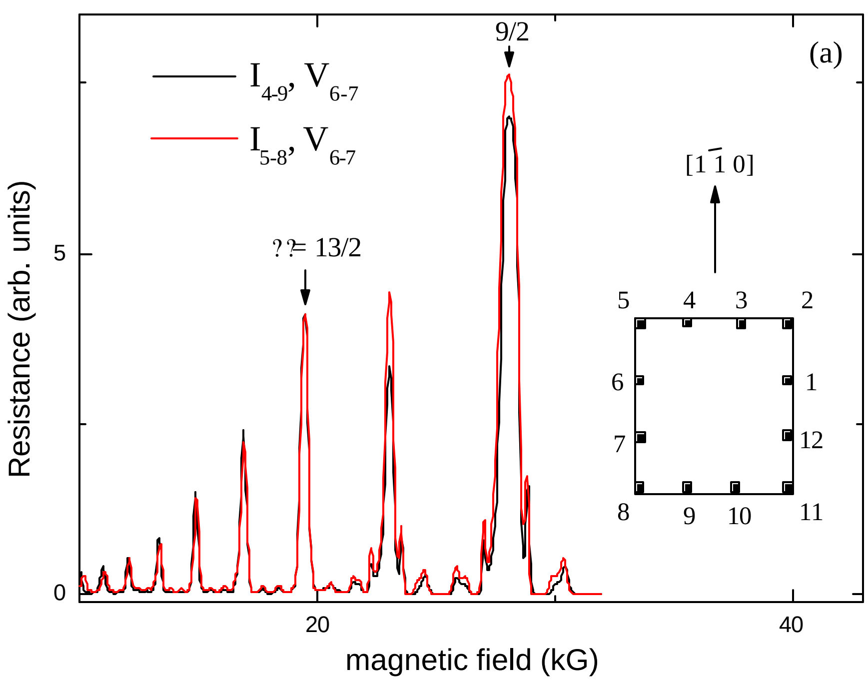

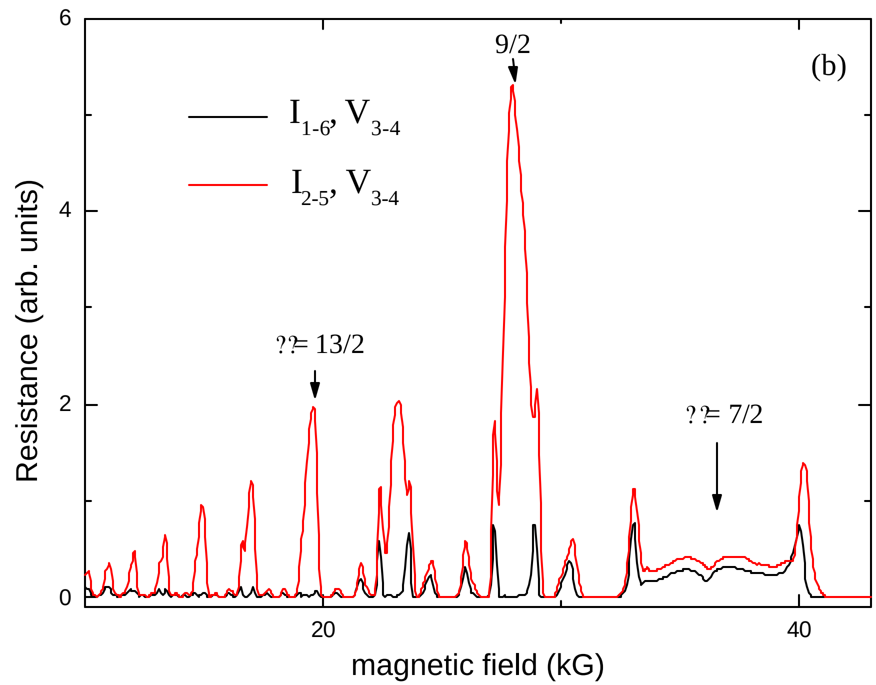

IV. Higher Landau Levels

C. 9/2: stripes and other things

As current/voltage contact separation increases little variation in voltage at 9/2 for current along (1$\bar{1}$0): not so for current across (1$\bar{1}$0)

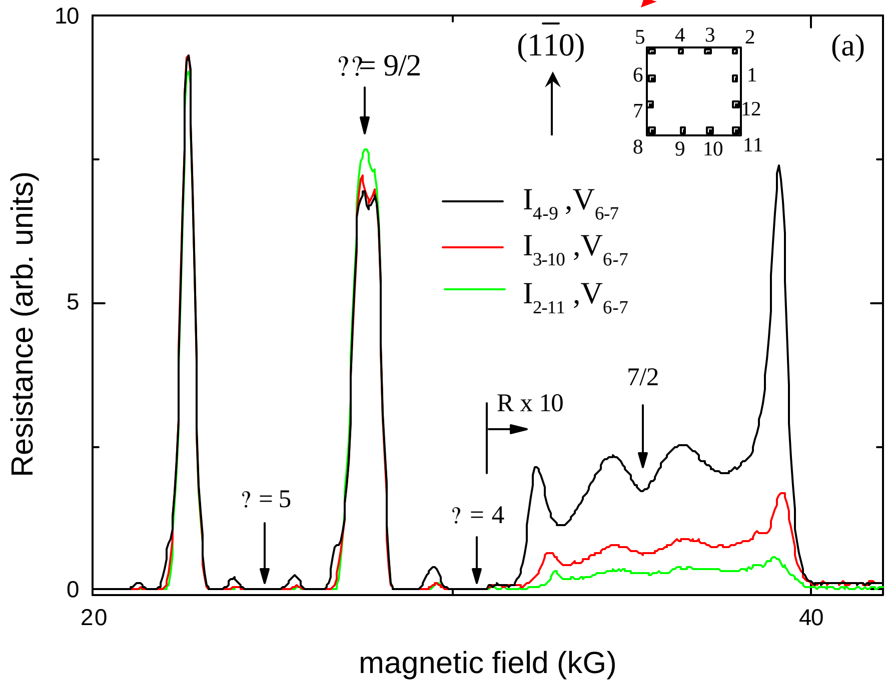

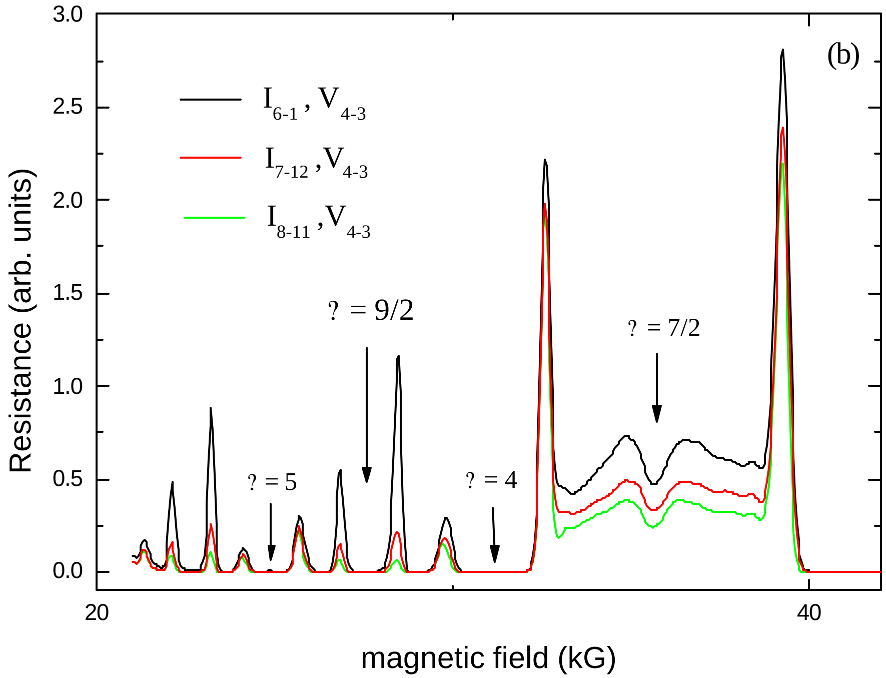

IV. Higher Landau Levels

C. 9/2: stripes and other things

As current/voltage contact separation increases large variation in voltage at 9/2 for current across (1$\bar{1}$0)

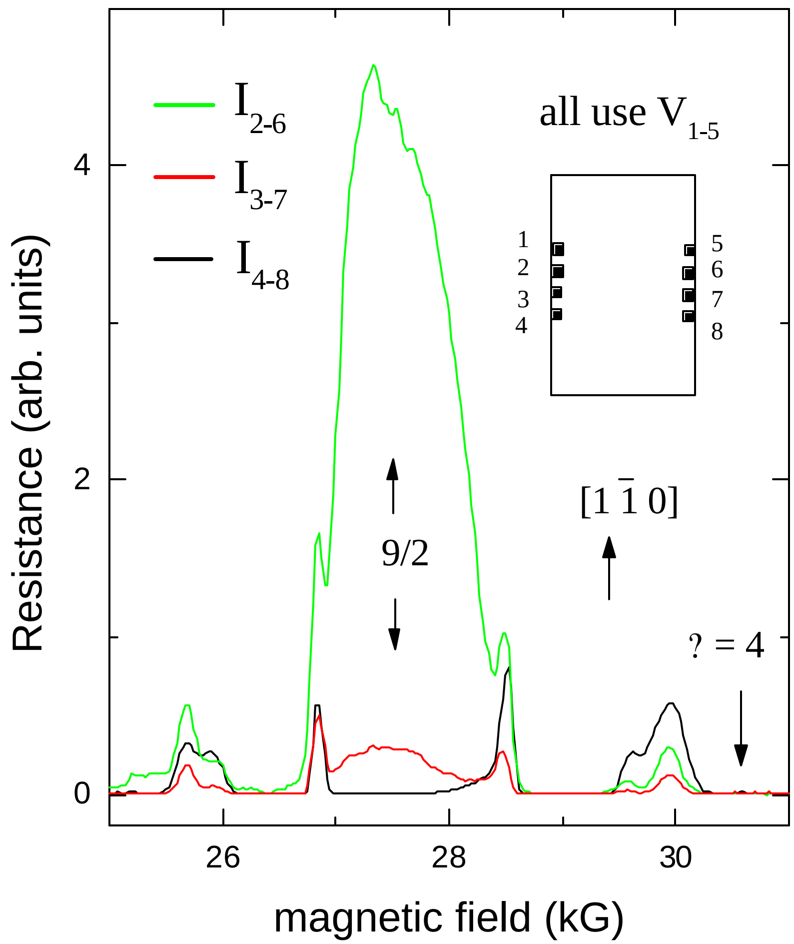

Current driven along (1 1bar 0) appears to spread along (110)

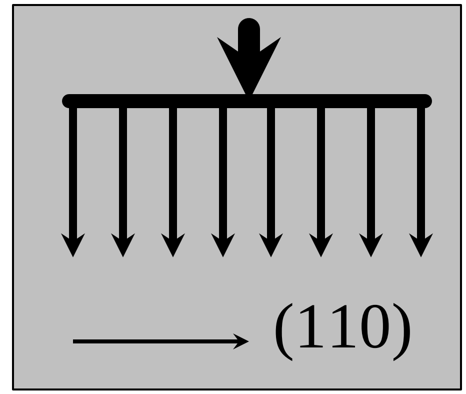

Current driven across (1 1bar 0) appears to channel along (110)

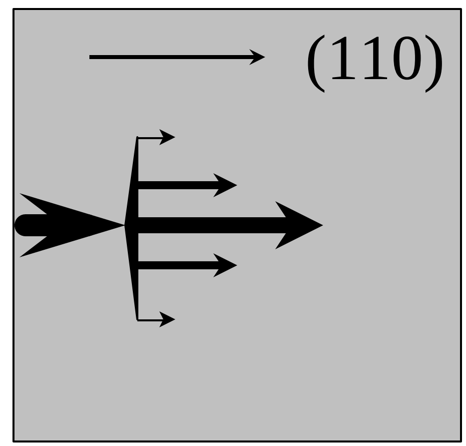

Intrinsic lines are alligned along (110)

IV. Higher Landau Levels

C. 9/2: stripes and other things

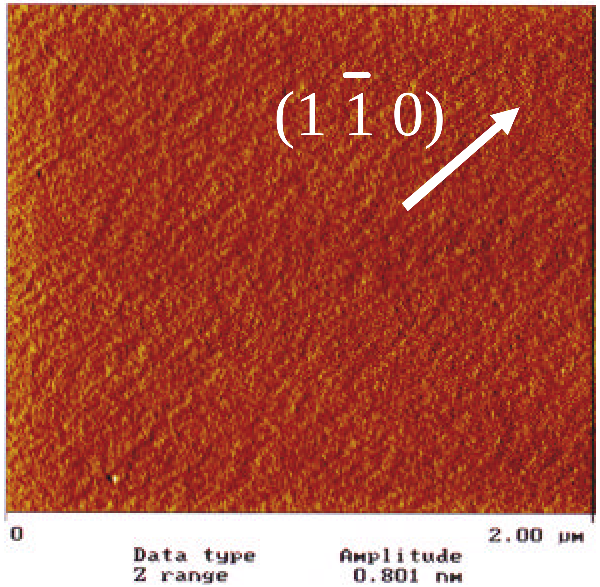

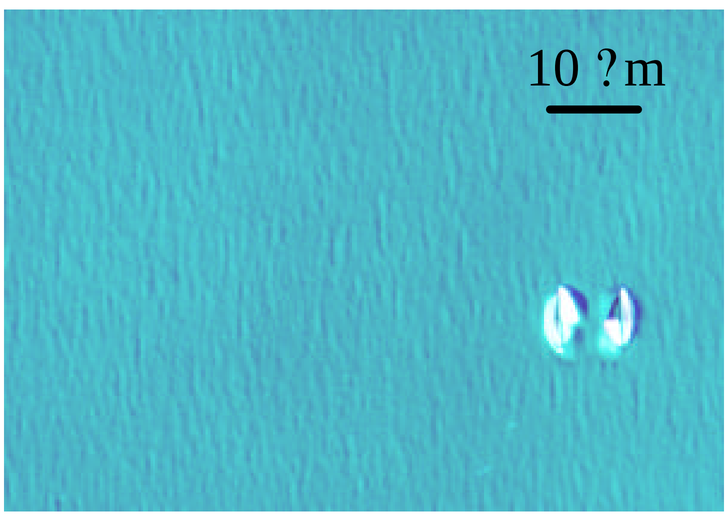

What establishes the anisotropy direction?

Surface lines visible in light microscopy and using atomic force microscopy: all samples examined show lines along (1 1bar 0)

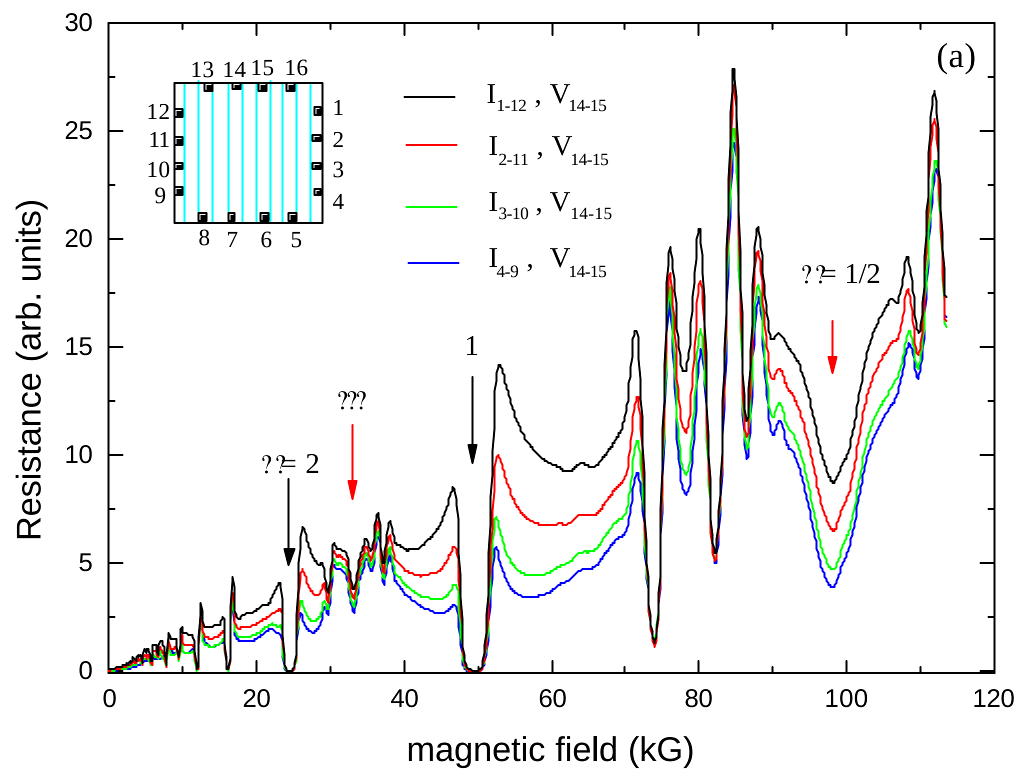

Artificial stripes induce common features

Open question

IV. Higher Landau Levels

C. 9/2: stripes and other things

Applying an in-plane field effects the anisotropy:

it re-orients the phases:

In plane direction establishes the high resistance direction

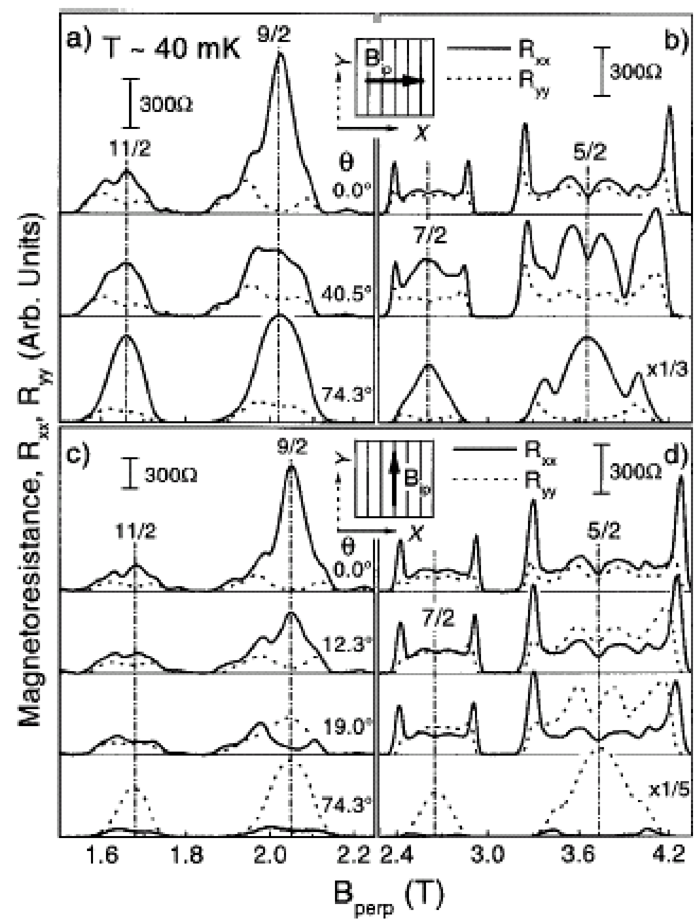

FIG. 2. Dependence of the magnetoresistance R_{xx} and R_{yy} around filling factor 9/2 and 11/2 as well as around 5/2 and 7/2 on angle, θ, and direction of a tilted magnetic field, B. B_{perp} represents the field perpendicular to the sample, $B_{\mathrm{perp}} = B\cos(\theta)$. The sample geometries are depicted as insets. The x and y directions are fixed with respect to the sample. Striples in the sample indicate the initial anisotropy of the 9/2 and 7/2 state. In panels (a) and (b) the sample is rotated around the y axis generating an increasing in-plane field $B_{\mathrm{ip}} = B\sin(\theta)$ along the hard direction, x, whereas in panels (c) and (d) the sample is rotated around the x axis generating an increasing B_{ip} along the easy direction y.

Pan PRL '99

Strongly Anisotropic Electronic Transport at Landau Level Filling Factor $\nu = 9/2$ and $\nu = 5/2$ under a Tilted Magnetic Field

W. Pan,[1,2] R. R. Du,[3,2] H. L. Stormer,[4,5] D. C. Tsui,[1] L. N. Pfeiffer,[4] K. W. Baldwin,[4] and K. W. West[4]
[1]*Department of Electrical Engineering, Princeton University, Princeton, New Jersey*
[2]*NHMFL, Tallahassee, Florida*
[3]*Department of Physics, University of Utah, Salt Lake City, Utah*
[4]*Bell Labs, Lucent Technologies, Murray Hill, New Jersey*
[5]*Department of Physics, Columbia University, New York, New York*
and Department of Applied Physics, Columbia University, New York, New York

(Received 12 March 1999)

IV. Higher Landau Levels

C. 9/2: stripes and other things

Using HIGFET, transition at ~2.5×10^{11}

Density adjustment also can induce reorientation

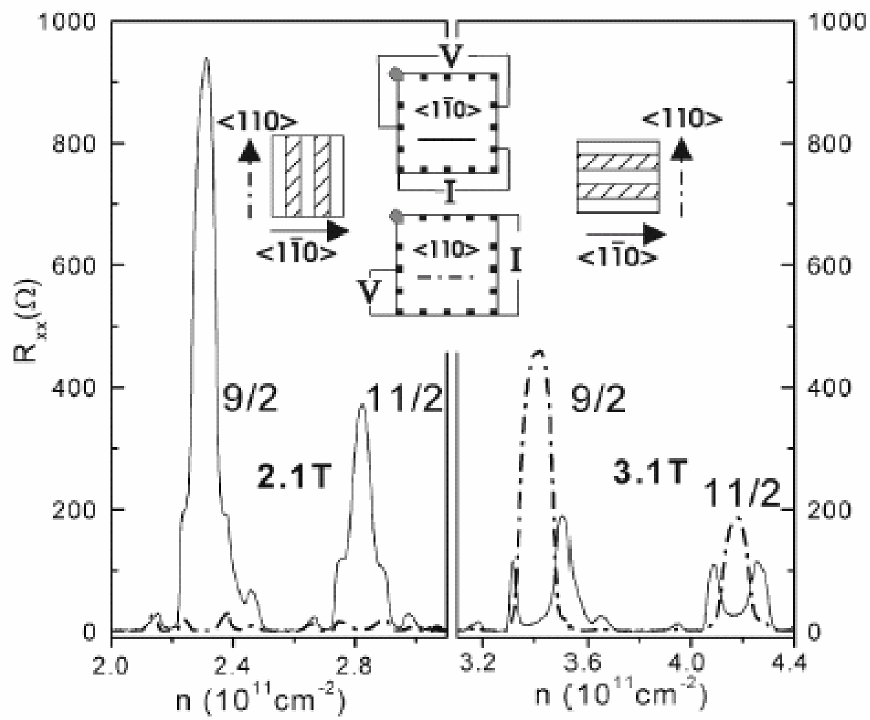

FIG. 1. Interchange of anisotropy axes of the $\nu = 9/2$ state with increasing densities. The two central insets show the contact configurations used to measure the anisotropy. Data from the $\langle 1\bar{1}0\rangle$ configuration are represented by solid lines and data from the $\langle 110\rangle$ configuration by dash-dotted lines. In the left panel, the stripes align along the $\langle 110\rangle$ direction. In the right panel, they align along the $\langle 1\bar{1}0\rangle$ direction. See insets.

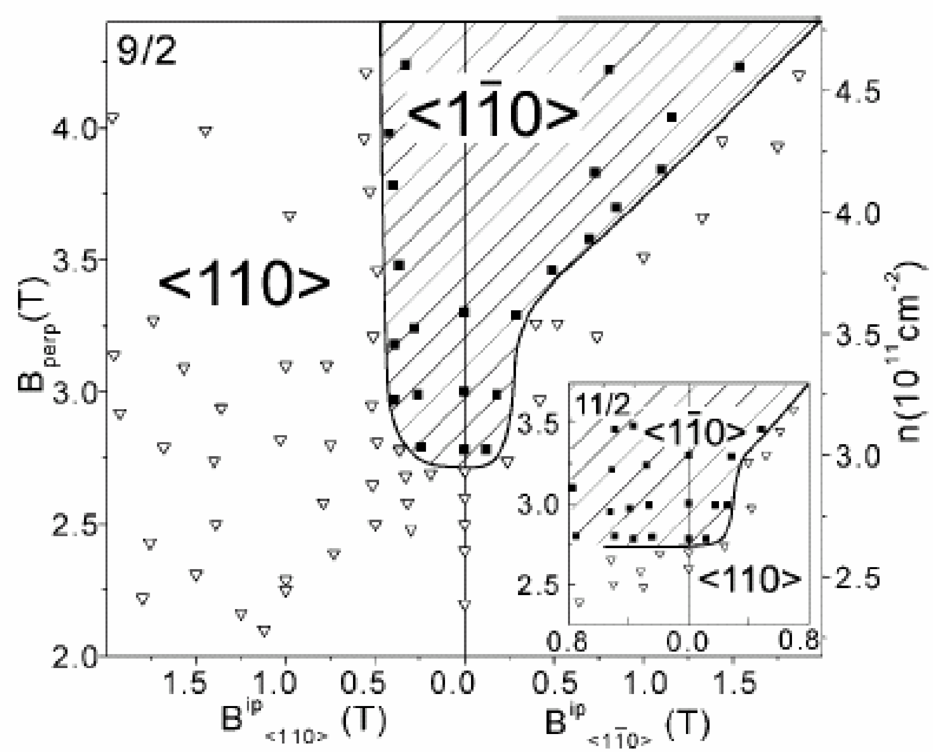

FIG. 3. Phase diagram of the orientation of the stripes at $\nu = 9/2$ in the B^{perp}-B^{ip} plane. Solid squares represent the $\langle 1\bar{1}0\rangle$ orientation of the stripes. Hollow triangles represent the $\langle 110\rangle$ orientation. In the left panel, B^{ip} points along the $\langle 110\rangle$ direction. In the right panel, B^{ip} points along the $\langle 1\bar{1}0\rangle$ direction. The inset shows the phase diagram at $\nu = 11/2$. Units are the same as in the $\nu = 9/2$ diagram.

Zhu PRL '02

IV. Higher Landau Levels

D. Higher Landau levels
experimental issues & future

In higher mobility samples complicated mixing of features of FQHE and stripes

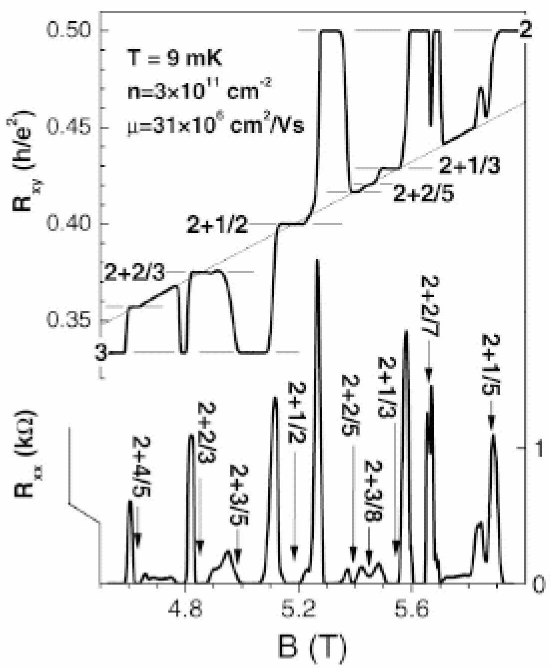

Re-entrant phases of stripes or bubbles at low temperatures:

Spill over of stripes to N=1

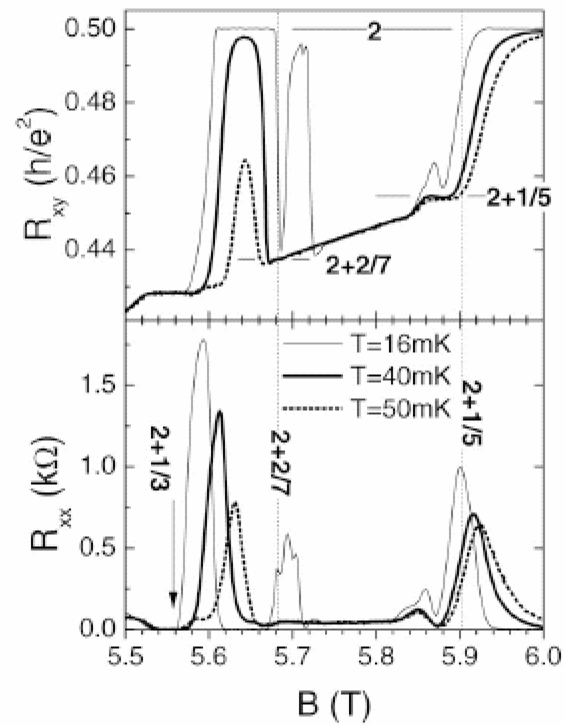

FIG. 1. R_{xx} and R_{xy} between $\nu = 2$ and $\nu = 3$ at 9 mK. Major FQHE states are marked by arrows. The horizontal lines show the expected Hall value of each QHE state. The dotted line is the calculated classical Hall resistance.

FIG. 3. Temperature dependence of R_{xx} and R_{xy} around the split Hall plateau and $\nu = 2 + 1/5$. The vertical lines mark the B field positions of the $\nu = 2 + 1/5$ and $2 + 2/7$ states. The horizontal lines mark the expected Hall resistance values for $\nu = 2 + 2/7$, $2 + 1/5$, and 2.

Electron Correlation in the Second Landau Level: A Competition Between Many Nearly Degenerate Quantum Phases

J. S. Xia,[1,2] W. Pan,[3,2,*] C. L. Vicente,[1,2] E. D. Adams,[1,2] N. S. Sullivan,[1,2] H. L. Stormer,[4,5] D. C. Tsui,[3] L. N. Pfeiffer,[5] K. W. Baldwin,[5] and K. W. West[5]

PRL '04

IV. Higher Landau Levels

C. 9/2: stripes and other things

Summary:

✍theory using higher Landau level structure predicts stripe and bubble phases

✍anisotropy in transport observed at 9/2,11/2, 13/2,…:
peak at 9/2 for current along [1 1bar 0],
minimum for current along [1 1 0]

✍anisotropy affected by in-plane field, density

✍What establishes direction of anisotropy and if same physics may be at play in N=1 are open questions

✍no direct observation of stripes yet achieved

IV. Higher Landau Levels

D. Higher Landau
experimental issues & future

Can stripes be visualized?

Imaging of localized electronic states in the quantum Hall regime

N. B. Zhitenev*, T. A. Fulton*, A. Yacoby*†, H. F. Hess*‡, L. N. Pfeiffer* & K. W. West*

** Bell Laboratories, Lucent Technologies, Murray Hill, New Jersey 07974, USA*
† Weizmann Institute of Science, Rehovot 76100, Israel
‡ Phasemetrics Inc., San Diego, California 92121, USA

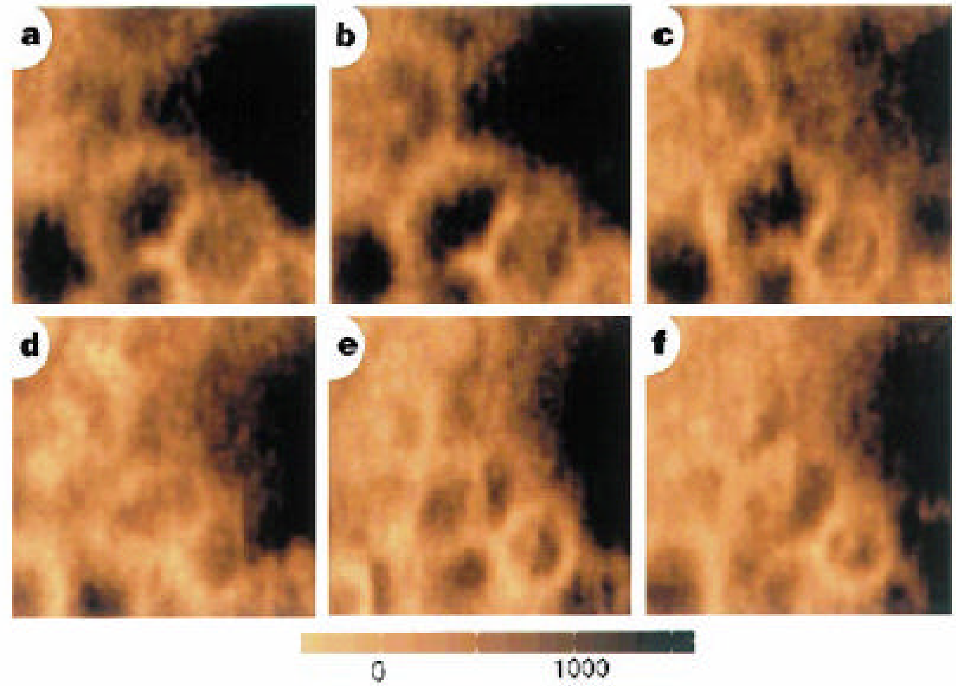

Figure 3 Interacting rings. **a–f**, Spatial images of the transparency signal over $1.0 \times 1.0\ \mu m^2$ area taken at six increasing densities. V_{bg} is changed by 5 mV between images which adds ~0.65 electron charges to the area of the panel. Filling factor is close to 1. As in Fig. 2, the transparency signals are large and positive in the centre of the cells, and small, or even negative, on the cell boundaries.

Scanning SET promising,
but with difficulties

IV. Higher Landau Levels

D. Higher Landau
experimental issues & future

1) Difficult to experimentally work here
   a) Low energy scales mean low temps needed
   b) Small energy gaps mean high mobility needed
   c) Any density perturbation creates problems

2) Important possibilities for exploring exotic statistics
   a) How do non-Abelian statistics manifest
   b) Can this be used in quantum computing?

3) Many open questions